UNIVERSITY OF GENOA

DEPARTMENT OF EXPERIMENTAL MEDICINE

PhD COURSE IN EXPERIMENTAL MEDICINE

Curriculum: Biochemistry

Title:

The role of CD38 and TRPM2 in adipose tissue and liver during thermogenesis

Candidate

Benzi Andrea

Tutor

Prof Bruzzone Santina

Coordinator of the PhD course

Prof Fedele Ernesto

Academic Year 2018-2022

XXXIV Cycle

Index

1. Introduction

The present thesis will explore the role of CD38, a Nicotinamide Adenine Dinucleotide (NAD^+) glycohydrolase mainly generating ADP-ribose, and of TRPM2, an ADP-ribose-gated ion channel, in adipose tissue and liver during thermogenesis. These tissues are fundamental for whole-body metabolism and their proper activity is necessary for a healthy life. My project focuses on the role of CD38 and TRPM2 in these tissues in mice exposed to a cold temperature: these proteins create a signal axis, which merges the regulation of the availability of the coenzyme NAD^+ with calcium homeostasis.

1.1 The adipose tissue

Adipose tissue is the largest endocrine organ in the body, and it plays an important role in thermogenesis, energy balance, glucose and lipid homeostasis.

Excessive nutrient-derived energy is mainly stored in adipose tissue and leads to the expansion of total body mass. Obesity is a consequence of altered energy balance and develops when energy intake exceeds total energy expenditure, which is dictated by the basal metabolic rate, physical activity, and thermogenesis. Obese people are at high risk for developing complications such as type 2 diabetes (T2D), cardiovascular disease, and the metabolic syndrome [Fenzl et al. 2014].

Adipocytes are lipid-rich cells, a feature from which is based its name. However, different types of adipocytes have been identified so far. Each one, exhibits specific functions in the body. The two mainly relevant types of adipose tissue in mammals are white adipose tissue (WAT) and brown adipose tissue (BAT). They are localized in different regions of the body and display different morphological and metabolic features. The origin of the name is based on tissue color [Giralt et al. 2013].

In addition, “beige adipocytes” have been described, although they do not constitute a distinguished tissue in the body. This type of adipocytes increases in WAT when the organism is subjected to certain stimuli (such as, but not limited to, norepinephrine and cold temperature) (see below). They share metabolic and morphologic features both with white and with brown adipocytes [Giralt et al. 2013].

Another type of adipose tissue, named pink adipose tissue, has been recently discovered: it rises only in mammary glands, in females during pregnancy and lactation period (see below) [Giordano et al. 2014].

1.1.1 White Adipose Tissue

Until the ’90s, WAT was commonly considered as an inert mass, whose functions were only to store lipids, as energy molecules to be used during fasting periods, as well as to play an important role in mechanical protection and thermal isolation [Martínez-Sánchez et al. 2020]. Approximately 30 years ago, WAT has been proposed under a different point of view: WAT was starting to be considered as an organ able to produce and release molecules affecting the whole organism. Indeed, the discovery of *ob* gene, which leads to leptin production, paved the way for a new concept of WAT, thereafter, considered as an endocrine organ [Zhang et al. 1994].

In mice and humans, WAT develops in different anatomical sites [Giralt et al. 2013]. The main human depots are:

- visceral: localized in omental, pericardial, mesenteric, perigonadal and mediastinal regions;
- subcutaneous: localized under the skin in abdominal and luteal-femoral regions.

In mice, the main white depots are inguinal, epididymal and subcutaneous (located in the anterior of the chest) [Martínez-Sánchez et al. 2020, Kwok et al. 2016, Ikeda et al. 2018]. White adipocytes contain a single large lipid droplet (90% of the cell volume) [Martínez-Sánchez et al. 2020]. The few mitochondria, Golgi complex, smooth and rough endoplasmic reticulum, nucleus, vesicles, and other organelles are pushed to the edge of the cell and appear elongated within a thin cytoplasmic layer [Bolsoni-Lopes et al. 2015]. Mature adipocytes are roundish and diameter range start from 30 to 160 μm. An average adult has 30 billion of fat cells with a weight of 14 kg [Torres et al. 2015].

WAT mainly functions as a homeostasis regulator: when calorie intake exceeds energy expenditure, it stores energy excess by synthetizing triglycerides (TGs); on the contrary, during long fasting period as well as when energy demand is high, it acts as an energy source by releasing non-esterified fatty acids (NEFAs) obtained during lipolytic processes [Zhang et al. 1994, Ikeda et al. 2018]. In plasma, TGs are carried inside chylomicrons (when of exogenous origin) and very-low-density lipoprotein (VLDL; when synthetized from the liver) and they could not be

internalized by adipose cells, thus these molecules need to be broken in NEFAs and monoacylglycerol by Lipoprotein lipase (LPL). This enzyme is attached to the vascular endothelium and displays its catalytic site in the lumen of the vessel. Through the LPL-catalyzed enzymatic activity, TGs-derived products resulting from this hydrolysis are allowed to be collected into white adipocytes. The internalization is mediated by diffusion or by several transporters, including CD36, Caveolin-1 and Fatty-acid binding protein. Intracellular NEFAs are trapped in the cytosol through their conversion in acyl-CoA by Acyl-CoA synthetase and then stored mainly in form of TGs into lipid droplet. This process is not only regulated by nutrient availability and different stimuli, including, but not limited to, insulin, are able to promote it [Zhang et al. 1994]. The other characterizing metabolism in white adipocytes is the degradation of lipids, subsequently released in the blood and utilized by the body to boost energy production. Lipolysis occurs, as it happens for lipogenesis, both in basal and in stimulated conditions. Different stimuli, such as glucagon and agonists of β3-adrenergic receptors, efficiently enhance lipolysis. Mainly, three enzymes are involved in TGs degradation, each one working on its preferential substrate and breaking just one of the ester bonds:

- Adipose triglyceride lipase (ATGL), acting on TGs, preferentially on C2-linked fatty acid, but broadening its activity range to the C1-linked fatty acid when associated with its coactivator;
- Hormone sensitive lipase (HSL), that better performs diacylglycerols breakdown, but it also slightly works on TGs;
- Monoacylglycerol lipase (MGL), which can complete the process separating the last fatty acid chain from the glycerol molecule.

In unstimulated status, basal lipolysis is mediated by ATGL, that stands on the surface of the lipid droplet. Upon lipolysis-promoting stimuli, the activated Protein kinase A (PKA) phosphorylates HSL and Perilipin A. This reaction leads to HSL mobilization from the cytosol to the surface of the lipid droplet and to a conformational change in Perilipin A, a lipid droplet-coating protein. Phosphorylated Perilipin A allows the lipid droplet to be more exposed to lipase activity. Moreover, an ATGL co-activator that usually is bound to Perilipin A is release upon phosphorylation and can interact with ATGL enhancing its activity. Most part of lipolysis-derived fatty acids is then released in the bloodstream, but a considerable part of them is kept by the adipose cell and undergoes re-esterification back to TGs or is utilized for the synthesis of membranes [Bolsoni-Lopes et al. 2015, Eichmann et al. 2012].

Another function characterizing WAT, discovered not so long ago, is the capability of producing and releasing up to 50 different molecules, defined as “adipokines” [Zhang et al. 1994, Travelli et al. 2015, Audrito et al. 2020, Eichmann et al. 2012]. Different WAT-resident cell types and not only adipocytes are able to influence the environment in autocrine/paracrine- and endocrine-manner. Among the adipokines, one of the most important is Leptin. It was the first one to be discovered. This adipokine is secreted by WAT and by gastric epithelial cells as well and plays a crucial role in feeding behavior and metabolic homeostasis, influencing insulin secretion and liver metabolism [Giralt et al. 2013]. Indeed, recent studies suggest Leptin as an important factor influencing adipocytes differentiation, lipolysis and beiging of WAT. It has been proposed that Leptin exerts its actions by influencing the central nervous system, but also an autocrine/paracrine role has been suggested [Leinninger et al. 2008, Siegrist-Kaiser et al. 1997]. Adiponectin is another meaningful factor secreted by WAT. Low levels of circulating Adiponectin have been shown to directly correlate with T2D, together with metabolic syndrome, and to inversely correlate with insulin resistance. When Adiponectin rises, β-oxidation and energy consumption increase in skeletal muscle and liver, inhibiting the gluconeogenic pathway in the latter [Zhang et al. 1994].

Nicotinamide phosphoribosyl transferase (NAMPT) is another noteworthy protein/enzyme that plays part in different pathways in WAT, including the endocrine signaling. Two forms of NAMPT, intracellular and extracellular, have been reported. Intracellular NAMPT (iNAMPT) is one of the enzymes involved in NAD^+ salvage pathways (see below), whereas extracellular NAMPT (eNAMPT, also known as Visfatin or PBEF, Pre-B-cell colony-enhancing factor) has been identified as a signaling protein acting on the whole body, while its physiological relevance is not well understood [Travelli et al. 2019, Audrito et al. 2020, Chang et al. 2011]. High Visfatin levels have been correlated with rising circulating concentration of TGs and LDL in patients with chronic kidney disease [Mu et al. 2011]. Furthermore, another study linked excessive Visfatin presence in plasma with obesity, T2D, metabolic syndrome and cardiovascular diseases onset and proposed it as a predictive marker to detect this kind of disease [Audrito et al. 2020, Chang et al. 2011]. Conversely, other studies reported Visfatin effects as beneficial. Indeed, Visfatin was observed to regulate glucose-induced insulin secretion in pancreatic β cells [Revollo et al. 2007]. Additionally, Vascular-endothelial grow factor (VEGF) production and release from the endothelial cells are promoted by Visfatin, resulting in an improved angiogenesis [Adya et al.

2008]. Likely, the most interesting effect of eNAMPT is represented by the results suggesting that it acts as an inter-organ modulator of NAD^+ biosynthesis. As a matter of fact, Visfatin was observed to be carried in extracellular vesicles across the bloodstream and, once internalized by cells, can boost NAD^+ synthesis [Yoshida et al. 2019, Yoon et al. 2015]. Moreover, NAMPT absence in adipocytes leads to adipose tissue dysfunction and insulin resistance in adipose tissue, liver, and skeletal muscle [Stromdorfer et al. 2016]. Other molecules released by WAT are growth factors (e.g.: VEGF, EGF, TGF-β), pro-inflammmatory (e.g.: TNFα, IL-1, IL-6) and anti-inflammatory (e.g.: IL-4, IL-10) cytokines and steroids (e.g.: estrogens, glucocorticoids) [Martínez-Sánchez et al. 2020, Kwok et al. 2016].

1.1.2 Brown adipose tissue

BAT represents the second main type of adipose tissue in mammals. It can be easily distinguished from WAT thanks to its color and to the specific localization in the body. Although it is a lipid-rich tissue, BAT exhibits peculiar features that render it different from WAT. Indeed, BAT is not able to store lipids as much as it can use them. This "expertise" makes it one of the major thermogenic sites of the organism. BAT is present in rodents and other small mammals, but in adult humans it has been long considered to be absent, whereas in infants it seems to be important for cold temperature survival [Saely et al. 2012]. In 2009, the presence of a functional brown adipose tissue in adult humans has been finally established by the use of radiolabeled molecules [van Marken Lichtenbelt et al. 2009, Cypress et al. 2009, Virtanen et al. 2009, Admiraal et al. 2013]. As WAT, BAT rises in different anatomical sites. In humans, abundant interscapular brown tissue can be found in infants. Differently, in adult humans it is largely localized in cervical and supraclavicular regions [Wang et al. 2021, Hankir et al. 2018]. In mice, more depots are present than in humans, and the interscapular is the main one [Hankir et al. 2018]. Furthermore, in both human and mice, some other secondary depots (such as axillary and perirenal) have been reported [Hankir et al. 2018].

Brown adipocytes, the main cell type populating BAT, do not share many morphological features with their white cousins. The brown adipose cells, in contrast to white adipocytes, are smaller, and their round nucleus is centrally positioned. Furthermore, the brown adipose cell contains multilocular small lipid droplets and a high number of mitochondria. This elevated mitochondria-content confers adipocytes the characteristic brown appearance and the possibility to produce energy by burning fat, that almost exclusively in this kind of cells will be converted in heat and

not in ATP [Martínez-Sánchez et al. 2020]. Thermogenin, or Uncopling protein 1 (UCP1), is the protein needed for this purpose. UCP1 is highly expressed in brown adipocytes and is a proton carrier inserted in the mitochondrial inner membrane. Exerting its action, respiration chain-derived protons are translocated through the mitochondrial inner membrane without ATP synthesis. This process results in a dissipation of energy produced by respiration, in the form of heat [Ricquier et al. 2011]. Thermogenic activity requires high substrate levels, and BAT is extremely vascularized, in order to allow a sufficient uptake of nutrients and O_2 [Jung et al. 2019]. Nevertheless, BAT also exhibits the ability to produce and release molecules, as referred as BATokines. Among these released regulatory factors, VEGF and nitric oxide are considered very important for their role in enhancing angiogenesis and vascularization, allowing brown adipocytes to better catch nutrients [Xue et al. 2009, Sun et al. 2014, Asano et al. 2001, Nisoli et al. 1988]. Other BATokines are known to target far tissues, such as liver, regulating their metabolism. For example, Fibroblast growth factor 21 (FGF21) is a hormone mainly produced and released by the liver, but BAT has also been proposed as a source of it. FGF21 into the bloodstream can affect liver metabolism, regulating glucose homeostasis and insulin sensitivity [Hondares et al. 2011].

1.1.3 Pink adipose tissue

Another type of adipose tissue has been discovered in mice in recent years, and it is only present in alveolar portion of mammary gland [Morroni et al. 2004]. In adult virgin mice, mammary glands do not present an alveolar portion. It appears during pregnancy and the lactation period, when white adipocytes undergo a trans-differentiation process toward epithelial cells that, in the end, results in the conversion to milk-producing glands formed by lipid-rich elements. These cells have been called “pink adipocytes” mainly because they are parenchyma-derived lipid-laden cells and because the primary mammary gland is pink at the macroscopic level [Giordano et al. 2014]. Pink adipocytes share features with epithelial glands by exhibiting epithelial junctions, apical microvilli and polarized, dense (protein-like) secretory granules. In addition, they display a well-developed Golgi complex, a robust rough endoplasmic reticulum and a large roundish centrally located nucleus, surrounded by a large amount of lipids [Correa et al. 2019]. The white-to-pink conversion is a case in point of the WAT plasticity in response to environmental stimuli, and it has been referred as “pinking” [Cinti et al. 2018].

1.2 Adipose tissue-related disorders

As already mentioned, adipose tissue exerts many functions, besides its storage role and it is well established that its activity is fundamental for the whole organism. Not surprisingly, there are different situations in which adipose tissue can act as a source of problems. An impairment in adipose tissue functions or a dysregulation in its size, are indeed associated to different metabolic disorders, such T2D and obesity [Burhans et al. 2018]. Diet-related disorders are turning epidemic, due to the modern lifestyle and the associated bad eating habits. Thus, an increase in global obesity and T2D prevalence has been reported [Flegal et al. 2016]. Moreover, aging positively correlates with a decline in cellular function and thus, with diseases onset, such as cancer, cardio-vascular diseases and T2D as well [Burhans et al. 2018]. While obesity in most of the cases is due to an overfeeding, T2D onset could be due to different factors, but a strong correlation exists between these two disorders [Burhans et al. 2018, Abdullah et al. 2010]. Insulin is the hormone responsible for glucose uptake by the cells, and for the inhibition of the lipolytic pathway. In liver, it is well known that insulin activates de novo lipogenesis while it blocks gluconeogenesis [Burhans et al. 2018]. In case of T2D, insulin resistance occurs, and pancreatic β-cells (insulin producers) are not able to compensate hyperglycemia [Kahn et al. 2006]. Persistent high glucose in the bloodstream, in turn promotes tissue dysfunction in affected subjects. Different events have been suggested as a link between obesity and T2D: adipose tissue chronic inflammation, free fatty acids (FFA) release and reduced levels of Adiponectin [Burhans et al. 2018]. It has been suggested that elevated adiposity may be related to insulin resistance because of the elevated FFA release exerted by the adipose tissue. This could be due to the lipotoxicity that these molecules trigger on pancreas [Kahn et al. 2006]. On the other hand, Adiponectin is one of the most important adipokines ameliorating adipose tissue inflammation and sensitizing the organism to insulin action. Through the interaction of Adiponectin with its receptors, different tissues, included liver, enhances their sensitivity to insulin. Adiponectin is inversely correlated to insulin resistance; indeed, diabetic subjects display lower plasma levels of this adipokine [Kahn et al. 2006]. Perhaps, the most fundamental factor involved in insulin resistance is the chronic inflammation of adipose tissue. Chronic inflammation occurs in obese subjects, as measured by the elevated pro-inflammatory marker levels observed in serum [Bastard et al. 2002]. One of the suggested hypotheses involves Hypoxia-inducible factor 1α

(HIF1α) expression. Indeed, obesity-related hypertrophy of adipocytes is associated to hypoxia. When hypoxia occurs, HIF1α is not degraded and can promote the expression of genes involved in different metabolism, including inflammation [Burhans et al. 2018]. In addition, high adiposity is also characterized by immune cells infiltration in adipose tissue. Leukocyte infiltration leads to increased pro-inflammatory molecules production, such as TNFα, IL-1β and IL-6 [Hotamisligil et al. 1995, Fried et al. 1998, Weisberg et al. 2003, Bing et al. 2015].

Several strategies are under investigation to counteract adipose tissue-related disorders, with diet as the first option. One of the most promising therapeutic approaches is the induction of beiging in WAT (see below), in order to increase energy expenditure, lipid metabolism and insulin sensitivity [Abdullah et al. 2010].

1.3 WAT beiging and BAT activation

The most interesting feature of adipose tissue is its extreme plasticity. During life, the organism is subjected to different stimuli that can influence the behavior of the adipose organ, and affect the characteristics exhibited by adipocytes and the rest of the resident cells in the organ. Due to this skill, currently one of the biggest challenges for scientists is to enhance the so called "browning/beiging" process and the activation of BAT. As already mentioned, BAT is specialized in thermoregulation, or the production of heat not associated to muscle activity. Upon cold exposure or proper stimulation, different factors are produced and released into the bloodstream. Liver, sympathetic nervous system (SNS) and adipose tissue itself are the main organs involved in this mechanism. These factors influence adipose tissue by enhancing lipases activity, UCP1 gene expression and activity, and heat production [Hankir et al. 2018].

UCP1 is the main source of heat production in adipocytes and its expression and activity are regulated by various pathways. The first and most known signaling affecting UCP1 expression and activity is norepinephrine (NE). NE is produced and released by the SNS and, when interacts with adrenoreceptors, affect UCP1 expression by stimulating Protein kinase A (PKA) activity. This kinase, in turn, mediates the activation of important factors, such as cyclic AMP (cAMP) responsive element-binding protein (CREB), that binds *UCP1* gene enhancing its expression. Moreover, NE stimulates lipolysis, inducing the release of long-chain fatty acids, known UCP1 activators [Hankir et al. 2018, Martinez-Sanchez et al. 2020, Jung et al. 2019].

Thyroid hormones are important for the correct gene expression pattern during thermogenesis. Thyroid hormone receptors (TRs) are expressed by the adipose tissue and their activation occurs upon interaction with 3,3',5-triiodothyronine (T3), the active form of 3,3',5,5' tetraiodothyroxyne (T4). The conversion between T3 and T4 is mediated by Iodothyronine Deiodinase 2 (DIO2), expressed in adipocytes, and induced by NE [Hankir et al. 2017]. Nevertheless, thyroid hormones also affect hypothalamus promoting SNS activity and enhancing thermogenesis [Hankir et al. 2017, Yau et al. 2020].

As mentioned, FGF21 is secreted mainly by the liver, but also adipose tissue is able to produce and use it as a paracrine/autocrine factor. FGF21, interacting with FGFR1, enhances UCP1 expression and promotes thermogenesis [Hondares et al. 2011].

Bile acids (BAs) constitute another important factor that promote thermogenesis in adipose tissue. These types of molecules are synthetized exclusively in the liver by two different enzymatic pathways. The first substrate in both enzymatic routes is cholesterol and the BAs generated, upon conjugation with taurine or glycine, are commonly used in lipid metabolism and absorption after a meal. Beside these functions, BAs are also related to thermogenesis: indeed, BAs can activate the G-protein coupled bile acid receptor, Gpbar1 (TGR5), increasing DIO2 activity and leading to higher levels of T3 hormone, thus enhancing thermogenic activity [Worthmann et al. 2017].

Besides the activation of BAT to increase energy expenditure, also WAT, as mentioned above, is considered a target for the treatment of diet-related and metabolic-related diseases. Indeed, WAT plasticity allows, under specific conditions, a metabolic and morphological reorganization of the tissue, that acquire brown-like features. This metabolic transformation is known as the beiging/browning of WAT and is triggered by the same stimuli needed to promote thermogenesis in BAT [Jung et al. 2019].

At the end of the beiging process, inducible adipocyte progenitor cells are induced to differentiate toward beige/brite cells. This phenomenon is paralleled by reduced amount of intracellular stored-lipids and an enhanced energy expenditure displayed by the tissue. Furthermore, these kinds of cells display low amounts of mitochondria and multilocular lipid droplets [Jung et al. 2019]. Although beige adipocytes express UCP1, which is commonly used as a marker to measure the browning rate after stimulus, it has been proposed that the route they utilize to produce heat is independent of this channel [Chang et al. 2019]. Thermogenesis in beige adipocytes occurs through an ATP-dependent mechanism, that involves Ca^{2+}: Ca^{2+} is moved

inside the endoplasmic reticulum and subsequently ejected back to the cytoplasm through the ryanodine receptor 2. Ca^{2+} entry into the endoplasmic reticulum is mediated by Sarco-endoplasmic reticulum calcium ATPase 2b (SERCA2b). This process consumes ATP and produces heat. An overexpression of SERCA2b occurring in beige adipocytes during thermogenesis, boosts this Ca^{2+} cycle and allows heat production even without UCP1 action [Chang et al. 2019].

However, induction of beiging in adipose tissue is reversible, thus the cells can differentiate again to white adipocyte. Moreover, it has been discovered that under specific conditions, adipocytes in BAT can change their morphology and functions and acquire white adipocyte features. This process is called "whitening "and is associated to obesity and aging, hence when BAT activity is reduced. Brown-to-white conversion has not been studied as much as the white-to-brown, but it seems that the mechanism begins with a reduced β-adrenergic signaling, inducing accumulation of lipid droplets and mitochondrial dysfunction. Furthermore, BAT becomes hypoxic due to VEGF silencing in adipocytes [Kotzbeck et al. 2018]. All the events described results in a reduced function of BAT.

Aiming to counteract obesity, T2D, and other metabolic disorders due to a massive expansion of WAT, one of the main strategies to which researchers pointed their attention is to fully understand the mechanism underlying adipose tissue plasticity, in order to promote energy expenditure and to reduce lipid accumulation in humans. Thus, recruitment and activation of the beige fat type have the potential to increase energy expenditure, countering obesity and its metabolic complications. Indeed, increasing BAT activity and the conversion of white adipocytes to brown fat-like cells (beiging/browning) have been found to protect from diet-induced obesity and insulin resistance in many rodent models [Lee et al. 2019, Bartelt et al. 2014]. A number of studies suggest that browning might represent a promising strategy to alleviate metabolic disturbances also in humans [Lee et al. 2019]: (i) BAT can act as an anti-diabetic organ by improving insulin sensitivity [Lee et al. 2014]; (ii) beige adipocytes in WAT are essential to maintain whole-body metabolic homeostasis during catabolic conditions [Rabiee et al. 2020, Brandao et al. 2021]; (iii) BAT activity has a significant negative correlation with BMI [van Marken Lichtenbelt et al. 2009]; (iv) subjects with an active BAT exhibit improved metabolic health compared with people with reduced BAT [Suchacki et al. 2021, Becher et al. 2021]. Thus, the loss of BAT and beige cell function can contribute to the development of insulin resistance and hyperlipidemia. In humans, the browning process is stimulated by different factors, including sympathetic stimulation upon cold exposure, beta adrenergic receptor activators and the

administration of Peroxisome proliferator-activated receptor (PPAR) agonists, a well-known regulator of lipid and glucose metabolism [Ahmadian et al. 2013]. However, these browning-inducing methods are not appropriate as therapeutic strategies: the effect of cold exposure is reversible and difficult to implement, and the other agonists/compounds induce adverse side effects.

Overall, mechanisms to induce long-lasting WAT browning are highly demanded in humans [Lee et al. 2019, Suchacki et al. 2021, Chait et al. 2020], because increased brown adipogenesis and WAT browning are considered promising new means for increasing energy expenditure and are suggested as potential therapeutic strategies to combat obesity and related metabolic disorders, including T2D. Indeed, agents capable of inducing WAT browning recently attracted the interest of researchers and stakeholders in the biomedical, nutritional and pharmaceutical fields.

1.4 Liver

Liver is one of the biggest solid organs in the body and constitutes the main metabolic hub of the organism and its functions are essential for a correct metabolic homeostasis. In liver, several metabolic pathways occur, depending on the hormones circulating in the bloodstream. Indeed, liver is largely irrorated, and can be influenced by metabolism-regulating hormones, such as insulin and glucagon. So, in fed state, glycolysis produces molecules that ca be redirected to fatty acids synthesis through de novo lipogenesis. Then, long-chain fatty acids are incorporated into triacylglycerol, phospholipids, and/or cholesterol esters in hepatocytes. Subsequently, these lipids are stored in membrane structures, or secreted into the circulation as VLDL.

Conversely, in the fasted state, liver generates glucose by breaking glycogen and through gluconeogenesis. Then glucose is secreted, aiming to support other organs [Rui et al. 2014, Ramnanan et al. 2011]. During prolonged fasting, lipolysis is promoted in adipose tissue, resulting in NEFAs release that are turned into ketone bodies in liver through ketogenesis. Ketone bodies, together with released glucose, provide a metabolic fuel for extrahepatic tissues. Aberrant hepatic function is correlated with insulin resistance, diabetes, and nonalcoholic fatty liver diseases (NAFLD) [Rui et al. 2014]. Recently, given the pivotal role of liver in regulating energy metabolism, hepatic function has been studied in the context of thermogenesis. Although BAT is considered the major site for thermogenesis in human and other mammals, other tissues are able to contribute to cold adaptation. Liver and muscle play an important role during this process. It has been established that cold exposure increases hepatic gluconeogenesis, total liver and

mitochondrial mass, respiration capacity of hepatocytes, and liver temperature [Abumrad et al. 2017]. Furthermore, liver was observed to influence thermogenesis by producing and releasing factors that act as metabolic booster. The first group of molecules promoting thermogenesis in peripheral tissues is BAs. As mentioned, BAs are exclusively synthetized in the liver, using two different enzymatic routes. Both routes start from cholesterol and result in the generation of the same BAs species. During cold acclimation, when heat generation is required, BAs levels were observed to increase in plasma, due to an upregulated synthesis in the liver. As already mentioned, in both mice and humans, bile acids increase energy expenditure via the stimulation of TGR5 on brown adipocytes. Thus, BAs production and release is one of the events making this organ very important for BAT activation and WAT browning [Chang et al. 2019, Worthmann et al. 2017].

The second known feature making the liver very important, is the ability to produce and release FGF21. Indeed, liver is considered one of the main FGF21 source in the body. As mentioned above, FGF21 is a factor promoting adipose tissue thermogenic activation, in response to specific stimuli [Hondares et al. 2011]. FGF21 is produced and secreted by the liver in response to prolonged fasting, re-feeding, and macronutrient imbalance. Despite adipose tissue has been observed to release FGF21, liver has been established as the major FGF21 producer. Released FGF21, affect the sympathetic nervous system and promotes thermogenesis in adipose tissue. Moreover, FGF21 can act directly on adipocytes, increasing the expression of numerous thermogenic genes [Hondares et al. 2011, Fisher et al. 2012].

An additional role for liver in thermogenesis, is the ability to produce acylcarnitine that acts as a fuel and enhance lipolytic metabolism in adipose tissue. Cold exposure, indeed, has been reported to induce FFAs release from WAT. The just released FFAs promote acylcarnitine production and release from the liver, that will be captured exclusively by BAT and boost heat production [Abmurad et al. 2017].

Thus, energy expenditure by liver and muscle, in addition to that exerted by BAT, could potentially be manipulated to modulate and improve metabolism in obese subjects.

1.5 Nicotinamide adenine dinucleotide: synthesis and utilization

NAD is one of the most important cofactors in living cells. It takes part in several enzymatic reaction thanks to its capacity of being reduced: a fundamental portion of the NAD^+ molecules is

the nicotinamide (NAM) ring, that can be easily reduced to form NADH. The reversible conversion of NAD between the oxidized and the reduced form is fundamental for cellular homeostasis and for the regulation of several metabolic processes [Covarrubias et al. 2021].

A few NAD-synthetizing metabolic pathways have been discovered. The "de novo" synthesis starts from tryptophan and, passing through kynurenine and quinolinate, results in nicotinic acid (NA) mononucleotide (NaMN) production. Another reaction starting from NA and involving the enzyme nicotinate phosphoribosyltransferase (NAPRT) leads to the same intermediate, NaMN. NaMN is then converted to nicotinic acid adenine dinucleotide (NaAD) and finally to NAD^+, by the enzyme NAD^+ synthase [Covarrubias et al. 2021, Belenky et al. 2007].

However, the pathway mostly utilized by mammalian cells to synthetize NAD^+ is the one involving the enzyme NAMPT, which convert NAM and phosphoribosyl pyrophosphate (PRPP) to produce nicotinamide mononucleotide (NMN). Then, nicotinamide mononucleotide adenylyltransferase (NMNAT) converts NMN to NAD^+, with ATP consumption [Covarrubias et al. 2021, Belenky et al. 2007].

All cell types display a specific metabolism depending on their role and function in the organism. Despite differences, a common feature shared by every living cell is the need to synthetize ATP for cellular homeostasis and function maintenance. ATP is produced in the glycolytic pathway, although the large majority of ATP is produced in mitochondria starting from a few substrates, in the oxidative phosphorylation process. The detail that makes NAD(H) so interesting is that all the catabolic pathways known so far converge in the NAD^+ reduction to NADH in the tricarboxylic acid cycle. NADH is in turn oxidized during the electron transport chain, in order to generate the proton gradient required for the synthesis of ATP.

NAD^+ can be also phosphorylated on C2 of the first ribose ring, by a specific kinase, to create $NADP^+$. NAD^+ kinase is the enzyme responsible for this reaction, and represents the only enzyme involved in maintaining the NADP(H) pool. Indeed, $NADP^+$, as its dephosphorylated form, act as a cofactor for redox reaction. These processes lead to the reduction of the NAM group and result in NADPH formation. The ratio between oxidized and reduced form of these two distinct pools gives information regarding cellular homeostasis. A specific NAD^+/NADH ratio is essential for cellular metabolism and mitochondrial function, whereas NADPH/$NADP^+$ ratio is a sensor of the cellular antioxidant potential since NADPH is involved in detoxification from reactive oxygen species [Xiao et al. 2018]. Nevertheless, NAD^+ plays an important role in cellular homeostasis independently from the redox reactions. Indeed, NAD^+ is also a substrate of NAD-consuming

enzymes, that affect several cellular processes by regulating gene expression, protein localization and activity, calcium homeostasis [Covarrubias et al. 2021, Belenky et al. 2007].

There are three main enzyme families able to utilize NAD^+, hydrolyzing the bond between the NAM ring and one the two riboses: Sirtuins (SIRTs), NAD^+-ase/ADP-ribosyl cyclase/cyclic ADP-ribose hydrolase, and Poly ADP-ribose polymerases (PARPs) [Covarrubias et al. 2021, Belenky et al. 2007].

SIRTs are NAD^+-dependent deacetylase/deacylase, which regulate gene expression and protein activities. The reaction requires NAD^+ as a substrate that acts as acetyl/acyl acceptor and releases NAM. Seven SIRTs have been discovered so far and they can be distinguished by their localization and preferential substrates [Covarrubias et al. 2021]. SIRT1 and SIRT6, for example, can regulate gene expression levels by removing acetyl and acyl groups from lysine residues of nuclear histones [Covarrubias et al. 2021]. Furthermore, being deacetylated or deacylated, several enzymes modify their activity and, as a consequence, some metabolic pathways are boosted or slowed down. For example, SIRT6 can deacetylate Glucose-6 phosphate dehydrogenase (G6PD), enhancing its activity and regulating the NADPH pool. Another fitting case is represented by NAMPT, which is targeted by SIRT1, and SIRT6 as well, on the same lysine residue. Despite deacetylation by both the SIRTs results in a promoted NAMPT activity, NAMPT release seems to be managed in a opposite manner by the activities of the two enzymes [Sociali et al. 2019, Yoon et al. 2015].

The second class of enzymes having a proven capacity of degrading NAD^+ is represented by PARPs. PARPs consume NAD^+ and, removing NAM, are capable of linking the resulting ADP-ribose (ADPR) to a target protein, influencing its activity. PARPs can attach more than one ADPR molecule to the protein target building long ADPR chains, that act as a post translational modification, known as poly ADP-ribosylation [Belenky et al. 2007].

The last category of enzymes regulating intracellular NAD amount is covered by NAD^+-glycohydrolases (NAD^+-ase) and includes two enzymes: SARM1 and CD38 [Covarrubias et al. 2021].

While SARM1 NAD^+-ase activity has just been recently discovered, tons of literature have been published on CD38 (see below), that seems to be the most active and widely expressed enzyme in this category [Covarrubias et al. 2021].

1.6 ADP-ribosyl cyclase/cyclic ADP-ribose hydrolase (CD38)

CD38 is a transmembrane multifunctional enzyme that is largely expressed by several cell types. The list of enzymatic activities in the repertoire of CD38 is long. The main activity is represented by the production of adenosine diphosphate ribose (ADPR) and cyclic adenosine diphosphate ribose (cADPR), by cleaving NAM from a NAD^+ molecule, and the hydrolysis of cADPR to ADPR. It has recently been reported that CD38 can also carry-out the 2'-deoxy-NAD^+ conversion to 2'-deoxy-ADPR (2dADPR) [Fliegert et al. 2017].

Another activity in the list is a base exchange reaction converting NAD^+ to (ADPR)2, by adding an ADPR moiety [De Flora et al. 1997] and the synthesis of three adenylic dinucleotides (diadenosine diphosphate and two isomers thereof) from cADPR and adenine [Basile et al. 2005].

In addition, it has been proposed that CD38 is able to perform a base-exchange reaction, starting from $NADP^+$ and using NA as the second substrate, that produce nicotinic acid adenine dinucleotide phosphate (NAADP). A further mechanism proposed, starts from 2'-phospho-cADPR and NA [Moreschi et al. 2006]. Anyhow, the conditions needed to obtain NAADP via CD38 are peculiar: in the first case, a very low pH is needed, while the second reaction consumes substrates that during physiological conditions are very low in cells [Guse et al. 2018, Leckie et al. 1998, Podestà et al. 2003, Franco et al. 2001]. Anyway, most of the CD38-derived enzymatic products act as Ca^{2+} mobilizers, and their role has been investigated in different cell lines [Howard et al. 1993, Guse et al. 2005, Malavasi et al. 2008]. CD38 inhibition has been largely considered as a promising approach to treat several pathological conditions, including, but not limited to allergic airway disease [Deshpande et al. 2017], cardiovascular diseases [Zuo et al. 2020], vascular thrombosis, disordered inflammation, and aberrant immune reactivity [Deaglio et al. 2011]. Anyway, the hematological malignancies represent the class of disorders in which CD38 pharmacological inhibition has been better studied. In this specific field of application, different anti-CD38 monoclonal antibodies have been developed and are currently in use or in clinical trials, especially in multiple myeloma [Van de Donk et al. 2018, Morandi et al. 2019]. Not all of the antibodies are inhibiting the enzymatic activity of CD38, and they trigger cell cytotoxicity with different mechanisms. In chronic lymphoid leukemia the block of the CD38-mediated signaling cascade has been demonstrated to represent a possible therapeutic strategy [Vaisitti et al. 2015]. Overall, the role of CD38 in hematological malignancies has been extensively studied, whereas the impact of targeting CD38 within solid tumors is less known.

Studies aimed at characterizing the infiltrating immune cell types expressing CD38 and identifying the most promising CD38 inhibitors/antibodies to use, are urgently needed [Konen et al. 2019]. For the aspects related to the potential CD38 targeting in cancer therapy, out of the scope of my thesis, I refer to the recently published review by Morandi et al. [Morandi et al. 2019].

On the other side, the fact that CD38 represents the major NAD^+ degrading activity, explains why the inhibition of this enzyme is also considered one of the most promising targets for the treatment of age-related disorders, when NAD^+ declines, leading to organ dysfunction [Hogan et al. 2019].

1.7 NAD^+ decline and pathological conditions

NAD^+ levels decrease during aging, obesity and obesity-related cardiometabolic diseases, in different tissues/organs, including liver and white adipose tissue [Yoshino et al. 2011, Kendrick et al. 2011, Braidy et al. 2011, Escande et al. 2013]. Thus, several strategies have been proposed aiming to boost intracellular NAD^+ and thereby to promote healthy aging and extend life span [Raiman et al. 2018, Chini et al. 2018]. Increasing intracellular NAD^+ levels by the systemic administration of NAD^+ biosynthetic precursors, such as nicotinamide riboside (NR) and nicotinamide mononucleotide (NMN) is one of the most promising approaches that has been extensively investigated in several pre-clinical studies and in human clinical trials [Radenkovix et al. 2020, Yoshino et al. 2021].

Recently, dihydronicotinamide riboside (NRH) has been demonstrated to be a natural precursor for the synthesis of NAD^+, via an NRH salvage pathway involving the enzyme adenosine kinase [Yang et al. 2020]. In addition, a reduced form of NMN (NMNH) was also identified as a new NAD^+ precursor, more efficient than NMN or NR at increasing intracellular NAD^+ concentrations in many organs and tissues: NMNH administration in mice determined the rise of NAD^+ levels in liver, kidney, muscle, brain, BAT, and heart, but not in WAT [Zapata-Pérez et al. 2021].

1.7.1 CD38 and adipose tissue

As mentioned above, a NAD^+ decrement occurs as a result of pathological dysfunctions, such as obesity- and age-related disorders. During the last decade, different studies investigated the mechanism guiding to this phenomenon in adipose tissue, from alternative points of views.

Interestingly, it has been observed that NAMPT expression and activity is impaired in obese mice, leading to lower NAD^+ levels in the tissue [Yoshino et al. 2011]. On the other side, NAD^+ degradation seems to contribute at reducing NAD^+ and thus, to exasperate the dysfunction. Indeed, CD38 expression rises in WAT of obese mice [Wang et al. 2018]. Moreover, a few studies reported the role of senescent cells in age-associated low-grade inflammation of adipose tissue. These cells mediate the secretion of factor influencing the environment. As a matter of fact, senescent cells secreted factors induce M1 polarization and a consequent CD38 overexpression in macrophages, resulting in a tissue inflammation [Covarrubias et al 2020, Chini et al. 2020]. Thus, blocking NAD^+ consumption by CD38 inhibition represents a strategy to boost NAD^+ levels. Several studies reported that CD38 knock out mice are protected against high-fat diet (HFD)-induced obesity, hyperglycemia and hyperinsulinemia, as a consequence of enhanced energy expenditure [Barbosa et al. 2007]. The pharmacological inhibition of CD38 recreates the effects observed by genetic deletion and improves several physiological and metabolic parameters. Specifically, administration of apigenin, a CD38 inhibitor, to obese mice increases NAD^+ levels and improves glucose and lipid homeostasis [Escande et al. 2013] and a new a potent CD38 inhibitor, 78c, improves several physiological and metabolic parameters, including glucose tolerance [Tarragò et al. 2018]. The beneficial outcomes of CD38 absence or inhibition seem to be a consequence of enhanced energy expenditure, and this effect is mediated at least in part via a NAD^+-dependent activation of SIRT-Peroxisome proliferator-activated receptor-γ coactivator-1α (PGC1α) axis, involved in the regulation of mitochondrial biogenesis and energy homeostasis [Barbosa et al. 2007].

1.7.2 CD38 and liver

Liver is another example of those tissues in which NAD^+ levels are affected by pathological dysfunction. Being the main metabolism-regulating center, its function is pivotal for the whole organism. Thus, impairment in NAD^+ levels in liver, may lead to severe dysfunction. During aging and overfeeding, NAD^+ levels decline as a consequence of a reduced synthesis and or a promoted overexpression. As happens in WAT, NAMPT is downregulated in liver of mice fed with HFD [Yoshino et al. 2011], leading to low NAD^+ levels in the organ [Kendrik et al. 2011]. Furthermore, senescent cells-derived factors induce a pro-inflammatory commitment in immune cells, leading to CD38 overexpression and NAD^+ reduction [Chini et al. 2020]. Another hepatic disorder is non-

alcoholic fatty liver disease (NAFLD) and is very common in western countries. NAFLD is characterized by fat accumulation in the liver, during the early phases, which results in liver cirrhosis [Bertolotti et al. 2014]. This pathological condition increases risk of T2D, cardiovascular and cardiac diseases, and chronic kidney disease [Mu et al. 2011, Byrne et al. 2015]. A few studies unveiled a link between CD38 and liver-associated disorders. Hepatic stellate cells are responsible for extracellular matrix proteins production upon activation, promoting hepatic fibrosis [Kim et al. 2010]. In this context, CD38 plays a role in promoting the activation of these cells by producing Ca^{2+}-mobilizing molecules. Furthermore, NAD^+ precursor administration contrasted the development of liver fibrosis in a mouse model fed with fat diet [Pharm et al. 2019].

Moreover, it has been reported that CD38 absence protects from NAFLD and hepatic steatosis induced by HFD. This protective phenotype is likely due to SIRTs activation [Xie et al. 2021]. These findings indicate that the detrimental role of CD38 in liver during these processes, is also associated to its NAD^+-consuming activity.

Being CD38 so important in pathological conditions in liver, further investigations are required to better understand its role in this tissue during thermogenesis.

1.8 TRPM2

The Transient Receptor Potential Melastatin 2 (TRPM2) is an ion channel that mediates Ca^{2+} influx, from the extracellular space towards the cytosol, and is gated by a few physiological agonists. The main agonist discovered so far is ADPR, and it has been reported to exhibit an EC_{50} value ranging within the low μM [Beck et al. 2006]. However, other ADPR-related endogenous molecules have been observed to evoke TRPM2 activation. A recent study identified the 2'-deoxyadenosine 5'-diphosphoribose (2dADPR) as an endogenous TRPM2 superagonist. 2dADPR is generated through two enzymatic steps: in the first one, NMN and 2'-deoxy-ATP are utilized by cytoplasmic NMNAT to generate 2'-deoxy-NAD^+, which is converted to 2dADPR by CD38 in the second step. In addition, by 2dADPR, is possible to get TRPM2 activated without NAD^+ consumption [Fliegert et al. 2017]. Hydrogen peroxide (H_2O_2) is another TRPM2 activator. However, it is still not well known whether TRPM2 activation by H_2O_2 is direct or indirect. Although TRPM2 Ca^{2+} influx is triggered upon H_2O_2 stimulation in a concentration-dependent manner, some studies proposed a direct interaction between H_2O_2 and TRPM2, but other groups

did not confirm this conclusion [Ishii et al. 2006, Wehage et al. 2002, Kuhn et al. 2004]. In addition, H_2O_2 is able to evoke 2dADPR rise in Jurkat T cell line, inducing a TRPM2-mediated calcium response [Fliegert et al. 2017]. Beside these three agonists, other molecules have been discovered to act as TRPM2 activators: cADPR and NAADP. NAADP and cADPR display only a weak (and controversial) effect on TRPM2. These two molecules can synergize with ADPR, but a direct effect on the channel have been proposed [Beck et al. 2006].

In the context of adipose tissue metabolism and thermogenesis, TRPM2 has not been studied that much. Only a few articles have been published so far and none of them is focused on the browning of WAT or the activation of BAT. TRPM2 was found be essential in insulin release from pancreatic β-cells. Insulin release requires intracellular calcium increase, that involves ATP-sensitive K^+ channels and TRPM2. Thus, pancreas lacking TRPM2 expression, is not able to release insulin into the bloodstream, causing hyperglycemia and T2D [Kunitoshi et al. 2014]. Conversely, other studies investigated the positive effects of TRPM2 deletion in the context of metabolism. They reported that *Trpm2*$^{-/-}$ mice displayed a higher glucose metabolism in peripheral tissues, and a higher insulin sensitivity. In addition, mice lacking TRPM2 displayed high protection to diet induced obesity, that was correlated with a higher energy expenditure of these mice and a lower AT inflammation [Zhang et al. 2012]. The pharmacological inhibition of TRPM2 was shown to improve insulin sensitivity in AT during Ang II-induced hypertension, suggesting that targeting TRPM2 may be a novel therapeutic strategy to treat hypertension-associated insulin resistance [Gao et al. 2018].

However, the role played by TRPM2 in adipogenesis and thermogenic response has not been established yet; nevertheless, TRPM2 expression in both BAT and WAT has been documented [Sun et al. 2017]. More data on browning are available regarding the involvement of another member of the TRP channels, TRPM8, expressed by WAT and BAT and representing the cold-sensing receptor in these cells, whose activation induces a rise in the intracellular Ca^{2+} concentration ($[Ca^{2+}]_i$) and UCP1 expression [Fonfria et al. 2006].

Thus, from the literature, TRPM2 can likely play distinct roles, both by regulating the endocrine system and metabolism in peripheral tissues. That is what makes TRPM2 an interesting target that could be pivotal during thermogenesis.

1.9 Aims of this study

This study aims to evaluate possible functions for the CD38-TRPM2 axis during cold-induced BAT activation and WAT browining. In addition, part of the project was focused on CD38 role in liver upon cold exposure.

Overall, the present thesis is composed by three parts:

- role of CD38 in BAT activation and WAT browning;

-role of CD38 in liver during cold-exposure;

-role of TRPM2 in BAT activation and WAT browning.

Understanding the mechanisms underlying WAT browning and BAT activation is a key research area for its implication in the possibility of finding new strategies against obesity and dysmetabolic conditions.

2. Material and methods

2.1 In vivo experiments

All *in vivo* experiments were conducted in the laboratory of Prof Jörg Heeren (University Medical Center Hamburg-Eppendorf, Hamburg, Germany), key collaborator of this project. All *in vivo* experiments were conducted in accordance with the laws and institutional guidelines for animal care and were performed with permission of the Animal Welfare Officers at University Medical Center Hamburg-Eppendorf. Mice were housed in temperature- and light-controlled conditions (12-h light cycle) with food and water ad libitum. *Cd38*$^{-/-}$ and *Trpm2*$^{-/-}$ mice were kindly provided by Prof Hans-Willi Mittrücker (University Medical Center Hamburg-Eppendorf). Three months old wild type (WT), *Cd38*$^{-/-}$ and *Trpm2*$^{-/-}$ mice were used for this study (7‑8 animals/group). Three groups (the two knockout mice and WT mice, used as control) were kept for 7 days at 30°C; the other animals were kept at 22°C and three groups were kept for the last 24 h at 6°C. Mice were fasted during the last 4 h before the end of the experiments. Mice were euthanized and interscapular BAT (iBAT) was collected and immediately processed for FACS analysis (see below) or collected, together with inguinal WAT (iWAT) and liver and flash frozen in liquid nitrogen for future investigations. Blood was also collected, centrifuged and plasma was frozen.

2.2 Indirect calorimetry and body temperature measurements

Indirect calorimetric measurements were performed using a Promethion Sable System. WT and *Trpm2*$^{-/-}$ mice were transferred to the measurement chamber in new cages without additional nesting material one day before the measurements started. During the experiments, mice were maintained at a 12-h light–dark rhythm with free access to a standard chow diet and water. Oxygen and carbon dioxide levels in each cage were measured every 15 minutes (min). The respiratory exchange ratio (RER) was calculated as the ratio of carbon dioxide produced (CO_2) to oxygen consumed (O_2). Energy expenditure (EE) was calculated using a modified Weir equation [Weir et al. 1949]. For gradual cold exposure studies, mice were acclimated at 30°C and gradually exposed to 5°C, for 6 days starting at 7:00 am. At the end of the experiment, mice were

acclimated at 30°C for 24 h and then injected with CL 316,243 (1 mg/kg body weight) to induce thermogenesis with a different stimulus.

2.3 Measurement of NAD(P)(H) content

NAD(P)(H) levels were evaluated in iWAT, iBAT and liver from WT and *Cd38*$^{-/-}$ mice. Nucleotides were extracted from the organs. Before their disruption with 0.6 M $HClO_4$ (PCA) or 0.1 M NaOH, samples were weighed to normalize nucleotide content. All the samples were subjected to sonication to homogenize them, followed by centrifugation at 15000xg for 10 min to pellet the insoluble fraction. Samples in PCA were neutralized by diluting the extracts in 100 mM sodium phosphate buffer (pH 8) and utilized to determine NAD^+ and $NADP^+$ content; samples in NaOH were warmed at 72°C for 10 min and were neutralized in 10 mM Tris-HCl, pH 6, and used for NADH and NADPH determination. NAD(H) content was assessed with an enzyme cyclic assay. The diluted samples were analyzed in a 96-multiwell plate by adding an equal volume of the enzymatic reaction mix [containing 2% (v/v) ethanol, 100 µg/ml Alcohol dehydrogenase, 20 µM resazurin, 5 µg/ml Diaphorase, 10 µM FMN, 10 mM NAM and 100 mM sodium phosphate, pH 8.0] to each well [Bruzzone et al. 2003]. NADP(H) were measured utilizing the same protocol, that exploits an alternative mix as the only difference from the previous one [10 mM Glucose-6 phosphate (G6P), 0.02U/ml G6PD, 20 µM resazurin, 5 µg/ml Diaphorase, 10 µM FMN, 10 mM NAM and 100 mM sodium phosphate, pH 8.0] in each well [Sociali et al. 2019]. Incubation of samples and the respectively mix leads to resazurin reduction to resorufin, its fluorescent product (544 nm excitation, 590 nm emission). The increase in resorufin-derived fluorescence was measured every minute over a time of 12 h, using a plate reader (Fluostar Optima, BMG Labtechnologies GmbH, Offenburg, Germany). To confirm the results obtained with the cycling assays, representative samples for each condition were also subjected to an HPLC analysis. The eluates from each analysis were collected in 1-min fractions and subjected to the cycling assays. In parallel, 100 pmol of standard NAD^+, NADH, $NADP^+$ or NADPH were exogenously added to the samples, analyzed, collected and subjected to the cycling assay, to determine the elution time and to calculate the % recovery, used in the calculation.

2.4 Glucose-6 Phosphate content

Livers from WT and *Cd38*$^{-/-}$ mice were weighed and then disrupted in 0.6 M PCA. After a brief sonication to better homogenize them, samples were centrifugated at 15000xg for 10 min at 4°C to obtain the soluble fraction. G6P content was evaluated by an enzymatic cycling assay [0.2 mM $NADP^+$, 0.02 U/ml G6PD, 20 µM resazurin, 5 µg/ml Diaphorase, 10 µM FMN, 10 mM NAM and 100 mM sodium phosphate, pH 8.0], in which sample-contained G6P is utilized by G6PD, producing NADPH. NADPH is subsequently oxidized to $NADP^+$ by Diaphorase, converting resazurin to resorufin, a fluorescent molecule. Resorufin-derived fluorescence was measured in a microplate reader (Fluostar Optima, BMG Labtechnologies GmbH, Offenburg, Germany) as in NADP(H) evaluation assay, see above.

Background was detracted from each respective sample, by measuring fluorescence from samples in which a modified mix was added [0.02 U/ml G6PD, 20 µM resazurin, 5 µg/ml Diaphorase, 10 µM FMN, 10 mM NAM and 100 mM sodium phosphate, pH 8.0]. A standard curve of G6P (ranging from 250 to 0.4 µM) was run in parallel.

2.5 Enzymatic assays

The collected organs were cut in small pieces and homogenized by sonication in lysis buffer (0.1 M Na_2HPO_4/NaH_2PO_4, pH 7.4), in the presence of protease inhibitors, and the lysate protein content was determined by the Bradford method. All assays of the different enzymatic activities were carried out using 25-50 µg protein of each lysate.

2.5.1 CD38 activities (ADP-ribosyl cyclase, GDP-ribosyl cyclase and NAD^+-ase activities)

ADP-ribosyl cyclase and NAD^+-ase activities were estimated by adding 0.4 mM NAD^+ as substrate to the incubation mixture (20 mM Tris-HCl, pH 7, 200 µl). Aliquots of the incubations were withdrawn at 0, 3 and 10 min: cADPR and ADPR content were evaluated using a cycling enzymatic assay [Bruzzone et al. 2003] and HPLC analysis [Grozio et al. 2013], respectively. Guanosine diphosphate (GDP)-ribosyl cyclase activity was measured by a fluorimetric assay, adding 0.02 mM nicotinamide guanine dinucleotide (NGD^+) to 20 mM Tris-HCl, pH 7, containing 25 µg lysate

proteins. NGD^+ is a NAD^+ analogue used to determine cyclase activity since the fluorescent product cyclic GDP-ribose (cGDPR) is not a substrate of the hydrolase activity [Graeff et al. 1994].

2.5.2 NAD^+ synthesis

NAD^+ synthesis starting from NAM, PRPP and ATP was evaluated as in [Zoppoli et al. 2010]. Briefly, the different lysates were added to 100 µl reaction mix (3 mM ATP, 5 mM $MgCl_2$, 0.5 mM PRPP, 2.5 mM NAM, 50 mM Tris-HCl, pH 7.4) and incubated at 37°C. Aliquots were withdrawn at 0, 45 and 90 min and the reaction was stopped by addition of PCA (0.6 M final concentration). NAD^+ content was measured by enzymatic cycling assay as described above.

2.5.3 NMNAT activity

NMNAT activity was evaluated by incubating each lysate in the presence of 0.5 mM NMN, 3 mM ATP, 5 mM $MgCl_2$, 50 mM Tris-HCl, pH 7.4. Aliquots were withdrawn at 0, 30 and 60 min. PCA (0.6 M final concentration) was added and NAD^+ content was evaluated by the enzymatic cycling assay [Bruzzone et al. 2003].

2.5.4 NAD^+ kinase activity

NAD^+ kinase activity was measured by incubating each lysate in the presence of 1 mM NAD^+, 10 mM ATP, 2 mM NAM, 10 mM $MgCl_2$ in 100 mM Tris-HCl, pH 7.8. Aliquots were withdrawn at 0, 30 and 90 min, the reactions were stopped by adding PCA (0.6 M final concentration) and $NADP^+$ content was evaluated using the cycling assay (see above).

2.5.5 Glucose-6 phosphate dehydrogenase activity

Approximately 20 mg of each organ was lysed in ice-cold buffer [25 mM Tris-HCl (pH 7.4), 1 mM EDTA, and protease inhibitors] by brief sonication. The lysates were centrifuged at 10,000xg for 10 min at 4°C and supernatants were collected. G6PD activity was measured on 25 µg protein of

each supernatant by measuring the reduction of $NADP^+$ in the reaction buffer [100 mM Tris-HCl (pH 7.4), 0.5 mM EDTA, 10 mM $MgCl_2$, 0.2 mM $NADP^+$, and 0.6 mM G6P] at 25°C as in [Sociali et al. 2019].

2.5.6 Glucose-6 phosphate phosphatase

Glucose-6 phosphate phosphatase (G6Pase) activity was evaluated by incubating each lysate with 5 mM G6P, in 100 mM Tris-HCl (pH 7.4), with 10 mM $MgCl_2$. G6P content was then measured in aliquots collected after 10 and 20 minutes, using the enzymatic cycling assay (see above).

2.5.7 LDH activity

LDH activity was measured using 50 or 25 ug proteins of each lysate by incubating them in the presence of L-(+)-Lactate (10 mM) and NAD^+ (3 mM) in Tris-HCl (40 mM final concentration, pH 8). The activity was measured following the reduction of NAD^+ to NADH, as detected by a fluorescence microplate reader (Em: 460 nm, and Ex: 350 nm, FLUOstar OPTIMA, BMG LabTech), at 25°C.

2.6 eNAMPT determination in plasma

eNAMPT levels were evaluated with a commercial ELISA kit (Adipogen AG, Liestal Switzerland).

2.7 Western blot analysis

iBAT, iWAT and liver were lysed in RIPA buffer (1 ml buffer/100 mg organ), with the addition of 0.1% SDS, protease inhibitor (Complete mini, EDTA-Free, Roche) and phosphatase inhibitor (bimake.com) and vanadate (1 mM; Sigma) using a tissue lyser. The homogenates were centrifuged, and the middle phase was collected. Lysates (20 μg proteins) were loaded on a 10% polyacrylamide gel, proteins were separated by SDS-PAGE and transferred to nitrocellulose membranes. Detection was performed with primary antibodies (see below), following incubation with the appropriate HRP-conjugated secondary antibodies and ECL detection (GE Healthcare,

Milan, Italy). Band intensity was quantified with the ChemiDoc imaging system (Bio-Rad, Milan, Italy).

The following primary antibodies were used: anti-CD38 (kindly provided by Prof. Fabio Malavasi, University of Torino, Italy); anti-HSL (Cell Signaling, #4107 Danvers, MA); anti-phospho-HSL (Cell Signaling, #4126 Danvers, MA); anti-Vinculin (Cell Signaling Technology, #4650 Danvers, MA); Anti-SOD2/MnSOD (acetyl K68) antibody (Abcam, ab137037, Boston, MA); anti-SOD2/MnSOD (Abcam, ab13533, Boston, MA); anti-Poly ADP-ribose (Merck Millipore, Clone 10H, AM80, Burlington, MA).

2.8 qPCR analyses

RNA was isolated from tissues using peqGOLD TriFast (Peqlab), by homogenizing tissues with TissueLyser (Qiagen) and purifying RNA by NucleoSpin RNAII Kit (Macherey-Nagel). Afterwards, cDNA was prepared with High-Capacity cDNA Archive Kit (Applied Biosystems). The cDNA was used as template for real-time PCR analysis: reactions were performed in an iQ5 real-time PCR detection system (Bio-Rad) following the experimental conditions described before [Sturla et al. 2009]. PCR primers were designed through Beacon Designer 2.0 Software (Bio-Rad) and are listed in Table 1; specific primers for *Ucp1*, *Pgc-1α* and for mouse housekeeping genes, ubiquitin and *β2-microglobulin*, were described in [Sturla et al. 2017]. Statistical analysis of the qPCR was performed using the iQ5 Optical System Software version 1.0 (Bio-Rad) based on the $2^{-\Delta\Delta}$Ct method [Livak et al. 2001]. The dissociation curve for each amplification was analyzed to confirm absence of unspecific PCR products.

2.9 miRNA analyses

RNA was isolated from BAT using miRNeasy (Qiagen). Total RNA was converted into cDNA with the miScript II RT kit (Qiagen) and subjected to real-time PCR analysis. Quantitative real-time PCR (RT-PCR) was performed in an iQ5 real-time PCR detection system (Bio-Rad) using miScript SYBR Green PCR Kit (Qiagen) in accordance with the manufacturer's protocol. The PCR reaction profile was: one initial activation step at 95°C for 15 min, 40 cycles at 95°C for 15 seconds, 55°C for 30 s and 72°C for 1 min, one step at 95°C for 15 min and the final step at 45°C for 15 min. PCR specific

primers for miR-140-3p, -140-5p, -708, -155 were designed using miRBase database (http://www.mirbase.org) and are listed in Table 1. PCR primer for small nuclear RNA 202 (snoRNA-202), used as internal control, was described in [Matouskova et al. 2014]. Statistical analysis of the qPCR was performed as described before in qPCR analyses.

Table 1 qPCR primers.

Target mouse gene	**Accession number**	**Sequence, 5′ -3′**
Nadk	NM_001159637	Forward 5′ -CCAAGTCTCGGAGCCTGTC-3′
		Reverse 5′ -AAATGTTGTCACTGGGCACG-3′
Nampt	NM_021524	Forward 5′ -AATGTCTCCTTCGGTTCTGGTG-3′
		Reverse 5′ -CCCGCTGGTGTCCTATGTAAAG-3′
Cd38	NM_007646	Forward 5′ -GGTCCTGATCGCCTTGGTAGTAG-3′
		Reverse 5′ -ATCTCCTGGCAGTTCTGATCTCTC-3′
Acaca	NM_133360	Forward 5′ -CACTGTGGCTTCTCCAGCA-3′
		Reverse 5′ -CACCGACGGATAGATCGCAT-3′
Fasn	NM_007988	Forward 5′ -ATGGGTGTGGAAGTTCGTCAG-3′
		Reverse 5′ -AGTGTGCTCAGGTTCAGTTGG-3′
Me1	NM_008615	Forward 5′ -GGACCCGCATCTCAACAAGG-3′
		Reverse 5′ -AGGGCGGCAACAATCCATGA-3′
G6pdx	NM_008062	Forward 5′ -TGATCGAGAAAAGCCCCAGC-3′
		Reverse 5′ -GTGAGGGTTCACCCACTTGT-3′
Gapdh	GU214026	Forward 5′ -CGTGCCGCCTGGAGAAACCTG-3′
		Reverse 5′ -TGGAAGAGTGGGAGTTGCTGTTGAAG-3
Pfk1	NM_001163487	Forward 5′ -AGTTGGTATCTTCACGGGCG-3′

		Reverse 5′ -CATAGACACGCTCTCCCACG-3′
Pdh	NM_008810	Forward 5′ -GATGGAGCTAAAGGCGGATCA-3′
		Reverse 5′ -TCCGTAGGGTTTATGCCAGC-3′
Trpm2	NM_138301	Forward 5′ -CCAATCTCCGACGAAGCAATAGC-3′
		Reverse 5′ -CATATTGGTGTGCGTGTGTGATGG-3′
G6pase	NM_008061	Forward 5′ -AGCCAAGAGATGGTGTGAGC-3′
		Reverse 5′ -TACATGCTGGAGTTGAGGGC-3′
MacroD1	NM_134147	Forward 5′ -TGAGCACCTCCACCGACT-3′
		Reverse 5′ -TGTTCCTCTCTCTGCTTGTCAC-3′
MacroD2	NM_001013802.3	Forward 5′ -AGCTGAAGTCCACAAAGATGAA-3′
		Reverse 5′ -TTGGGAAGTTCTTGGTCACACA-3′
Oard1	NM_001289490	Forward 5′ -TGGAGGCCATGAAGTCCCAT-3′
		Reverse 5′ -CCGATCCAGACCACATCCAA-3′
Adprs	NM_133883	Forward 5′ -TCCTGAGTCACGTCGAGAGC-3′
		Reverse 5′ -TGGCAGTGTCATCTGTGTAGT-3′
Mitochondrial DNA	AP014941	Forward 5′ CCGTCACCCTCCTCAAATTA-3′
		Reverse 5′-GGCTAGGATTAGTTCAGAGTG-3′
β-2 Microglobulin	NM_009735	Forward 5′-CGGTCGCTTCAGTCGTCAG-3′
		Reverse 5′-CAGTTCAGTATGTTCGGCTTCC-3′
Ubiquitin	NM_019639	Forward 5′-GACAGGCAAGACCATCAC-3′
		Reverse 5′-TCTGAGGCGAAGGACTAAG-3′
Tbp	NM_013684	Forward 5′-GAAGCTGCGGTACAATTCCAG-3′
		Reverse 5′-CCCCTTGTACCCTTCACCAAT-3′
miR-140-3p	MI0000165	5′ -TACCACAGGGTAGAACCACGG-3′
miR-140-5p	MI0000165	5′ -CAGTGGTTTTACCCTATGGTAG-3′

miR-708	MI0004692	5′ -AAGGAGCTTACAATCTAGCTGGG-3′
miR-155	MI0000177	5′ -TTAATGCTAATTGTGATAGGGGT-3′

2.10 FACS analysis

Mice were exposed to cold temperature for 24 h (see above), or at 22°C. iBAT was collected, washed in PBS, dried quickly on paper, cut in small pieces and incubated in the digestion buffer [PBS with Collagenase from Clostridium histolyticum 1.5 U/ml (Sigma), Bovine Serum Albumine (BSA) (Sigma) 1 mg/ml and $CaCl_2$ 10 mM, 1 ml/g of adipose tissue] at 37°C for 40 min with constant agitation. Digestion was stopped adding complete medium (DMEM with 10% FBS) and the cell suspension was filtered on a cell strainer (70 μm diameter). Cell suspension was incubated with Peridinin Chlorophyll Protein Complex-cyanin 5.5 (PerCPCy5.5) conjugated anti-mouse CD45.2 antibody (BD Biosciences), with Brilliant Violet (BV) 480 anti-mouse CD38 antibody (BD Biosciences), Syto 16 dye (Thermo Fisher) to select nucleated cells and Fixable Viability Stain 780 (BD Biosciences) to evaluate live cells. After staining procedures, cells were analyzed by a FACSCanto II flow cytometer (BD Biosciences) using FACSDIVA 6.0 software (BD Biosciences).

2.11 Mass spectrometry

BAT and WAT from WT and *Cd38*$^{-/-}$ mice were deproteinized by mincing them in 0.6M PCA. Afterwards, samples were neutralized with 2 M K_2CO_3 until they reached a neutral pH and ADPR quantification was performed by HPLC/MS, using a reversed-phase XBridge C18 column (Waters, 150 × 1 mm, 3 μm). The standards and samples were separated using a mobile phase consisting of water/methanol (95:5, v/v) with 4 mM dibutylamine acetate (eluent A) and water/acetonitrile (25:75, v/v; eluent B). The mobile phase was 0% B initially, which then increased to 80% over 10 min and then to 100% over 5 min. The mobile phase was held at 100% B for 5 min and then re-equilibrated to 0% B and held for 15 min. The flow rate was 30 μl/min. A diverter valve was employed to reduce the introduction of matrix components in the spectrometer. The mass spectra were acquired using electrospray ionization in negative-ion mode in the 100–800 m/z range, and ion charged control with a target ion value of 100,000 and an accumulation time of 300 ms. MS and MS/MS were used for the specific detection of each analyte. The settings of the ESI source were as follows: capillary voltage of 3300 V, nebulizer pressure of 15 psi, drying gas of 8 l/min, dry temperature of 325°C, and 2 rolling averages (averages: 5) were the parameters set

for the MS detection. MS/MS analysis was conducted using an amplitude optimized time by time for each compound [Fu et al. 2019].

2.12 Statistical analyses

Groups were compared by an unpaired Student's t test, or by one way ANOVA followed by Tukey's Test, using GraphPad software. Values of $p < 0.05$ were considered significant.

3. Results

3.1 Decreased CD38 levels lead to NAD(P)(H) saving and boost thermogenesis in white and brown adipose tissues in cold-exposed mice

3.1.1 Thermogenic markers expression is enhanced in *Cd38*$^{-/-}$ mice

To investigate the impact of the genetic ablation of *Cd38* during thermogenesis, RT-PCR analyses were performed on iBAT and on iWAT, harvested from WT and *Cd38*$^{-/-}$ mice kept for one week at 22°C or for 6 days at 22°C and the last day at 6°C: as expected, increased expression of the thermogenic genes *Pgc-1α* and *Ucp1* was observed in both iBAT and iWAT from WT mice exposed to 6°C, compared with those at 22°C (Fig 1A–D).

Of note, *Pgc-1α* mRNA levels were significantly higher in iBAT and iWAT from *Cd38*$^{-/-}$ mice kept at 6°C, compared with WT mice equally exposed to cold (Fig 1A, B). Likewise, *Ucp1* gene upregulated expression was significantly higher in iBAT and iWAT from *Cd38*$^{-/-}$ mice housed at 6°C, compared with corresponding WT mice (Fig 1C, D). In addition, cold exposure increased the levels of the phosphorylated, i.e. activated, hormone-sensitive lipase (p-HSL) form, in BAT from control mice, as detected by Western blot analysis: HSL activation was even more pronounced in BAT from *Cd38*$^{-/-}$ mice (Fig 1F). Body weights of chow-fed mice were similar after cold exposure (Fig 1E).

Altogether, these data indicate that genetic deletion of CD38 increases expression of both the pivotal browning gene *Ucp1* and the master regulator of mitochondrial activity *Pgc-1α.*

Figure 1

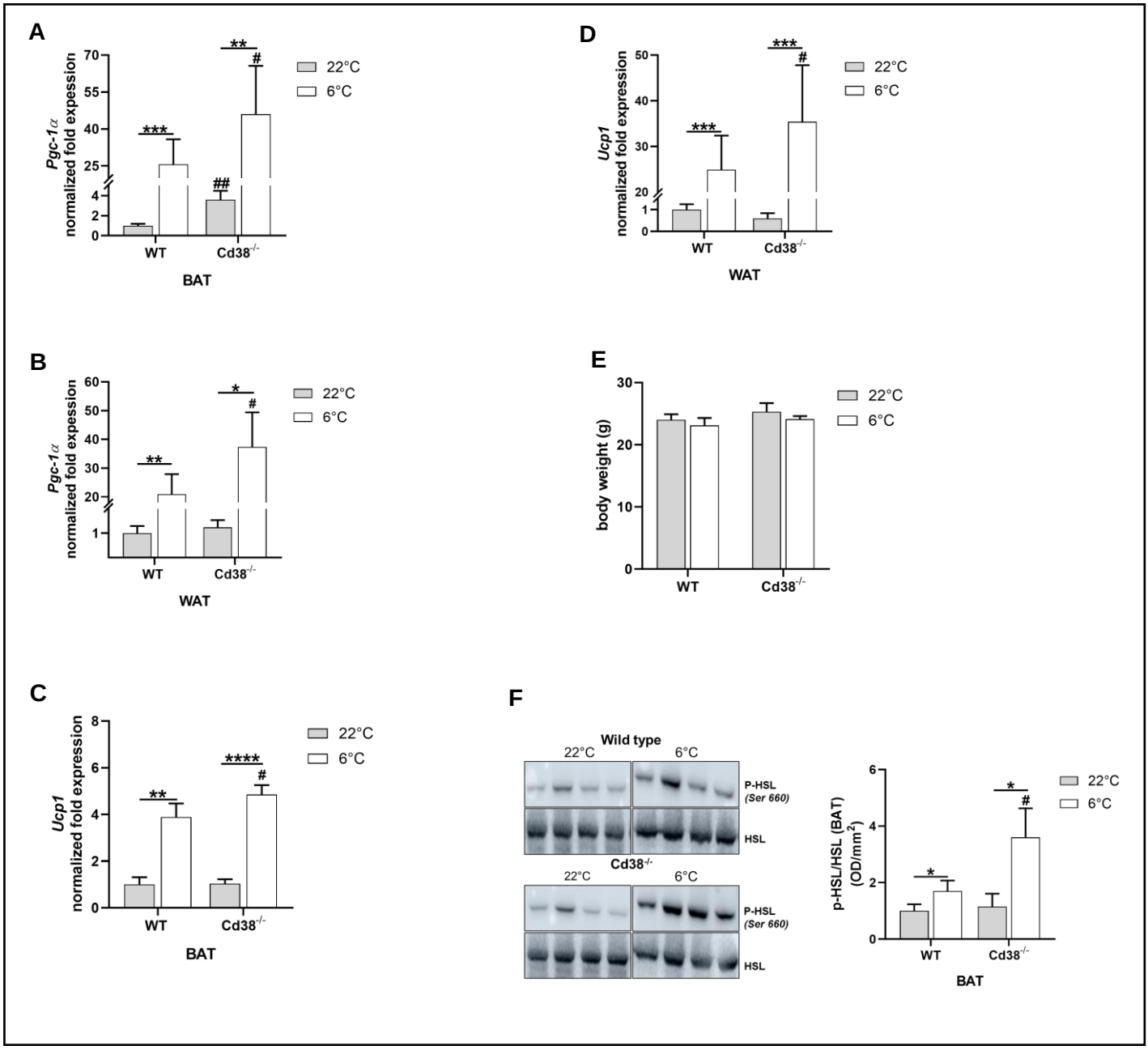

Fig 1 Lack of CD38 enhances cold exposure-induced iBAT activation and iWAT browning.

iBAT and iWAT were collected from WT and *Cd38*$^{-/-}$ mice kept at 22°C for 1 week (22°C), or at 22°C for 6 days and at 6°C for 1 day (6°C). RT-PCR analysis was performed to evaluate mRNA levels of: A, *Pgc-1α* in iBAT; *Pgc-1α* in iWAT (B); *Ucp1* in iBAT (C); *Ucp1* in iWAT (D). Results are mean ± SD of determinations on tissues from different animals (n = 4 for *Pgc-1α* in iWAT; n = 6–7 for all the others). Body weight in the two groups (E). Western blot analyses were performed to compare the phosphorylated form of the hormone-sensitive lipase (P-HSL) and HSL total protein level in BAT (F). Results of quantifications are mean ± SD from n = 4 animals for each condition. Data analyzed by Student's *t* test: *, $p < 0.5$, **, $p < 0.01$, ***, $p < 0.001$, ****, $p < 0.0001$; $^{\#}$, $p < 0.05$, $^{\#\#}$, $p < 0.01$, compared with the corresponding WT.

3.1.2 NAD^+ levels increase in BAT upon cold exposure

Since CD38 is one of the major NAD^+-consuming enzyme, and its absence is associated with increased levels of this dinucleotide [Zocchi et al. 1998, Young et al. 2006], the NAD^+ and NADH content in adipose tissue from mice housed at different temperatures was evaluated, using a cycling assay. In order to confirm results obtained with this assay, a few representative samples were analyzed by HPLC, followed by cycling assay on the collected fractions (as described in Material and methods).

In WT mice, NAD^+ levels, expressed as nmol/g of tissue, appeared to be very high in BAT, compared with WAT: approximately 300 vs 20 nmol/g tissue in BAT and WAT, respectively (Fig 2A, C). In addition, the amount of protein contained in each type of adipose tissue have been measured: 22 ± 8 mg protein/g WAT (n = 42 determinations) and 121 ± 36 mg protein/g BAT (n = 29 determinations). When expressed relative to tissue protein content, NAD^+ levels were closer between BAT and WAT, i.e. 2.5 vs 1.0 nmol/mg protein, respectively.

As expected, NAD^+ levels were significantly higher in both BAT and WAT from *Cd38*$^{-/-}$, compared with WT animals (Fig 2). Specifically, the lack of CD38 increased NAD^+ by approximately 2–2.5 fold in iBAT and by approximately 6 fold in iWAT in animals kept at 30°C or 22°C (Fig 2A, C). Interestingly, a massive increase in NAD^+ levels occurred in BAT from WT animals kept at cold temperature, compared to animals at 22°C or 30°C (Fig 2A). Indeed, the significant difference in NAD^+ levels was lost at 6°C in BAT from WT and *Cd38*$^{-/-}$ mice (Fig 2A). This result suggests that NAD^+ is involved in regulating thermogenesis and energy metabolism in BAT. NADH levels were slightly, although significantly, increased in BAT and WAT from cold-housed mice, compared to controls (Fig 2B). As a consequence, the NAD^+/NADH ratio was significantly higher in BAT from WT animals exposed to cold temperature. Importantly, the fact that both the oxidized and the reduced form of NAD were increased upon cold exposure in BAT, indicates that the total NAD pool (NAD^+ + NADH) is increased. Thus, the change in the oxidized form is not merely due to an accelerated oxidation of the reduced form, which may occur during thermogenesis.

Figure 2

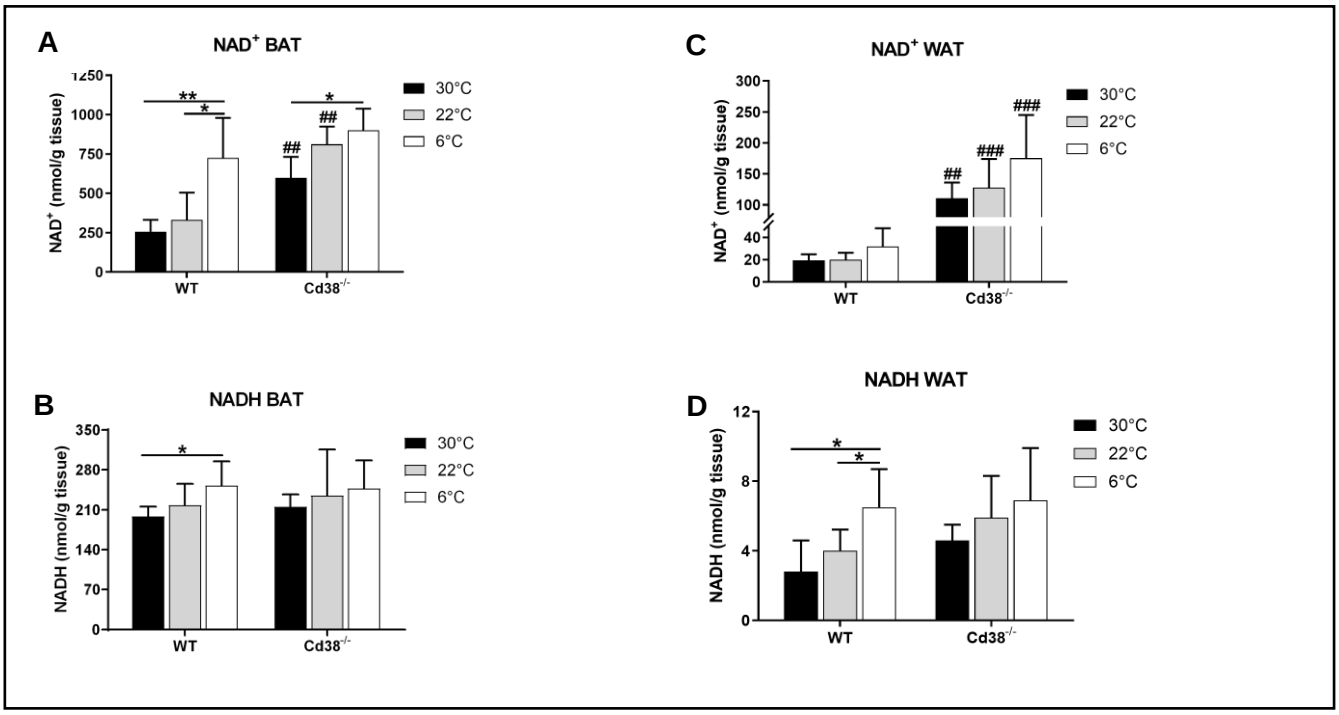

Fig 2 Cold exposure increases NAD$^+$ levels in BAT from WT mice.

Adipose tissues (iBAT and iWAT) were harvested from WT and *Cd38*$^{-/-}$ mice housed at 30°C for 7 days (30°C, black bars), or at 22°C for 7 days (22°C, grey bars), or at 22°C for 6 days and at 6°C for 1 day (6°C, white bars). The collected tissues were chopped in PCA or NaOH and used to evaluate NAD$^+$ or NADH levels, respectively. NAD$^+$ in iBAT (A); NADH in iBAT (B); NAD$^+$ in iWAT (C); NADH in iWAT (D). Results are expressed as nanomoles of the respective dinucleotide forms normalized to tissue weight (g) and represent means ± SD of determinations from 5 to 6 different mice for each condition. Data analyzed by ANOVA with Tukey's test: *, $p < 0.05$, **, $p < 0.01$; data analyzed by Student's t test: ##, $p < 0.01$, ###, $p < 0.001$ compared with the corresponding WT.

In order to identify the molecular mechanism underlying the observed boost in NAD^+ levels in BAT from mice exposed to 6°C, *Nampt* expression was evaluated by RT-PCR. *Nampt* expression was significantly increased, by approximately 2 fold, in both iBAT and in iWAT (Fig 3A, B). Nevertheless, the total NAD^+-synthesizing activity from NAM, measured in homogenates from BAT and WAT obtained from 22°C- and 6°C-exposed mice, was not significantly different (Fig 3C, D), likely as a consequence of the fact that the NMNAT enzymatic activity (from NMN to NAD^+) was not significantly affected by cold exposure (127 ± 55 and 96 ± 59 pmol NAD^+/min/mg protein for 22°C and 6°C, respectively, n = 4). Also, plasma levels of eNAMPT were not significantly different in mice kept at neutral or cold temperature (Fig 3E), likely ruling out the possibility that NAMPT be released from cold-activated BAT and/or WAT. Moreover, the lack of CD38 did not affect eNAMPT levels (Fig 3E).

Figure 3

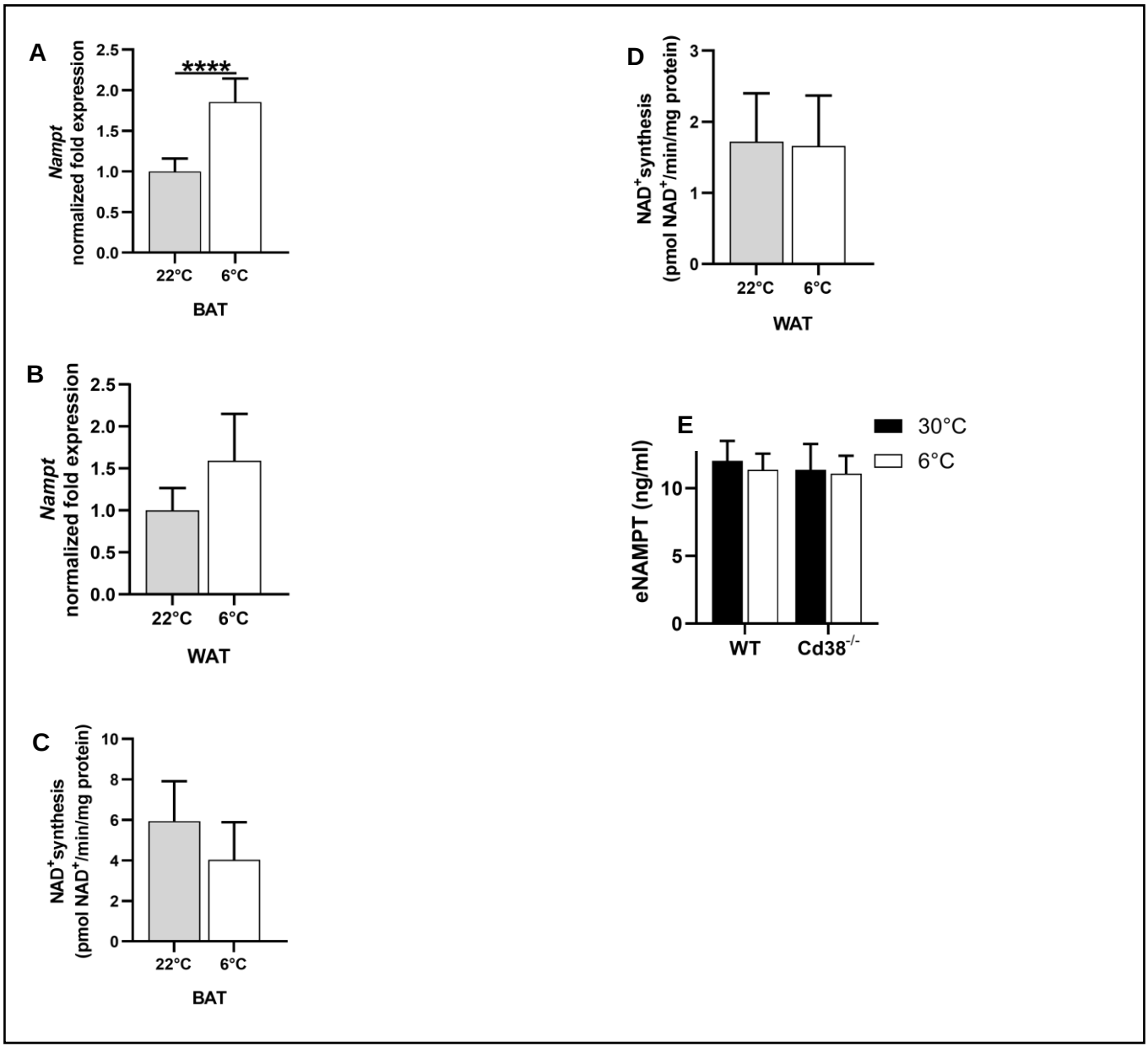

Fig 3 Cold exposure affects *Nampt* mRNA levels, but not NAD^+-synthesizing activity in BAT and in WAT.

iBAT and iWAT were collected from WT mice kept at 22°C for 1 week (22°C), or at 22°C for 6 days and at 6°C for 1 day (6°C). RT-PCR analyses were performed to evaluate *Nampt* mRNA levels in iBAT (A) and iWAT (B). iBAT (C) and iWAT (D) were lysed and NAD^+ synthesis was evaluated by adding NAM, PRPP and ATP as substrates. eNAMPT levels in plasma were evaluated by ELISA (E). All results are means ± SD of results of 4–5 independent determinations for each condition. Data analyzed using Student's t test: ****, $p < 0.0001$.

3.1.3 Cold exposure downregulates CD38 expression in BAT

Being CD38 one of the major NAD^+-consuming enzyme, a change in its expression or activity, could represent a possible explanation for the increased NAD^+ levels observed in iBAT of cold-exposed WT mice.

Indeed, *Cd38* expression was decreased by approximately 45%, as evaluated by RT-PCR (Fig 4A). Western blot analysis confirmed that CD38 expression is significantly reduced (by approximately 50%, Fig 4B). Accordingly, the CD38 enzymatic activities in BAT proved to be decreased by cold exposure; NAD^+-ase, ADP-ribosyl cyclase and GDP-ribosyl cyclase activities were reduced by 82%, 67% and 77%, respectively, in homogenates from BAT obtained from cold-exposed mice, compared with control mice at 22°C (Fig 4C, D, E). Thus, the NAD^+ increase that occurs in BAT from mice kept at 6°C proves to be due to reduced expression of CD38. The fact that the significant difference in NAD^+ levels was lost at 6°C in BAT from WT and *Cd38*$^{-/-}$ mice (Fig 2A) indicates that the spontaneous downregulation of CD38 in WT animals at 6°C, is metabolically equivalent to its genetic ablation. All the three CD38-related activities were undetectable in iBAT from *Cd38*$^{-/-}$ mice (data not shown).

Figure 4

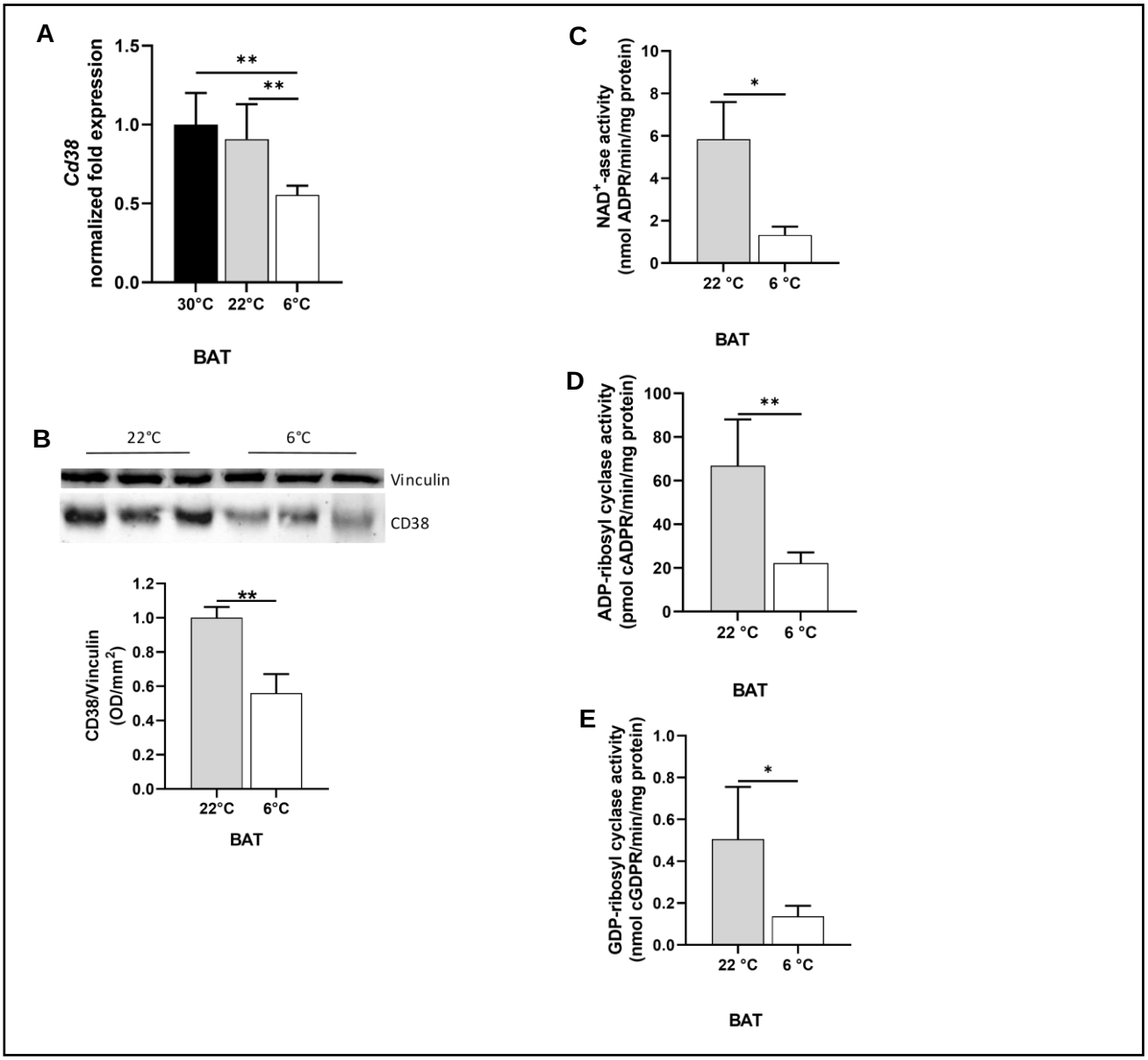

Fig 4 Cold exposure determines downregulation of CD38 expression in iBAT of WT mice.

iBAT was collected from WT mice kept at 22°C for 1 week (22°C), or at 22°C for 6 days and at 6°C for 1 day (6°C). CD38 levels were evaluated at the mRNA level by RT-PCR analysis (A), and at the protein level by Western blot analysis (B). Western blot graph shows values normalized against Vinculin, as housekeeping protein. C–E, CD38-related enzymatic activities were evaluated on iBAT lysates by measuring: ADPR (from NAD^+, C), cADPR (from NAD^+, D) or cGDPR (from NGD^+, E). All results are means ± SD of 4–5 independent determinations for each condition. Data analyzed by ANOVA with Tukey's test (A) or by Student's t test (B–E): *, $p < 0.05$, **, $p < 0.01$.

Next, in order to identify the cell lineage that downregulates CD38 expression, BAT from WT animals exposed to 22°C or 6°C was dissociated and analyzed by flow cytometry. The percentage of BAT-infiltrating $CD45^+$ leukocytes was significantly decreased upon cold exposure (Fig 5A, B), but the frequency of $CD38^+$ cells on $CD45^+$ population was not affected (Fig 5A, C). Interestingly, the percentage of $CD38^+$ in $CD45^-$ cells (i.e. adipocytes) was significantly decreased (Fig 5D) and a distinctive change of CD38 was observed, when adipocytes were stratified in CD38bright, CD38dim and $CD38^-$ subsets (Fig 5E). Specifically, the % of CD38bright cells was decreased, and the % of $CD38^-$ cells was increased upon cold exposure (Fig 5E). Thus, the decreased level of CD38 in BAT is a consequence of both a decrease in number of infiltrating $CD45^+/CD38^+$ leukocytes, and of a downregulation of CD38 expression in brown adipocytes.

miR-140-3p and miR-708 have been demonstrated to regulate the TNFα-induced CD38 expression in human airway smooth muscle cells [Jude et al. 2012, Dileepan M 2014]. Moreover, target prediction algorithms have identified other binding sites for two additional miRNAs (miR-155 and miR-499-5p) in *Cd38* 3' UTR [Deshpande et al. 2017]. The levels of miR-155 were evaluated in our samples, since this miRNA has recently been characterized as a regulator of both brown and white adipogenesis [Goody et al. 2019]. Interestingly, the level of miR-140-3p was significantly increased in BAT upon cold exposure (Fig 5F), suggesting that this may represent a possible mechanism for CD38 downregulation. Conversely, levels of miR-708, miR-155 and miR-140-5p, evaluated as control, were not affected by cold exposure (Fig 5F).

Figure 5

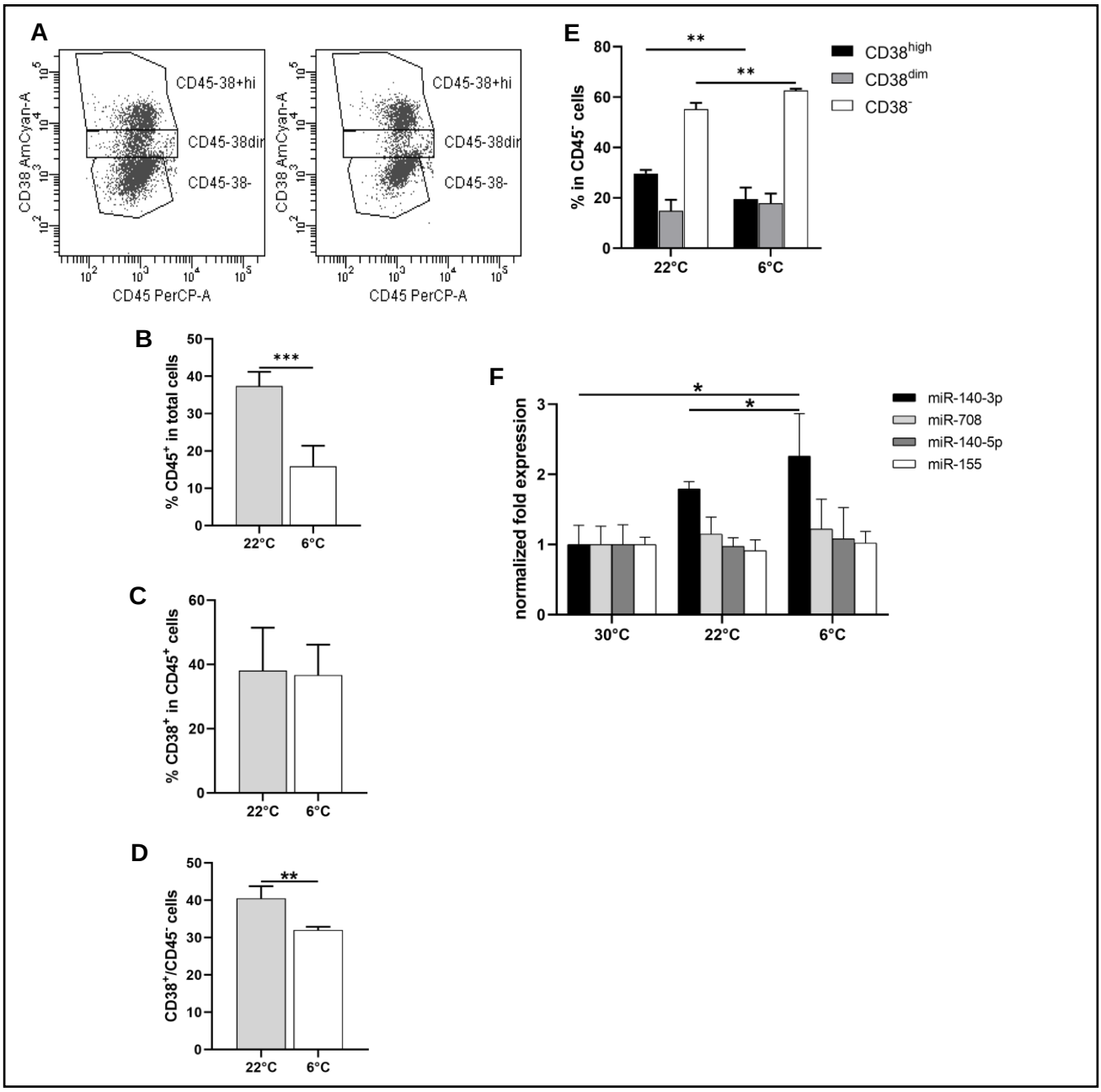

Fig 5 Identification of cells responsible for the cold exposure-related downregulation of CD38 expression in iBAT of WT mice.

iBAT was collected from WT mice kept at 22°C for 1 week (22°C), or at 22°C for 6 days and at 6°C for 1 day (6°C). iBAT was dissociated and FACS analyses were performed on samples stained with antibodies against CD45 and CD38, and with Syto 16 dye and Fixable Viability Stain, to select nucleated cells and live cells, respectively: a representative plot for each condition is shown (A); % $CD45^+$ cells in total cells (B); % $CD38^+$ cells in $CD45^+$ cells (C); % $CD38^+$ cells in $CD45^-$ cells (D); % cells expressing CD38 at different levels ($CD38^{bright}$, high expression; $CD38^{dim}$, low expression; $CD38^-$, no expression), within $CD45^-$ cells (E). Levels of miRNA 140-3p, 708, 140-5p, 155 in iBAT (F). Results are means ± SD of 4–5 independent determinations for each condition. Data by analyzed by Student's t test (B–E) or by ANOVA with Tukey's test (F): *, $p < 0.05$, **, $p < 0.01$, ***, $p < 0.001$.

3.1.4 NADP(H) levels increase in WAT upon cold exposure

In WAT, as in BAT, cold exposure determined a significant decrease in CD38 expression, as measured by RT-PCR analyses (by approximately 50%, Fig 6A), Western blot analysis (by approximately 55%, Fig 6B) and NAD^+-ase activity (by 85%, Fig 6C). The CD38 protein and NAD^+-ase activity were undetectable in iWAT from *Cd38*$^{-/-}$ mice (data not shown). Nevertheless, the decrease in CD38 expression translated in only a slight (not statistically significant) increase in NAD^+ levels in WAT from mice exposed to cold temperature (Fig 2C).

Figure 6

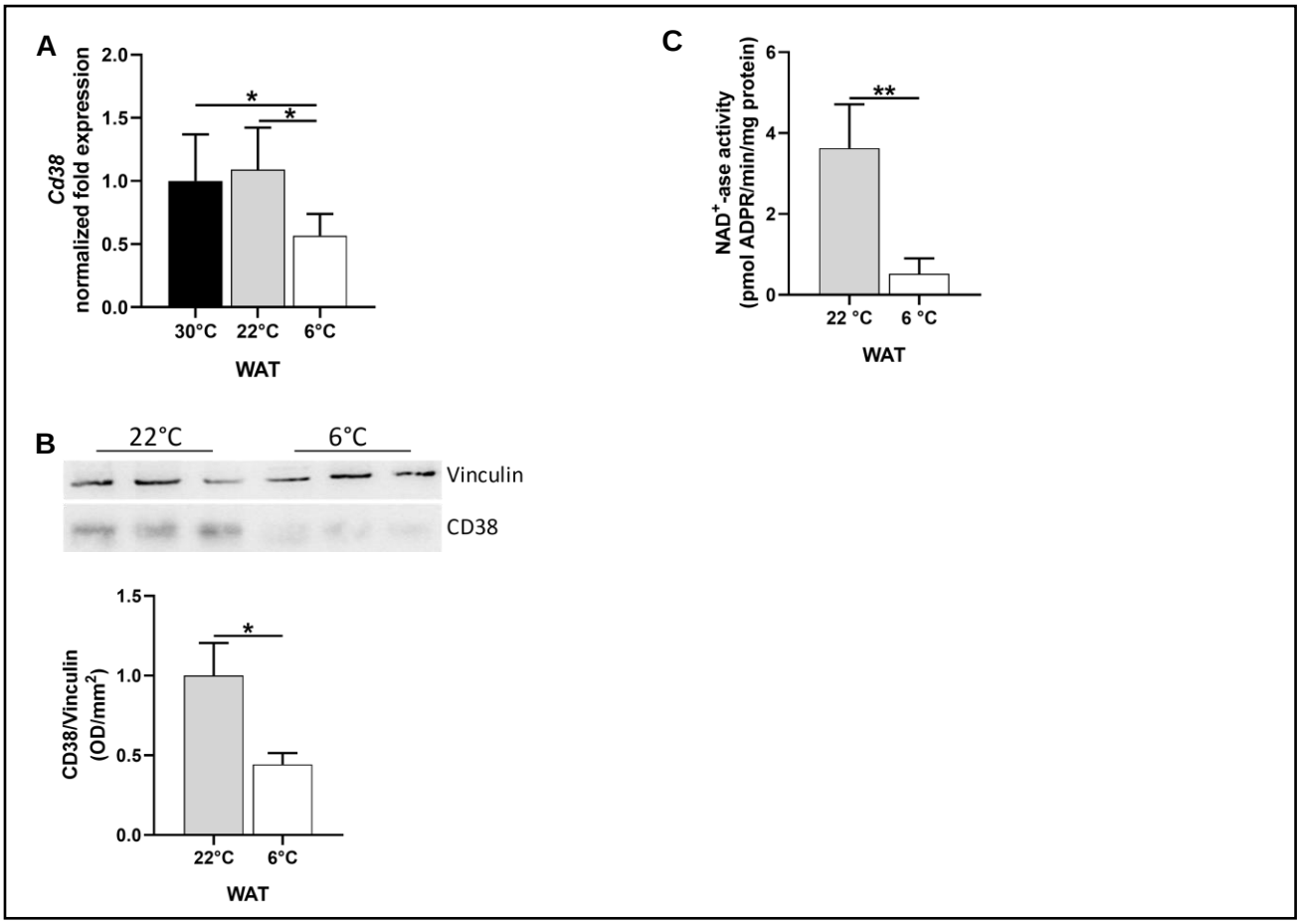

Fig 6 Cold exposure determines downregulation of CD38 expression in iWAT from WT mice.

iWAT was collected from WT mice kept at 22°C for 1 week (22°C), or at 22°C for 6 days and at 6°C for 1 day (6°C). CD38 levels were evaluated at the mRNA level by RT-PCR analysis (A), and at the protein level by Western blot analysis (B). Western blot graph shows values normalized against Vinculin, as housekeeping protein. NAD^+-ase enzymatic activity was evaluated on iWAT lysates by measuring ADPR production from NAD^+ (C). All results are means ± SD of 4–5 independent determinations for each condition. Data analyzed by ANOVA with Tukey's test (A) or by Student's t test (B–C): *, $p < 0.05$, **, $p < 0.01$.

Hence, the levels of the phosphorylated dinucleotide forms $NADP^+$ and NADPH were also evaluated in adipose tissue of mice exposed to different temperatures. In iBAT, the lack of CD38 was mirrored by a slight increase in $NADP^+$ (by approximately 1.4 fold, Fig 7A), but not in NADPH (Fig 7B), in mice housed at 30 and 22°C, compared with 6°C. Conversely, in iWAT, the lack of CD38 was accompanied by a marked increase, by approximately 3 and 2 fold, in $NADP^+$ and NADPH, respectively, in mice housed at 30 and 22C° compared to animals kept at 6°C (Fig 7C, D).

Figure 7

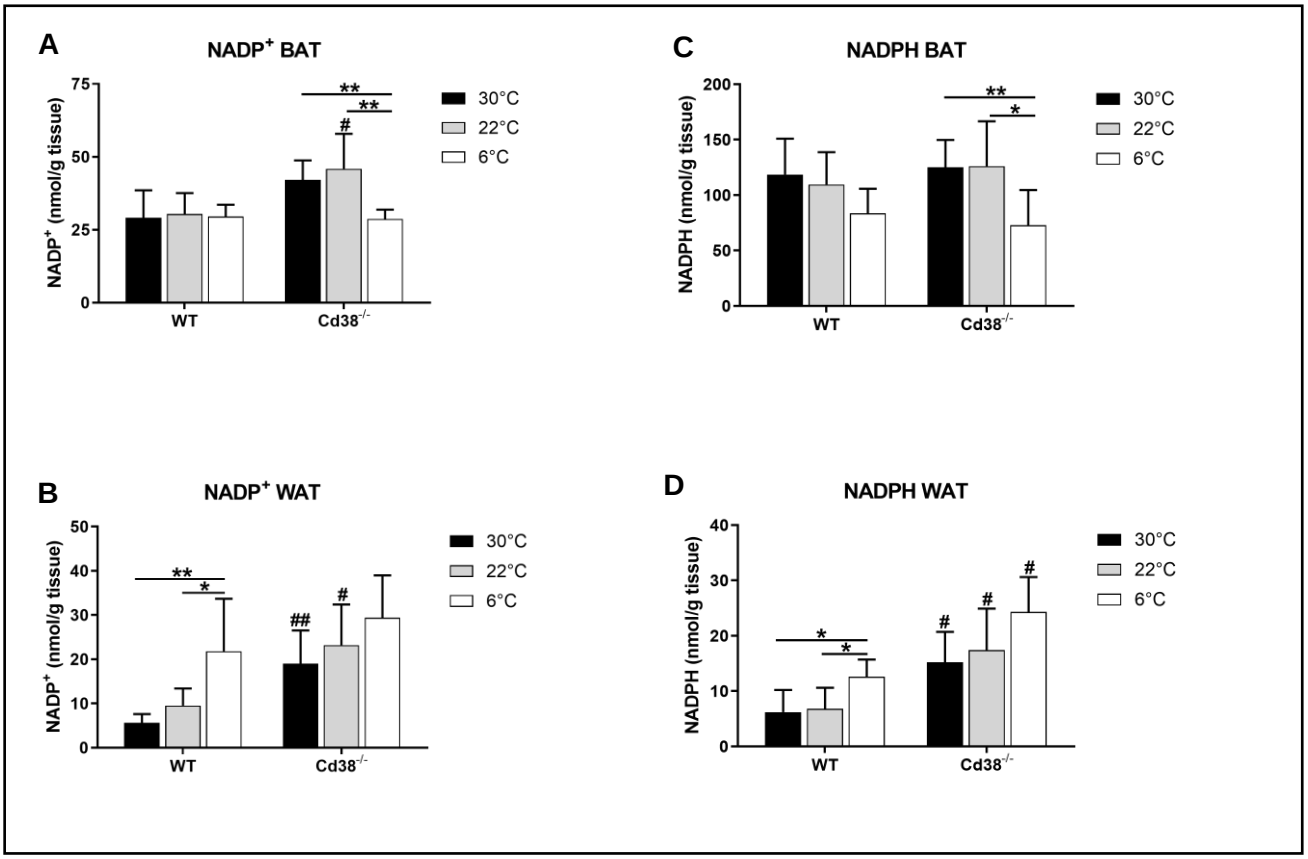

Fig 7 Cold exposure increases NADP$^+$ and NADPH levels in iWAT from WT animals.

Adipose tissues (iBAT and iWAT) were harvested from WT and *Cd38*$^{-/-}$ mice housed at 30°C for 7 days (30°C, black bars), or at 22°C for 7 days (22°C, grey bars), or at 22°C for 6 days and at 6°C for 1 day (6°C, white bars). The collected tissues were chopped in PCA or NaOH and used to evaluate NADP$^+$ or NADPH levels, respectively. NADP$^+$ in iBAT (A); NADPH in iBAT (B); NADP$^+$ in iWAT (C); NADPH in iWAT (D). Results are expressed as nanomoles of the respective dinucleotide normalized to tissue weight (g) and represent means ± SD of determinations from 5 to 6 different mice for each condition. Data analyzed by ANOVA with Tukey's test: *, $p < 0.05$, **, $p < 0.01$; data analyzed by Student's t test: #, $p < 0.05$, ##, $p < 0.01$ compared with the corresponding WT.

No increase whatsoever in $NADP^+$ levels was observed in iBAT from WT mice at cold temperature (Fig 7A). On the contrary, when WT mice were exposed to cold, a remarkable increase (by approximately 4 fold) in $NADP^+$ levels occurred in iWAT, compared with animals kept at 22°C or 30°C (Fig 7C). Indeed, $NADP^+$ levels in iWAT from WT or *Cd38*$^{-/-}$ mice at 6°C, were not statistically different (Fig 7C). These data suggest that, differently from what observed in iBAT, the CD38 downregulation occurring in iWAT upon cold exposure (Fig 6) was followed by NAD^+ being re-directed to its phosphorylated form.

Consonant with this hypothesis, NAD^+ kinase mRNA levels (Fig 8A) and enzymatic activity (Fig 8B) were found to be significantly up-regulated in iWAT from cold-exposed mice. Also, NADPH levels were significantly enhanced in iWAT from cold-exposed mice (Fig 7D), likely to foster the FA synthesis occurring in WAT during thermogenesis. Indeed, mRNA level of both enzymes determining FA synthesis, Acetyl-CoA carboxylase 1 (*Acaca*) and Fatty acid synthase (*Fasn*), were found to be significantly upregulated in iWAT from mice exposed to 6°C (Fig 8C, D). In agreement, the mRNA level (Fig 8E) and activity (Fig 8F) of the major NADPH-generating enzyme G6PD were found to be upregulated in iWAT from mice housed at 6°C. Notably, also gene expression of Malic enzyme *(Me1)*, another fundamental enzyme catalyzing the formation of NADPH, was strongly increased upon cold exposure in iWAT (Fig 8G).

In iBAT, NAD^+ kinase mRNA (Fig 8H) and enzymatic activity (Fig 8I) were slightly, although not significantly, increased by cold exposure, possibly in line with the lack of increase in $NADP^+$ content (Fig 7A). Also *G6pdx* mRNA levels were not affected in iBAT from animals exposed to low temperature (Fig 8L).

Figure 8

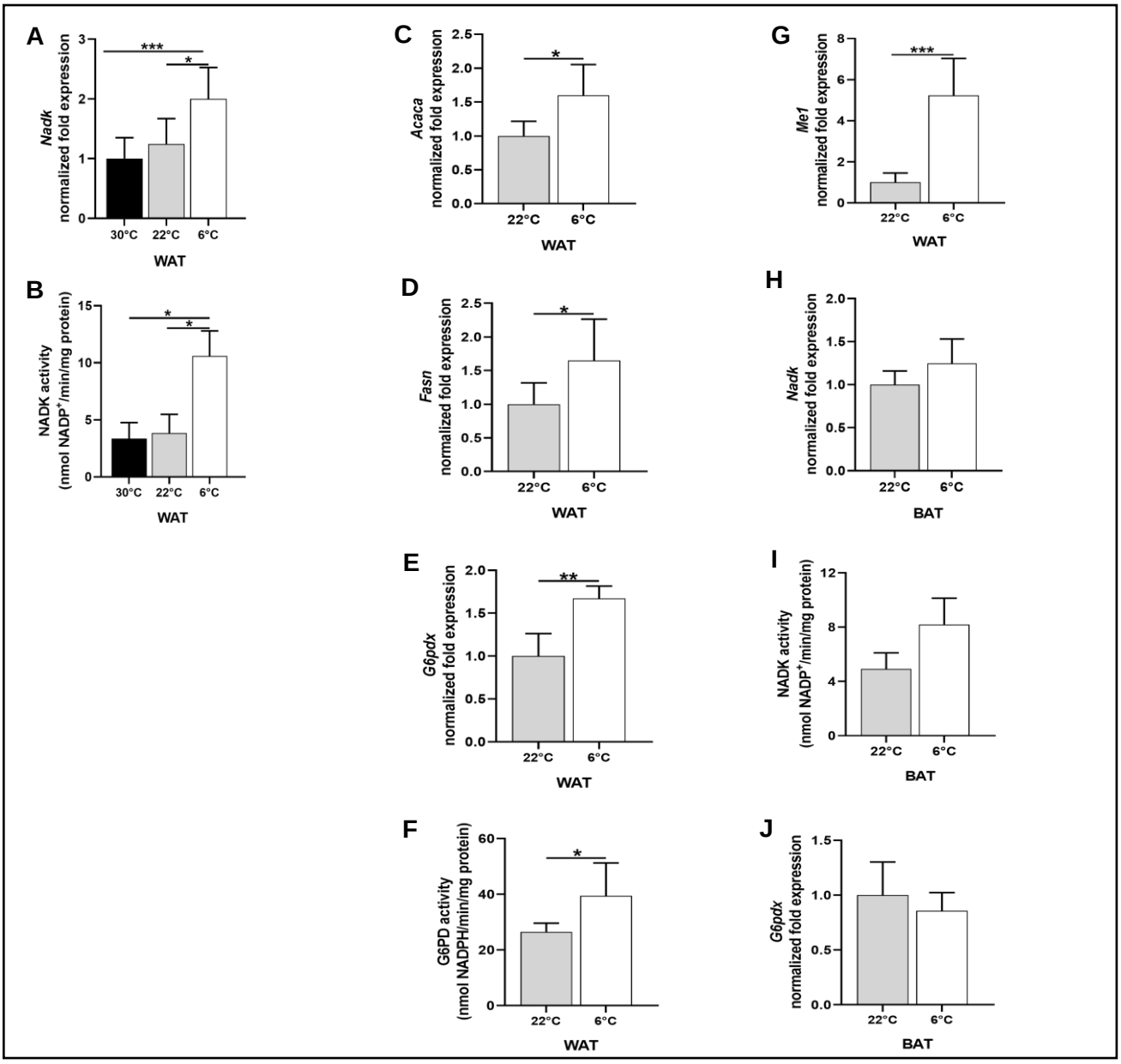

Fig 8 Cold exposure increases NAD$^+$ kinase, acetyl CoA carboxylase, fatty acid synthase, G6PD and Malic enzyme levels in iWAT.

NAD$^+$ kinase levels were evaluated on iWAT collected from WT mice kept at 30°C for 1 week (30°C), or at 22°C for 1 week (22°C), or at 22°C for 6 days and at 6°C for 1 day (6°C) (A, B). RT-PCR analysis was performed to evaluate mRNA levels (A), and enzymatic activity was evaluated by adding NAD$^+$ and ATP as substrates (B). *Acaca*, *Fasn*, *G6pdx* and *Me1* levels were evaluated on iWAT collected from WT mice kept at 22°C for 1 week (22°C), or at 22°C for 6 days and at 6°C for 1 day (6°C) (C-G). RT-PCR analysis were performed to evaluate mRNA levels (C, *Acaca*; D, *Fasn*; E, *G6pdx*; F, *Me1*, malic enzyme), and G6PD enzymatic activity was evaluated by adding G6P and NADP$^+$ as substrates (F).

NAD$^+$ kinase levels were evaluated on iBAT collected from WT mice kept at 22°C for 1 week (22°C), or at 22°C for 6 days and at 6°C for 1 day (6°C) (H-I). RT-PCR analysis was performed to evaluate mRNA levels (H), and enzymatic activity was evaluated by adding NAD$^+$ and ATP as

substrates (I). *G6pdx* mRNA levels were evaluated by RT-PCR on iBAT collected from WT mice kept at 22°C for 1 week (22°C), or at 22°C for 6 days and at 6°C for 1 day (6°C) (J). Results are means ± SD of measurements from different animals from each condition (n = 5–7 animals for RT-PCR analysis; n = 4 animals for enzymatic activities).
Data analyzed by ANOVA with Tukey's test (A–B) or by Student's t test (C–J) *, $p < 0.05$, **, $p < 0.01$, ***, $p < 0.001$.

3.2 Cold-exposure affects NAD(P)(H) levels in liver and CD38 deletion impairs gluconeogenesis and glycolysis regulation

3.2.1 NAD(H) and NADP(H) levels are modified in liver of mice during cold exposure as a consequence of CD38 downregulation

Since cold exposure led to increased levels of NAD(H) in BAT, and to NADP(H) in WAT, we evaluated the impact of this stimulus on NAD(P)(H) in liver, the main metabolic hub in the body. NAD(H) levels were measured by an enzymatic cycling assay, on liver of WT and *Cd38*$^{-/-}$ mice exposed to cold, or housed at 30°C and 22°C. Both NAD^+ and NADH levels were increased (by 1.3 and 1.8 fold, respectively) in liver of cold-exposed WT mice (Fig 9A, B). No differences were detected comparing the other two experimental conditions, with mice housed at 22°C and 30°C. The NAD^+/NADH ratio was reduced in WT mice exposed to cold, compared with mice housed at 30°C (by approximately 1.5 fold), indicating that during thermogenesis, liver metabolism is highly promoted.

In line with results obtained in adipose tissue, livers harvested from *Cd38*$^{-/-}$ mice exhibited exceptionally high levels of NAD(H) in comparison with WT mice (approximately 2.5-fold higher for both NAD^+ and NADH at all temperatures; Fig 9A, B). No significant changes were detected in liver from *Cd38*$^{-/-}$ at the three different housing temperatures. This result indicates that CD38 is the major NAD^+-consuming enzyme also in liver. Thus, we hypothesized that a decrease in CD38 expression may cause the NAD(H) increase, as occurred in BAT (see paragraph 3.2.2). No significant differences were detected in NAD^+/NADH ratio when cold-exposed *Cd38*$^{-/-}$ mice were compared with *Cd38*$^{-/-}$ mice housed at 30 and 22°C.

In WAT, the downregulation of CD38 expression was followed by increased levels of the phosphorylated NAD pool (Fig 7). $NADP^+$ and NADPH were measured also in liver, harvested from animals housed at 30°C, 22°C and 6°C. As evaluated by the specific enzymatic cycling assay, $NADP^+$ levels were not modified in liver from mice exposed to cold temperature, neither in WT nor in *Cd38*$^{-/-}$ (Fig 9C). On the other hand, NADPH levels in liver were negatively affected by cold exposure. In WT mice, cold exposure led to a decline of NADPH in liver by approximately 45% in comparison with 30°C-housed mice and 35% in comparison with 22°C-housed mice. In line with

this, in liver from *Cd38*$^{-/-}$ mice, cold exposure determined a reduction in NADPH levels by approximately 35% in comparison with 30°C-housed mice and 20% in comparison with 22°C-housed mice (Fig 9D). NADP(H) levels in *Cd38*$^{-/-}$ were significantly higher than in WT mice (Fig 9C, D), indicating that CD38 activity affects the amount of the NADP(H) pool, beside the NAD(H) one.

3.2.2 Increase in NAD(H) levels during cold exposure are a consequence of CD38 downregulation

To investigate whether changes in CD38 expression occur in liver, as observed for BAT and WAT, CD38 levels were evaluated using three different approaches: at the mRNA level, by RT- PCR and at the protein level, by Western blot analyses and by evaluating the CD38-related enzymatic activity. In liver, as in BAT (Fig 4) and in WAT (Fig 6), cold exposure determined a significant decrease in *Cd38* expression, as measured by RT-PCR analyses (by approximately 60% Fig 9H), Western blot analysis (by approximately 40%, Fig 9I) and NAD^+-ase activity (by 27% Fig 9J). Thus, CD38 downregulation could account for NAD(H) increase at cold temperatures.

To identify other possible explanations for the increased NAD(H) levels observed in liver upon cold exposure, we verified whether the NAD^+-synthetizing activities were upregulated in liver upon cold exposure. NAMPT is the main enzyme in the salvage pathway, converting NAM to NMN: *Nampt* mRNA levels were evaluated by RT-PCR in livers harvested from WT and *Cd38*$^{-/-}$ mice housed at 30°C or at 6°C. *Nampt* expression levels were significantly higher in WT mice exposed to cold, in comparison with mice housed at 30°C (Fig 9E). However, we did not observe cold-mediated modulation in NAD^+-synthetizing activity (starting from NAM and PRPP and producing NAD^+ by utilizing ATP) (Fig 9F). Then, the NMNAT enzymatic activity (converting the NAMPT-produced NMN to NAD^+, with ATP consumption) was measured in livers from WT and *Cd38*$^{-/-}$ mice, to obtain a complete view on the NAD^+ salvage pathway in liver. NMNAT enzymatic activity was not different among the different conditions, demonstrating that the cold stimulus did not influence NMNAT activity (Fig 9G).

Figure 9

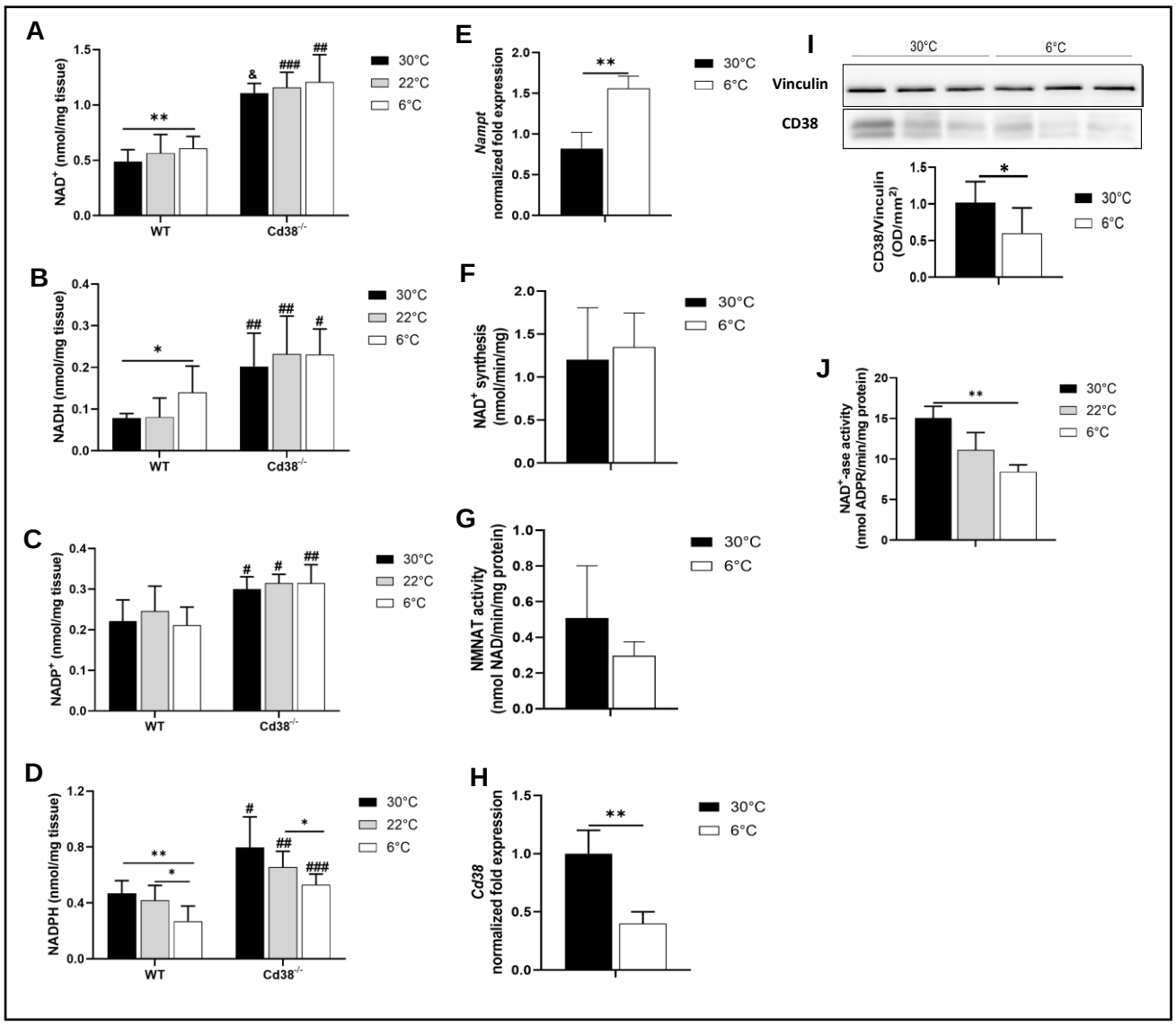

Fig 9 Cold exposure increases NAD(H) levels, decreases NADPH levels, and down-regulates CD38 levels in liver from WT mice.

Livers were harvested from WT and *Cd38*$^{-/-}$ mice housed at 30°C for 7 days (30°C, black bars), or at 22°C for 7 days (22°C, grey bars), or at 22°C for 6 days and at 6°C for 1 day (6°C, white bars). For nucleotide content assay, tissues were minced on ice and then deproteinized in PCA or NaOH. Acid-extracted samples were used to evaluate NAD^+ and $NADP^+$ (A, C), whereas base-extracted samples were used to determine NADH and NADPH levels (B, D). *Nampt* gene expression levels were evaluated by RT-PCR (E). NAD synthesis and NMNAT enzymatic activity were measured by evaluating NAD^+ production starting from NAM, PRPP and ATP, or starting from NMN and ATP, respectively (F, G). *Cd38* expression was measured by RT-PCR (H) and by western blot analyses (I), and CD38 enzymatic activity was evaluated by measuring ADPR production starting from NAD^+ (J). Results are means ± SD (n= 4-5). Data analyzed by ANOVA with Tukey's test: *, $p < 0.05$, **, $p < 0.01$; data analyzed by Student's t test: $^{\#}$, $p<0.05$, $^{\#\#}$, $p < 0.01$, $^{\#\#\#}$, $p < 0.001$, $^{\&}$, $p < 0,00001$, compared with the corresponding WT.

3.2.3 Reduction of G6PD and malic enzyme is responsible for the decrease in NADPH in liver of WT and Cd38$^{-/-}$ mice upon cold stimulation

With the goal of understanding the mechanisms leading to NADPH decrease in liver during thermogenesis, level of expression of NAD^+ kinase, G6PD and Malic enzyme were evaluated. NAD^+ kinase is responsible for $NADP^+$ production starting from NAD^+; G6PD and malic enzyme are the main enzymes involved in $NADP^+$ reduction to NADPH. *Nadk* gene expression was upregulated (by 60%) in liver in WT mice upon cold exposure (Fig 10A). On the other hand, *Cd38*$^{-/-}$ mice did not exhibit *Nadk* gene regulation in basal conditions, compared with WT mice (Fig 10A). NADK enzymatic activity in total liver lysates, showed a trend to be increased at 6°C, but this value was not significantly different from values at 22°C or 30°C (Fig 10B).

Gene expression analyses unveiled a remarkable downregulation in *G6pdx* and *Me1* expression occurring upon cold exposure in WT and *Cd38*$^{-/-}$ mice, compared with mice housed at control temperature (Fig 10C, D). *Cd38*$^{-/-}$ mice displayed higher *Me1* expression than WT mice (Fig 10D). G6PD activity was lower in liver of cold-stimulated mice than in liver from mice at 22 and 30°C. This trend was observed both in WT and in *Cd38*$^{-/-}$ (Fig 10E).

Altogether, results from the G6PD and Malic enzyme expression are in line with the observed decrease in NADPH content in liver and suggest that the entrance of hepatic G6P in the pentose phosphate pathway is reduced during thermogenesis, in both WT and *Cd38*$^{-/-}$ mice, the reduction being stronger in the latter animals.

Figure 10

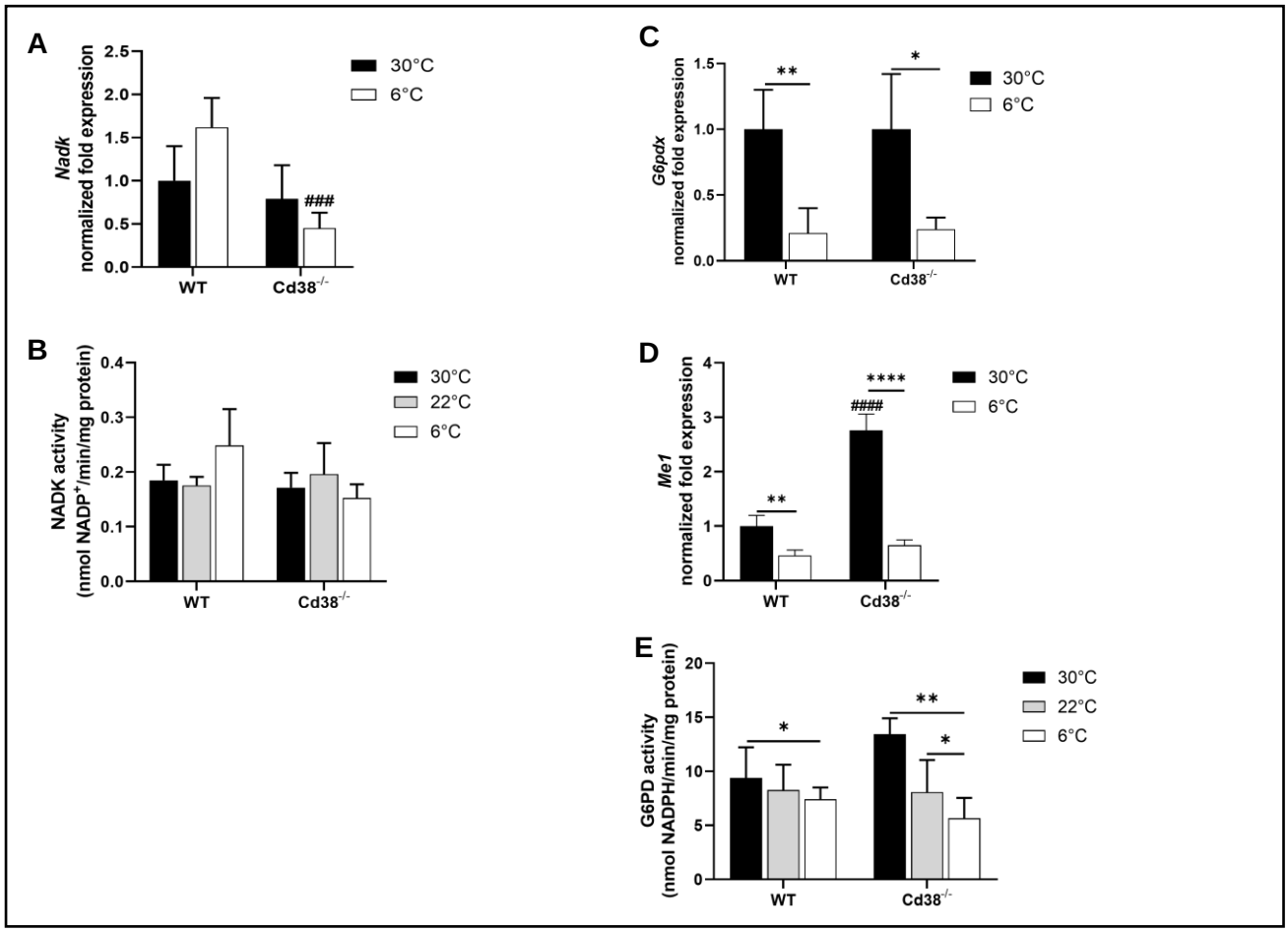

Fig 10 G6PD and Malic enzyme are downregulated in liver of WT and *Cd38*$^{-/-}$ mice.

Livers were harvested from WT and *Cd38*$^{-/-}$ mice housed at 30°C for 7 days (30°C, black bars), or at 22°C for 7 days (22°C, grey bars), or at 22°C for 6 days and at 6°C for 1 day (6°C, white bars). *Nadk*, *G6pdx* and *Me1* expression was measured by RT-PCR (A, C, D). NADK activity was evaluated by measuring the $NADP^+$ production, starting from NAD^+ and ATP (B). G6PD activity was evaluated by measuring NADPH production, starting from G6P and $NADP^+$ (E). Results are means ± SD (n= 4-5). Data analyzed by ANOVA with Tukey's test: *, $p < 0.05$, **, $p < 0.01$, ****, $p < 0.0001$; data analyzed by Student's t test: ###, $p < 0.001$, ####, $p < 0.0001$ compared with the corresponding WT.

3.2.4 Glycolytic and gluconeogenic pathways are not affected by cold exposure in Cd38$^{-/-}$ mice.

To investigate hepatic G6P destiny in liver during thermogenesis in WT and *Cd38*$^{-/-}$ mice, the expression of enzymes involved in the main glucose pathways was analyzed. *Pfk1* (Phosphofructokinase 1) and *Gapdh* (Glyceraldhyde-3-phosphate dehydrogenase) expression and LDH (Lactate dehydrogenase) activity were tested to estimate the glycolytic pathway rate in WT and *Cd38*$^{-/-}$ mice. *Pfk1* and *Gapdh* expression levels were significantly lower in liver of WT mice exposed to cold, than in mice housed at 30°C (by approximately 2.5 and 8 folds, respectively). Conversely, this downregulation was abrogated in *Cd38*$^{-/-}$ mice, in which even a trend to increase *Pfk1* and *Gapdh* levels was detected in cold-exposed mice (Fig 11A, B). In line with this, a marked reduction in LDH enzymatic activity was detected in liver from WT mice exposed to cold temperature, compared with mice housed at 22°C and 30°C (Fig 11C). However, no statistical differences in hepatic LDH activity were detected in *Cd38*$^{-/-}$ upon cold exposure (Fig 11C).

Next, G6Pase gene expression and activity were evaluated. As shown in Fig 11D andE, cold exposure determined a marked increase in G6Pase expression and activity (approximately 2.5 and 2 fold respectively) in WT mice; on the contrary, the cold stimulus did not affect G6Pase expression and activity *Cd38*$^{-/-}$ mice (Fig 11D, E). Hepatic G6P levels were evaluated using a cycling assay. In line with what observed for G6Pase, the amount of released glucose was higher in WT mice, than in *Cd38*$^{-/-}$ mice upon cold exposure (Fig 11F). Interestingly, glycogen levels were higher in *Cd38*$^{-/-}$ mice housed at 30°C, in line with observations reported by [Rah et al. 2015] and were drastically decreased in both WT and *Cd38*$^{-/-}$ mice exposed to cold. The remaining glycogen was significantly higher in liver from cold-exposed *Cd38*$^{-/-}$ mice, than in liver from WT mice (Fig 11G). Altogether, these data suggest that upon cold exposure, liver metabolism is shifted from glycolytic to gluconeogenetic, and CD38 plays a role in this cross-regulation. Indeed, in the absence of CD38, this metabolic switch is impaired, and glucose entrance in the glycolytic pathway is not reduced. Moreover, higher glycogen levels in knockout mice act possibly as a bigger glucose reservoir to promote glycolysis when energy and heat production are required, such as during cold exposure.

Next, hepatic lipid metabolism was compared in the two mice strains at different temperatures. First of all, *Cd38*$^{-/-}$ mice had a reduced content of TGs compared to WT mice, when housed at 30°C (Fig 11H). In line with liver assembling triglycerides to be exported to the other organs in

VLDL during thermogenesis, the levels of TGs were greatly increased during cold-exposure, both in WT and in *Cd38*$^{-/-}$ mice (Fig 11H).

Glycerol levels were also evaluated: notably, glycerol levels were dramatically decreased in liver from *Cd38*$^{-/-}$ animals upon cold exposure (Fig. 11I), suggesting that glyceroneogenesis, as gluconeogenesis, is not properly activated during thermogenesis, in the absence of CD38.

Next, the expression of *Acaca* and *Fasn* was evaluated in liver of WT and *Cd38*$^{-/-}$ mice. *Acaca* gene expression levels were not affected by cold exposure in WT mice, whereas the expression of *Fasn* was significantly reduced (by approximately 2.5 fold) in WT cold-exposed mice, in comparison with WT mice housed at 30°C (Fig 11J, K). In *Cd38*$^{-/-}$, *Acaca* and *Fasn* expression levels were significantly downregulated in mice exposed to cold temperature, in comparison with *Cd38*$^{-/-}$ mice housed at 30°C (by approximately 2 and 3 fold for *Acaca* and *Fasn*, respectively) (Fig 11J, K). Interestingly, the expression of *Acaca* and *Fasn* was higher in *Cd38*$^{-/-}$ mice than in WT mice at 30°C (by approximately 1,9 and 1.75 fold, respectively). However, the expression of these two enzymes was unchanged in 6°C-housed *Cd38*$^{-/-}$ mice, in comparison with WT mice housed at 6°C (Fig 11J, K).

Figure 11

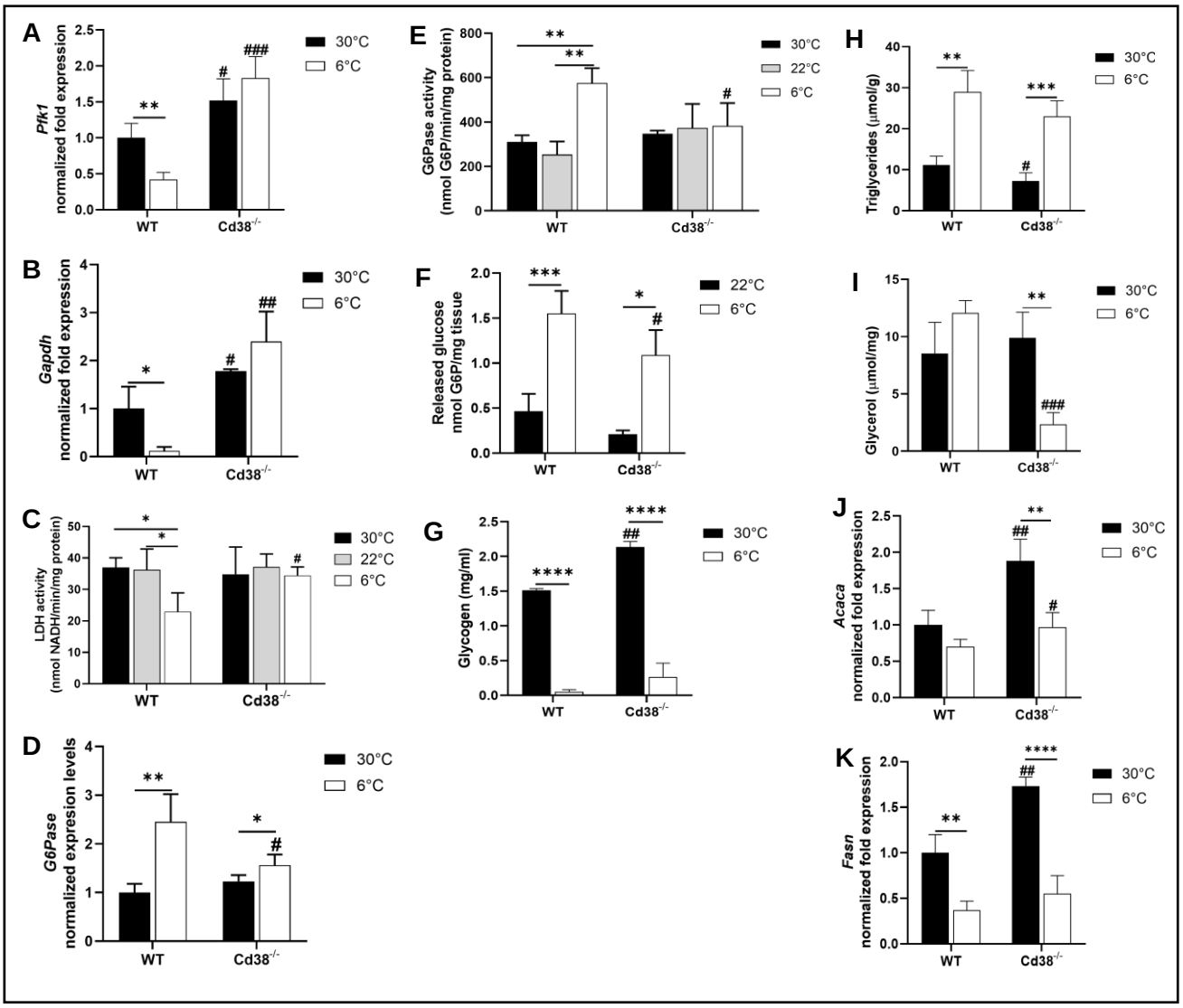

Fig 11 Cold exposure determines a metabolic switch, from glycolysis to gluconeogenesis, in WT mice, but not in mice lacking *Cd38*$^{-/-}$ mice.

Livers collected from WT and *Cd38*$^{-/-}$ mice housed at 30°C for 7 days (30°C, black bars), or at 22 °C for 7 days (22°C, grey bars), or at 22°C for 6 days and at 6°C for 1 day (6°C, white bars) were utilized for gene expression and enzymatic activity quantification. *Pfk1*, *Gapdh*, *G6pase*, *Acaca* and *Fasn* gene expression levels were measured by RT-PCR (A, B, D, J, K). LDH activity was measured by quantifying NADH produced incubating liver lysates with NAD^+ and L(+)-lactate (C). G6Pase activity was evaluated by quantifying G6P depletion from the incubation of liver lysates with G6P (E). G6P levels were measured in acid-extracted samples, using cycling assay (F). Hepatic glycogen, TGs and glycerol were measured in fresh minced tissues. Glycogen levels were determined by glucose quantification, upon glycogen hydrolysis, using a commercially available kit (G). TGs and free glycerol were detected by quantitative fluorometric assay, using a commercially available kit (H, I). All results are means ± SD of 4-5 independent determinations for each condition.

Data analyzed by ANOVA with Tukey's test: *, $p < 0.05$, **, $p < 0.01$, ***, $p< 0,001$, ****, $p < 0.0001$; data analyzed by Student's t test: #, $p<0.05$, ##, $p < 0.01$, ###, $p < 0.001$, compared with the corresponding WT.

3.2.4 Cold-exposure and CD38 deletion enhance SIRT3 enzymatic activity in liver

Given the results regarding differences in glucose metabolisms occurring in WT and *Cd38*$^{-/-}$ mice during thermogenesis, Pyruvate dehydrogenase (*Pdh*) expression was evaluated by RT-PCR. *Pdh* levels were significantly reduced in liver from *Cd38*$^{-/-}$ mice compared to WT mice (Fig 12A). Upon cold-exposure, *Pdh* expression was significantly reduced. As for the enzymes in the glycolytic pathway, *Pdh* regulation was lost in the absence of CD38.

Since SIRT3 (a member of the Sirtuin family) is a master regulator of mitochondria metabolism, and SIRT3 activity is known to be activated during thermogenesis (Shi et al. 2005), we compared SIRT3 activity in the different conditions. SIRT3 activity was evaluated measuring the acetylation levels of SOD2 (Superoxide dismutase 2, one of its known substrates), as revealed by Western blot analysis, using a specific antibody against the acetylated form, normalized on total SOD2 expression. The higher is the value (i.e. the most SOD2 is acetylated), the lower is SIRT3 activity. Western blot analyses were performed on liver lysates: SOD2 acetylation levels were lower (by approximately 50%) when WT mice were exposed to cold, confirming that SIRT3 was activated during cold exposure in WT mice (Fig 12C). Nevertheless, in liver from *Cd38*$^{-/-}$ mice, SIRT3 activity was not enhanced by cold exposure (Fig 12D), suggesting that CD38 (likely via modulation of NAD^+ levels) is crucial also for SIRT3 regulation. As shown in panel E of Fig 12, when mice were housed at 30°C, SIRT3 is more active in liver from *Cd38*$^{-/-}$ than in liver from WT mice, as if it had already reached the highest achievable activity; indeed, *Cd38*$^{-/-}$ mice displayed higher SIRT3 activity in their liver, at both temperatures, in comparison with liver from WT mice (Fig 12E, F).

The enhanced SIRT3 activity recorded in liver from *Cd38*$^{-/-}$ mice was not due to a higher mitochondria content. Indeed, *mt-DNA* expression levels unveiled lower mitochondrial amount in *Cd38*$^{-/-}$ mice, compared with WT mice, housed at 30°C (Fig 12B). In WT mice, cold exposure strongly enhanced mitochondria content (by approximately 3-fold, Fig 12B). Similarly, in *Cd38*$^{-/-}$ mice, mitochondria content was enhanced by cold exposure, although the levels were far from reaching levels in WT mice (Fig 12B).

Figure 12

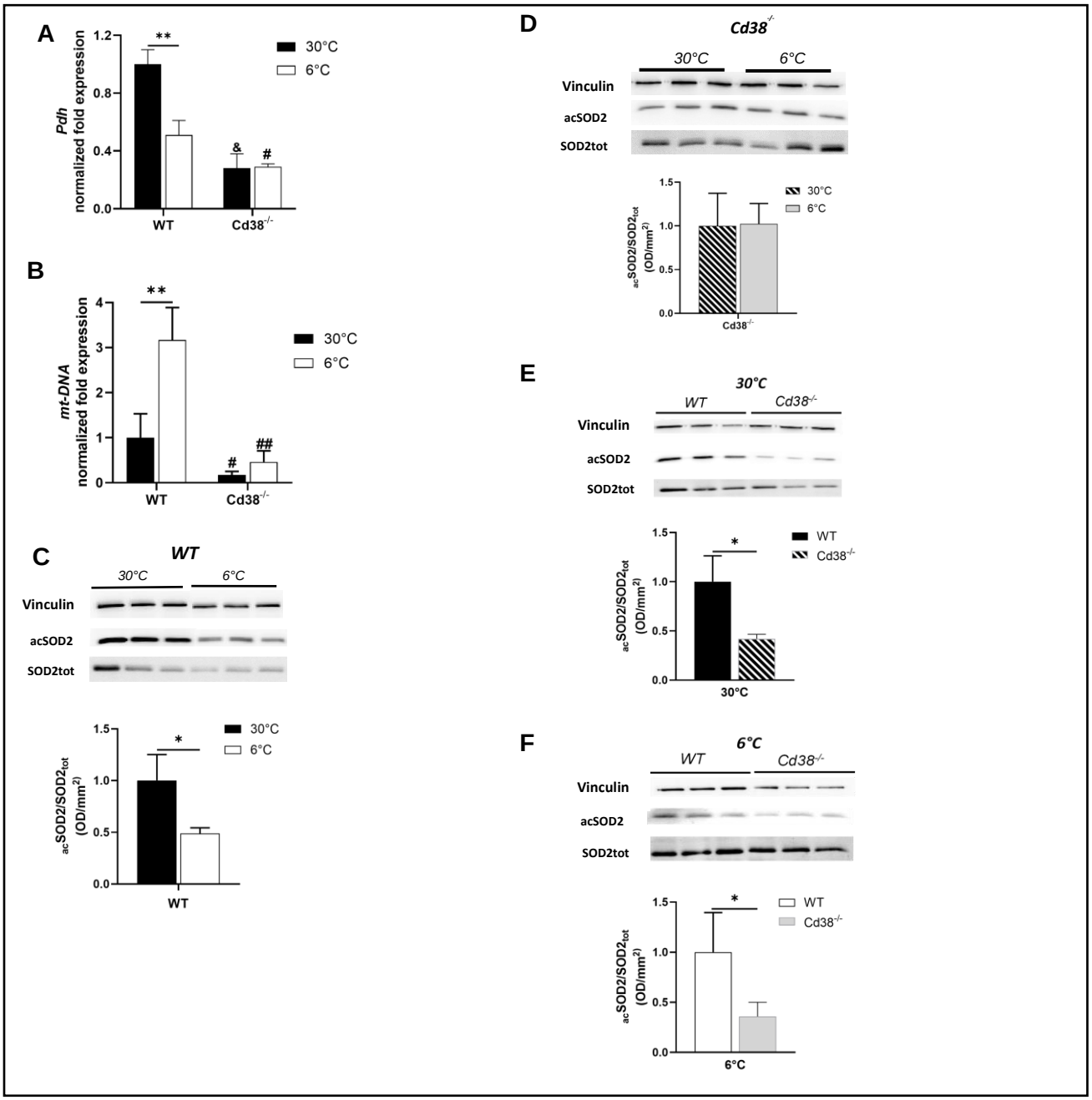

Fig 12 Cold exposure increases mitochondrial content and SIRT3 activity in WT, but not in *Cd38*$^{-/-}$ mice, and SIRT3 is over-activated at warm temperature in *Cd38*$^{-/-}$ mice.

Livers from WT and *Cd38*$^{-/-}$ mice, kept for 1 week at 30°C (black bars) or 6 days at 22°C followed by 1 day at 6°C (white bars) were used to evaluate mitochondrial content and SIRT3 activity. *Pdh* and *mt-DNA* expression were evaluated by RT-PCR (A, B). SIRT3 activity was evaluated by western blot, measuring the acetylation level of SOD2, a substrate of SIRT3 activity (C, D, E, F). Results of quantification are mean ± SD from n = 3 animals for each condition. Data analyzed by ANOVA with Tukey's test: *, p< 0.05, **, p< 0,01; data analyzed by Student's t test: #, p< 0.05, ###, p< 0,001, &, p< 0,00001 compared with the corresponding WT.

3.3 TRPM2 is necessary for BAT activation and WAT browning

3.3.1 Trpm2$^{-/-}$ mice exhibit lower respiration and energy expenditure when thermogenesis is stimulated

To investigate whether the cation channel TRPM2, gated by ADPR, an NAD^+-derived second messenger (see Introduction), plays a role in thermogenesis, we performed experiments using *Trpm2*$^{-/-}$ mice, in collaboration with Prof Nolte, Mittrücker and Heeren (University Medical Center Hamburg-Eppendorf, Hamburg, Germany). WT and *Trpm2*$^{-/-}$ mice were subjected to two different stimuli: cold acclimation and β-adrenergic agonist administration. These methods were used to trigger the thermogenic response in mice, while they were constantly monitored to register and calculate the following parameters: O_2 consumption, CO_2 production, EE and RER.

When thermogenesis is stimulated, metabolic changes in the body lead to increased O_2 consumption and CO_2 production. In addition, EE rises as a consequence of the accelerated metabolism and the RER decreases.

As expected, when mice were housed at decreasing temperature for 6 days, both O_2 consumption and CO_2 production were observed to rise day by day. In addition, EE rose in a temperature-dependent manner, while RER decreased (Fig 13A-G). High RER, ranging from 0.9-1, suggests that glucose is used as a main source to support cellular function, whereas low RER, 0.8-0.7, indicates that lipid oxidation is occurring. All the obtained results indicated that thermogenesis was triggered both in WT and *Trpm2*$^{-/-}$ mice.

Interestingly, *Trpm2*$^{-/-}$ mice displayed lower O_2 consumption and CO_2 production when cages reached the cold temperature, in comparison with WT mice. These results were observed especially during the day. However, during the night, when mice are more active, knockout mice displayed the same trend although statistical significance was not reached during the whole experiment (Fig 13A, D). Furthermore, the reduced respiration displayed by *Trpm2*$^{-/-}$ mice led to a reduced EE and a higher RER, in comparison with WT mice (Fig 13E, G). Next, administration of CL-316,243 (a β-adrenergic agonist) was used to activate adrenergic receptors and stimulate thermogenesis in mice. Not surprisingly, CL316,243 mimicked the exposure to cold temperature, as seen by the higher O_2, CO_2, EE, and the lower RER displayed by mice upon the treatment (Fig 13H, M). However, *Trpm2*$^{-/-}$ mice exhibited attenuated thermogenic response when compared with WT mice. Indeed, CL-316,243-treated *Trpm2*$^{-/-}$ mice exhibited lower O_2 production, CO_2

consumption and EE in comparison with WT treated mice (Fig 13H, K). Moreover, RER was higher in *Trpm2*$^{-/-}$ mice in comparison with WT mice (Fig 13L, M).

All the data obtained by these *in vivo* experiments suggest that TRPM2 plays a role in thermogenesis and seems to influence the type of macromolecules utilized to produce energy upon thermogenic stimulation.

Figure 13

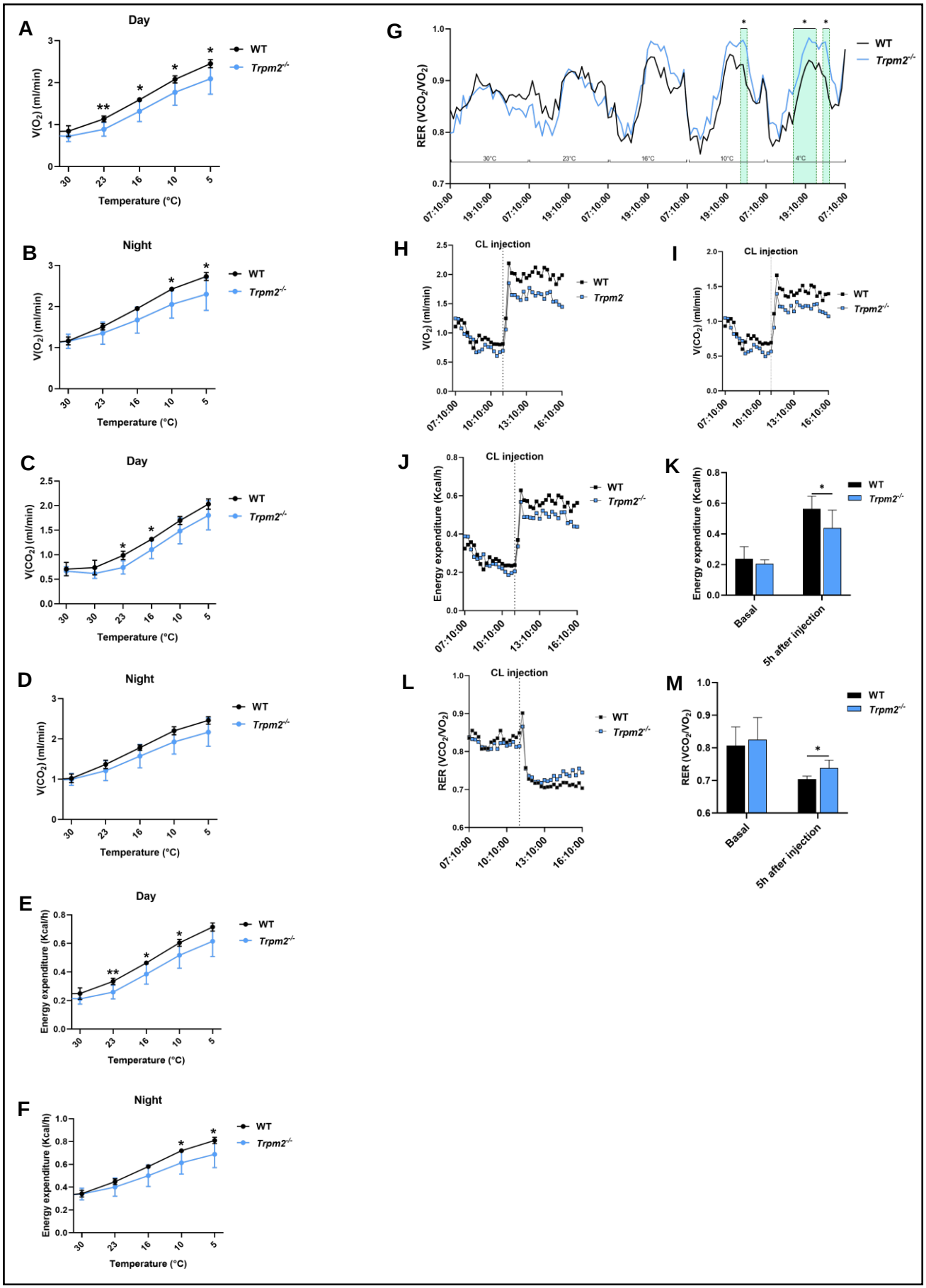
A
Day
V(O2) (ml/min)
Temperature (°C)
WT
Trpm2-/-
B
Night
C
Day
V(CO2) (ml/min)
D
Night
E
Day
Energy expenditure (Kcal/h)
F
Night
G
RER (VCO2/VO2)
30°C
23°C
16°C
10°C
4°C
H
CL injection
I
CL injection
J
CL injection
K
Basal
5h after injection
L
CL injection
M
Basal
5h after injection

Fig 13 Impaired response to thermogenesis in *Trpm2*$^{-/-}$ mice.

In vivo measurements performed on WT (black lines) and *Trpm2*$^{-/-}$ mice (blue lines)
O_2 consumption, CO_2 production and EE of *Trpm2*$^{-/-}$ and WT mice in response to 5 days of decreasing environmental temperature (from 30°C to 5°C) during the light time (Day) (A, C, E) and the dark time (Night) (B, D, F). RER of WT and *Trpm2*$^{-/-}$ mice in response to the cold acclimation (G). O_2 consumption, CO_2 production, EE and RER of *Trpm2*$^{-/-}$ and WT mice upon CL316,243 administration (H, I, J,L). Monitoring started approximately 4 h before the treatment and finished 5 h after the injection. Graphic representation of basal EE and RER (1 h before the injection) and upon the treatment (5 h after injection) in WT (black bars) and *Trpm2*$^{-/-}$ mice (blue bars) (K, M). Data are presented as mean ± SD (n=6). ***** $p \leq 0.05$ and ****** $p \leq 0.01$ by two-tailed unpaired Student's t test.

3.3.2 Trpm2$^{-/-}$ mice display attenuated upregulation of thermogenic markers in white and brown adipose tissue after cold exposure

In order to unveil the role of TRPM2 during thermogenesis in adipose tissue, *Pgc1-*α and *Ucp1* gene expression levels, two thermogenic markers, were measured on iBAT and iWAT, harvested from WT and *Trpm2*$^{-/-}$ mice, housed for 6 days at 22°C and a final day at 6°C, or 7 days at 22°C, as control condition. As expected, an upregulation of these genes was observed in iBAT and iWAT from WT mice exposed to 6°C, in comparison with the control temperature (Fig 14A, B, D, E). Notably, the cold-induced upregulation of *Pgc1-*α and *Ucp1* levels was attenuated in iWAT and iBAT from *Trpm2*$^{-/-}$ (Fig 14A, B, D, E). TRPM2 has been demonstrated to regulate the expression of CREB (Chen SJ 2020). CREB is a well-known gene master regulator which promotes expression of several genes, including *Pgc1-*α and *Ucp1,* involved in different metabolism. Therefore, *Creb* mRNA levels were evaluated in both WAT and BAT of WT and *Trpm2*$^{-/-}$ mice, exposed to cold or housed at 22°C. As expected, *Creb* expression rose in WAT and BAT of WT mice upon cold exposure (by 7 and 9 fold in BAT and WAT and, respectively, when compared with the respective tissue from mice housed at 22°C) (Fig 14C, F). On the other hand, *Creb* mRNA upregulation was greatly attenuated in BAT and WAT from *Trpm2*$^{-/-}$ mice after 1 day at 6°C: *Creb* expression increased only by 2 and 1.5 fold in BAT and WAT, respectively, when compared with adipose tissue from *Trpm2*$^{-/-}$ mice housed at 22°C (Fig 14C, F).

Taken together, these data suggest that TRPM2 channels, likely through the regulation of intracellular Ca^{2+} movements, may be involved in WAT browning and in BAT activation in response to cold.

Figure 14

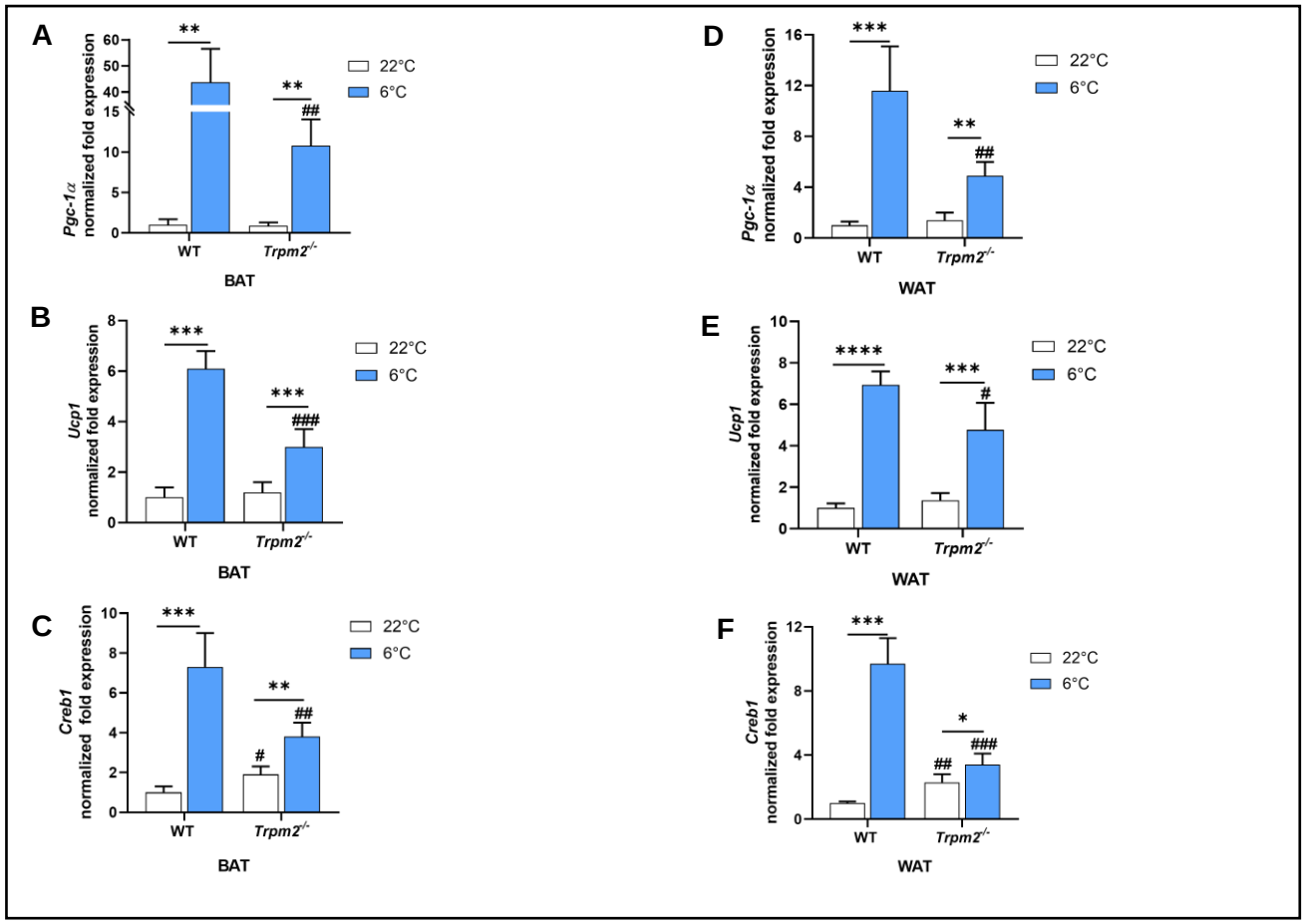

Fig 14 Lack of TRPM2 impairs cold exposure-induced iBAT activation and iWAT browning.

iBAT and iWAT were collected from WT and *Trpm2*$^{-/-}$ mice kept at 22°C for 1 week (white bars, 22°C), or at 22°C for 6 days and at 6°C for 1 day (blue bars). RT-PCR analysis was performed to evaluate mRNA levels of: *Pgc-1α* in iBAT (A); *Pgc-1α* in iWAT (D); *Ucp1* in iBAT (B); *Ucp1* in iWAT (E); *Creb1* in iBAT (C); *Creb1* in iBAT (F). Results are mean ± SD of determinations on tissues from different animals (n = 4). Data analyzed by ANOVA with Tukey's test: *, $p < 0.05$, **, $p < 0.01$, ***, $p < 0.001$; data analyzed by Student's t test: $^{\#}$, $p<0.05$, $^{\#\#}$, $p < 0.01$, $^{\#\#\#}$, $p < 0.001$ compared with the corresponding WT.

3.3.3 Trpm2 is overexpressed and ADPR levels rise in adipose tissues during cold exposure

To further investigate whether TRPM2 has a role during cold-induced thermogenesis, *Trpm2* expression was evaluate by RT-PCR in WT mice of each experimental condition. Interestingly, *Trpm2* expression was markedly increased in both types of adipose tissue after 24 h hours of cold exposure (Fig 15A). Likewise, *Trpm2* expression was highly up-regulated in both WAT and BAT from *Cd38*$^{-/-}$ mice. The lack of CD38 led to increased expression of browning markers in mice upon cold exposure (Fig 1): in fact, *Trpm2* mRNA levels were higher in cold exposed *Cd38*$^{-/-}$ mice, in comparison to WT, both in WAT and in BAT (Fig 15B). These data clarify that TRPM2 upregulation is not mediated by CD38.

In order to verify whether *Trpm2* upregulation occurs in adipocytes or in other cell types in the tissue, BAT from cold-exposed and control WT mice, was collected and processed: RT-PCR analyses were then performed on the BAT-isolated adipocyte fraction. An approximately 12 fold higher *Trpm2* expression was observed in brown adipocytes isolated from BAT from mice exposed to cold, in comparison to control mice-derived adipocytes (Fig 15C), indicating that this channel could be required for an appropriate thermogenic response to cold environment in adipocytes.

ADPR is a well-known TRPM2 agonist, produced by NAD^+ degradation in a number of enzymatic processes (see Introduction). CD38 is considered as one of the major ADPR producing enzymes, and for this reason its expression and activity are often linked to intracellular Ca^{2+} signaling. As shown in Figs 4 and 6, CD38 expression is regulated in BAT and WAT when mice are exposed to cold. Thus, we aimed at evaluating whether ADPR levels are modulated during thermogenesis. To this purpose, mass spectrometry analyses were performed on lysates of BAT and WAT from WT and *Cd38*$^{-/-}$ mice exposed or not to cold temperature. Surprisingly, and despite the fact that CD38 is downregulated in the same condition (Figs 4 and 6), ADPR levels were higher in both BAT and WAT from WT mice upon cold exposure (Fig 15D, E). Furthermore, ADPR was increased even in BAT from *Cd38*$^{-/-}$ mice (Fig 15D). Altogether, these data indicate that the cold-induced ADPR production is due to the activity of other enzymes, rather than of CD38. Nevertheless, ADPR levels were significantly reduced in *Cd38*$^{-/-}$ mice kept at 22°C, indicating that CD38 represent a source of ADPR is basal condition, in BAT (Fig 15D). ADPR was not detectable in WAT from *Cd38*$^{-/-}$ mice.

Fig 15

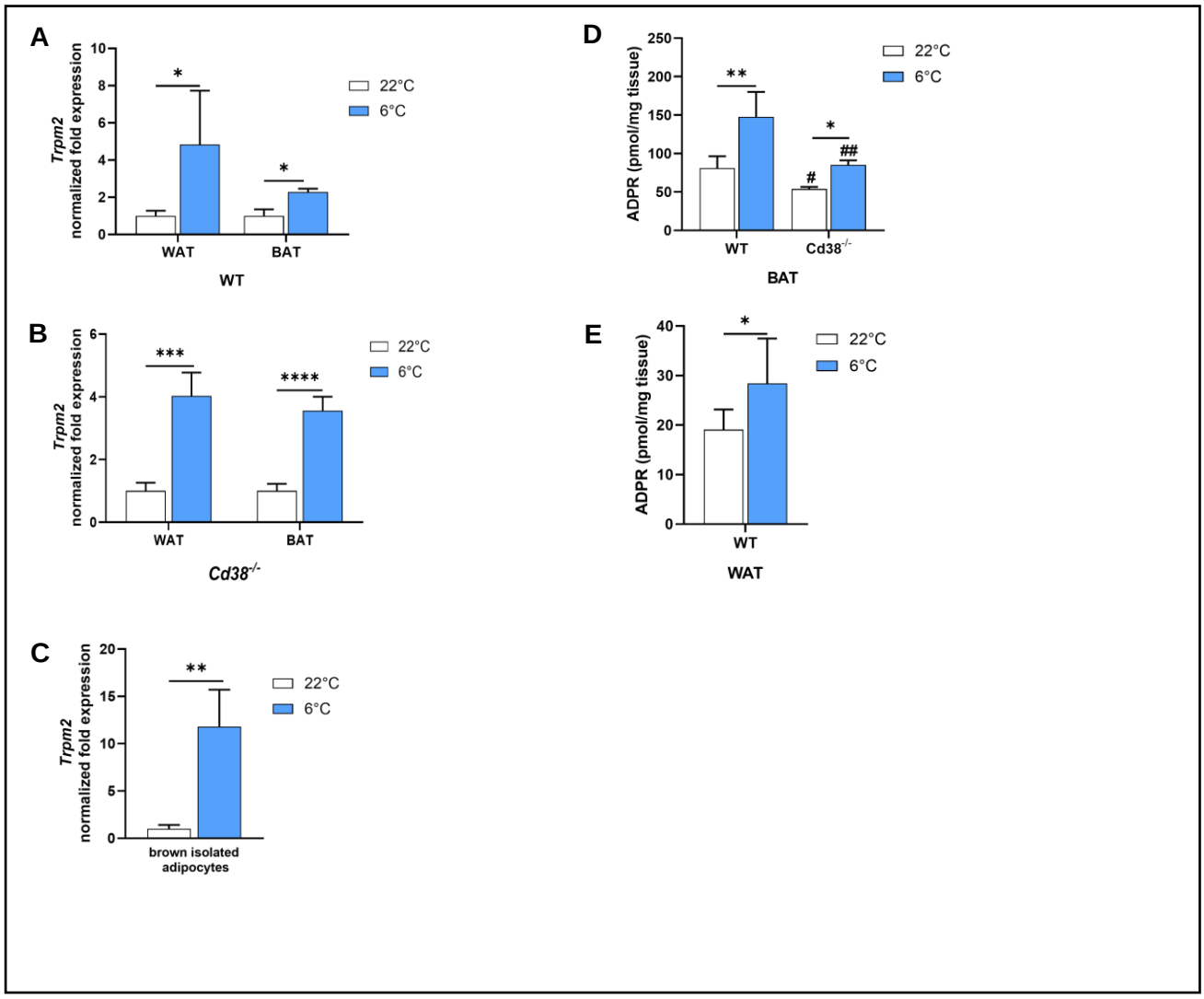

Fig 15 Cold exposure determines the increase in *Trpm2* and ADPR levels in adipose tissue.

A,B, RT-PCR were performed on iBAT and iWAT collected from WT (A) and *Cd38*$^{-/-}$ (B) mice kept at 22°C for 1 week (white bars), or at 22°C for 6 days and at 6°C for 1 day (blue bars) and *Trpm2* mRNA levels were evaluated. **C**, RT-PCR performed on isolated brown adipocytes obtained from iBAT of WT mice kept at 22°C for 1 week (white bars), or at 22°C for 6 days and at 6°C for 1 day (blue bars). **D,E,** ADPR levels were measured by mass spectrometry analyses on iBAT (D) and iWAT (E) of WT and *Cd38*$^{-/-}$ mice kept at 22°C (white bars), and mice exposed to cold (blue bars). ADPR levels mice were undetectable in iWAT from *Cd38*$^{-/-}$. Results are mean ± SD of determinations on tissues from different animals (n = 4 in A, B, C; n=6 in D, E). Data analyzed by ANOVA with Tukey's test: *, $p < 0.5$, **, $p < 0.01$, ***, $p < 0.001$, ****, $p < 0.0001$; data analyzed by Student's t test: $^{\#}$, $p<0.05$, $^{\#\#}$, $p < 0.01$ compared with the corresponding WT.

3.3.4 Enhanced Poly-ADPR polymers degradation is responsible for increased ADPR levels in WAT and BAT of cold exposed mice

PARPs are enzymes using NAD^+ to build poly-ADPR chains on amino acid residues, influencing protein localization and activity. The process of poly-ADPR chains degradation results in a release of ADPR monomers. To identify the pathway responsible for the observed ADPR increase, Western blot analyses were performed on BAT from WT and *Cd38*$^{-/-}$ mice, using an antibody against poly-ADPR polymers. Interestingly, the amount of ADPR polymers was reduced when mice were exposed to cold in comparison with controls, both in WT and in *Cd38*$^{-/-}$ mice (Fig 16A). Thus, we hypothesized that an accelerated degradation of ADPR polymers represents the cause for ADPR increase. and we performed several RT-PCR analyses on BAT and WAT from cold-exposed and control WT mice, as well as from *Cd38*$^{-/-}$ mice, to follow the expression of the major ADPR hydrolases identified so far, i.e. *MacroD1*, *MacroD2*, *Oard1*, *Parg* and *Adprs*. Gene expression measurements unveiled a marked upregulation of all these enzymes, in WAT and in BAT, when WT mice were exposed to cold temperature (Fig 16B, C). Although WT mice displayed a similar trend for all the different enzymes, *Cd38*$^{-/-}$ mice did not exhibit the same pattern (Fig 16B, C). Specifically, in WAT from *Cd38*$^{-/-}$ mice, the expression of none of the enzymes was increased during cold exposure (Fig 16B). In BAT from *Cd38*$^{-/-}$ mice, *Parg* and *Adprs* were significantly upregulated upon cold exposure (Fig 16C). *Parg and MacroD1* were more expressed in both BAT and WAT from *Cd38*$^{-/-}$ mice compared with WT controls, housed at the neutral temperature (Fig 16B, C).

Fig 16

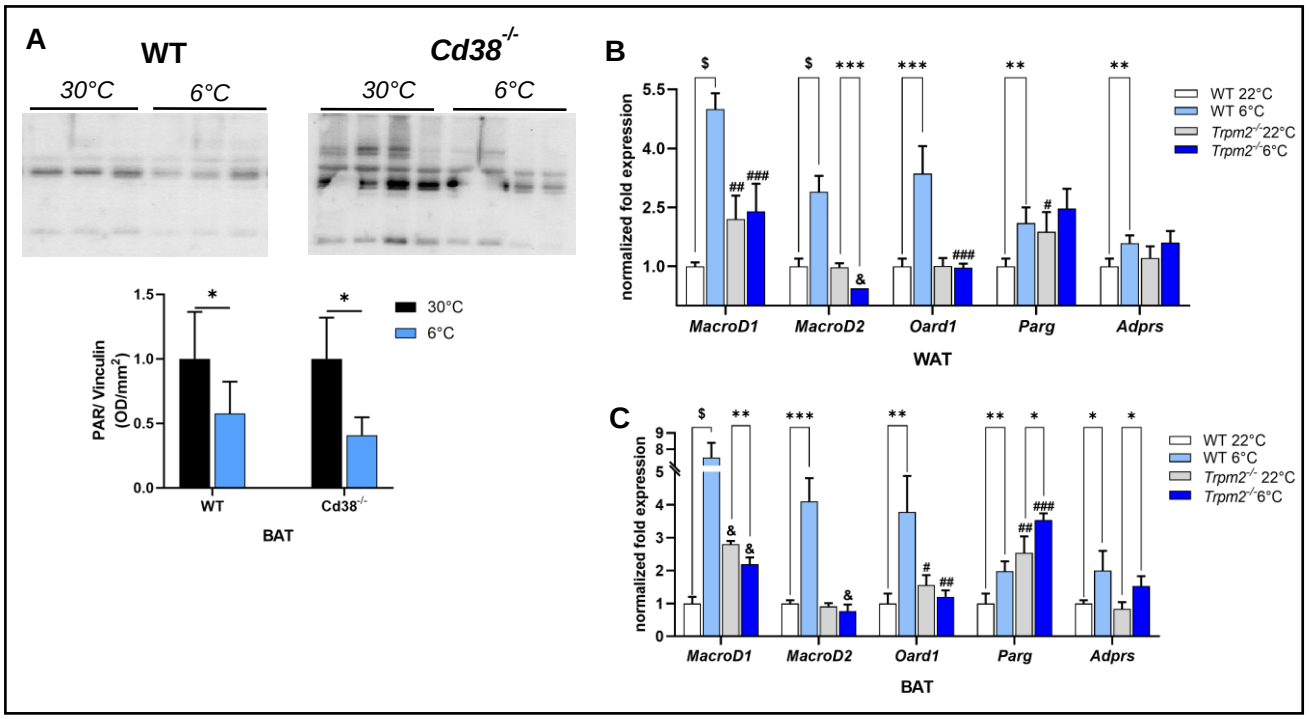

Fig 16 Poly-ADPR polymers are a source of ADPR during cold through overexpression of its degrading enzymes, in WT and *Cd38*$^{-/-}$ mice.

Western blot displaying poly-ADPR levels was performed in iBAT of WT and *Cd38*$^{-/-}$ mice housed at 30°C (black bars) or at 22°C for 6 days and 1 day at 6°C (blue bars) (A). Gene expression levels were measured by RT-PCR on iWAT (B) and iBAT (C) of WT and *Cd38*$^{-/-}$ mice housed at 22°C (white and grey bars) or at 22°C for 6 days and 1 day at 6°C (light blue and blue bars). mRNA levels of the following genes were quantified: *MacroD1*, *MacroD2*, *Oard1*, *Adprs1*, *Parg*. Results are mean ± SD of determinations on tissues from different animals (n = 3 in A; n=4 in B, C).
Data analyzed by ANOVA with Tukey's test: *, $p < 0.5$, **, $p < 0.01$, ***, $p < 0.001$, $, p< 0.00001; data analyzed by Student's t test: $^{\#}$, $p<0.05$, $^{\#\#}$, $p < 0.01$, ###, $p< 0.001$, &, $p < 0.00001$ compared with the corresponding WT.

4. Discussion

4.1 The role of CD38 in WAT and BAT during thermogenesis

The first aim of this study was to elucidate the role of CD38 in WAT, BAT and liver, during cold-induced thermogenesis. A schematic representation of the main results is shown in Fig 17. Overall, our results indicate that the lack of CD38 improves WAT and BAT responses to cold temperature: key physiological regulators of thermogenic and mitochondrial genes, *Ucp1* and *Pgc-1α*, were significantly more upregulated in *Cd38*$^{-/-}$ than in WT animals (Fig 1A–D). Moreover, HSL was more activated in *Cd38*$^{-/-}$ mice, as determined by its phosphorylation levels (Fig 1F). Thus, the absence of CD38 seems to potentiate the browning process and BAT activation. Cold temperature generated broad alterations in NAD biology of WT mice, in adipose tissues and in liver as well. In BAT, cold exposure determined a remarkable increase in NAD^+ levels (Fig 2A), indicating that NAD^+ biology and metabolism play a fundamental role in thermogenesis in this tissue. In line with our observation, the group of Yoshino recently reported a significant increase of NAD^+ in BAT upon cold exposure and demonstrated that the expression of NAMPT (involved in NAD^+ biosynthesis by converting NAM to NMN) was up-regulated in these conditions [Yamaguchi et al. 2019]. Our data confirm *Nampt* overexpression in BAT from cold-exposed mice (Fig 3A); nevertheless, the total activity of NAD^+ biosynthesis from NAM failed to be significantly affected by cold temperature (Fig 3C). Our present findings indicate that, beside NAMPT overexpression, an additional and major mechanism underlying the cold-induced increase of intracellular NAD^+ is the marked downregulation of CD38 in both BAT and WAT. The reduction in CD38 expression was confirmed at the mRNA and protein level, as well as by measuring CD38 enzymatic activities (namely, NAD^+-ase, ADP-ribosyl cyclase, and GDP-ribosyl cyclase). To the best of our knowledge, this is the first process in which a physiological decrease in CD38 is documented. CD38 is the major enzyme involved in NAD^+ consumption: its levels markedly affect NAD^+ content, as demonstrated by modulating its expression in cell lines [Zocchi et al. 1998], or in different organs (i.e. muscle, lung, kidney and brain) from *Cd38*$^{-/-}$ mice [Young et al. 2006, Barbosa et al. 2007]. Here we observed that the genetic ablation of *Cd38* per se strongly increases NAD^+ levels also in BAT and WAT from mice kept at 30–22°C: specifically, the absence of CD38 induced a more than doubled NAD^+ content in BAT, whereas in WAT the effect was even more pronounced, with NAD^+ being 6-fold higher in *Cd38*$^{-/-}$ mice (Fig 2A, C). Therefore, the

processes triggered by exposure of mice to low temperature and resulting in iBAT activation/WAT thermogenesis involve a lower expression of CD38 impacting on significant changes of NAD(H) and NADP(H) levels in both cell types. Overall, our results indicate that the regulation of NAD^+ metabolism is an important event during cold exposure, in line with the study by Yoshino and coll., in which the key role of NAD^+ synthesis has been investigated by the use of brown adipocyte-specific *Nampt* knockout mice as a model [Yamaguchi et al. 2019]. In BAT, NAD^+ levels are significantly higher in *Cd38*$^{-/-}$ mice compared with WT controls, at 30 and 22°C. This difference is lost at 6°C (Fig 2A), and this observation holds true also for $NADP^+$ levels in WAT (Fig 7C). Altogether, these data suggest that, in terms of the impact on $NAD(P)^+$ and their controlled metabolic pathways, the physiological cold exposure mimics the condition of CD38 ablation. The increased levels of NAD^+ in BAT are likely necessary to foster the activity of NAD^+-dependent protein deacetylases sirtuins: both SIRT1 and SIRT6 have been demonstrated to be fundamental in the orchestration of thermogenesis and BAT functions [Xu et al. 2016, Yao et al. 2017]. Furthermore, NAD^+ levels in liver of *Cd38*$^{-/-}$ mice were higher than WT control mice (30°- and 22°-housed mice), confirming what previously observed by Chini and coll. [Camacho-Pereira et al. 2016]. The fact that NAD^+ also increase in liver, suggested that this is an important factor driving thermogenic response. Also in liver, CD38 absence is accompanied by increased NAD^+ levels, proving that also in liver CD38 is one of the major enzymes degrading NAD^+. Regarding CD38 regulation, different reports documented the increase in its expression and enzymatic activities, as a consequence of different stimulation in various cell systems, to increase the production of cADPR and ADPR [Bruzzone et al. 2003, Deshpande et al. 2017, Morita et al. 1997, Munshi et al. 2002, Bruzzone et al. 2007]. As already mentioned, CD38 overexpression is induced by different cytokines in airway smooth muscle and is involved in asthma pathogenesis: this process is more enhanced in airway smooth muscle from asthmatic subjects [Deshpande et al. 2017]. Regulation of CD38 expression in these cells is achieved by different kinases and transcription factors, and also post-transcriptionally by microRNAs. Specifically, miR-140-3p and miR-708 were demonstrated to down-regulate TNFα-induced CD38 overexpression in airway smooth muscle cells [Jude et al. 2012, Dileepan et al. 2014]. Although in a completely different setting, this was the only reported mechanism of CD38 downregulation, and based on this study we investigated the levels of miR-140-3p and miR-708, and the levels of miR-155, predicted to bind to *Cd38* 3' UTR [Deshpande et al. 2017] and to change during adipogenesis [Goody et al. 2019]. During cold exposure, among the evaluated miRNAs, miR-140-3p expression is increased

in BAT (Fig 5F) and might account for CD38 downregulation and for its downstream metabolic consequences. The involvement of other miRNAs, beside miR-140-3p in cold-induced CD38 regulation cannot be excluded: indeed, it has been reported that different miRNAs regulate the browning process [Goody et al. 2019]. miRNAs are produced by the activity of the nuclear RNase III Drosha, together with its key cofactor Dgcr8: adipose tissue-specific Dgcr8 knockout mice exhibited decreased expression of genes characteristic of brown fat and were intolerant to cold exposure [Kim et al. 2014]. It would be also interesting to explore the possible involvement of cold shock proteins in the regulation of CD38 expression. Cold shock proteins are multifunctional RNA/DNA binding proteins, characterized by the presence of one or more cold shock domains, which regulates transcription, splicing and translation, as well as orchestration of exosomal RNA content [Lindquist et al. 2018]. Anyway, to the best of our knowledge, cold-induced thermogenesis in BAT and WAT is the first "physiological" stimulus inducing a decrease in CD38 expression. The fact that occurrence of CD38 in adipose tissue from cold-exposed mice is also due to a reduced number of infiltrating $CD38^+/CD45^+$ leukocytes (Fig 5B, C) may suggest that in obesity and/or obesity-related abnormal metabolism, the presence of inflammatory $CD38^+$ cells [Kusminski et al. 2016] might be responsible for interfering in the browning process. Interestingly, a study conducted on ferrets demonstrated that cold acclimation produces an inhibition of immune response-related pathways in perivascular adipose tissue, indicative of an anti-inflammatory response, that may be exploited for the enhancement/maintenance of cardiovascular health [Reynes et al. 2017]. Possibly, CD38 downregulation is also occurring in perivascular adipose tissue upon cold exposure, accounting for the regulation of CD38-controlled inflammatory processes. In parallel with the downregulation of CD38 expression, our study also unveiled the upregulation of NADK, the enzyme responsible for NAD^+ phosphorylation to $NADP^+$, occurring especially in WAT (Fig 8A, B) and leading to increased $NADP^+$ levels (Fig 7C). Intriguingly, the fact that NADK activity is upregulated upon cold exposure was reported long ago in winter rape plant [Maciejewska et al. 1990]. Few reports documented a regulation of NADK levels and activity in mammals. In WAT, *Nadk* mRNA levels are regulated by nutrition levels, with fasting increasing and a high-fat diet decreasing its levels [Zhang et al. 2013]. In this respect, a cold exposure might functionally mimic fasting in WAT, with WAT providing FA to the other organs. Upon cold exposure, also NADPH levels were increased in WAT (Fig 7D), likely as a consequence of increased $NADP^+$ availability (Fig 7C), and of the associated increased G6PD and malic enzyme expression (Fig 8E, G) and G6PD activity (Fig 8F). The specific increase in NADPH

was not reported to take place during cold exposure, although this likely supports fundamental biochemical processes during cold exposure and specifically lipid biosynthesis in WAT and thermogenesis in BAT [Mottillo et al. 2014, Hao et al. 2015]. Admittedly, the molecular mechanisms affecting *Nadk*, *G6pdx* and *malic enzyme (Me1)* expression, and thus the destiny of the NAD(P) pool to support FA synthesis and the metabolic hallmarks specific for BAT and WAT, remain to be defined. Expression of key enzymes in FA synthesis was indeed upregulated in iWAT upon cold exposure (Fig 8C, D). It is also of note that the cold-induced increase in NADPH is observed specifically in WAT but not in BAT, indicating the higher demand for NADPH as reductive power for anabolic processes important for vascularization and differentiation of adipocyte precursors observed during sustained cold exposure in WAT [Sheja et al. 2016].

Fig 17

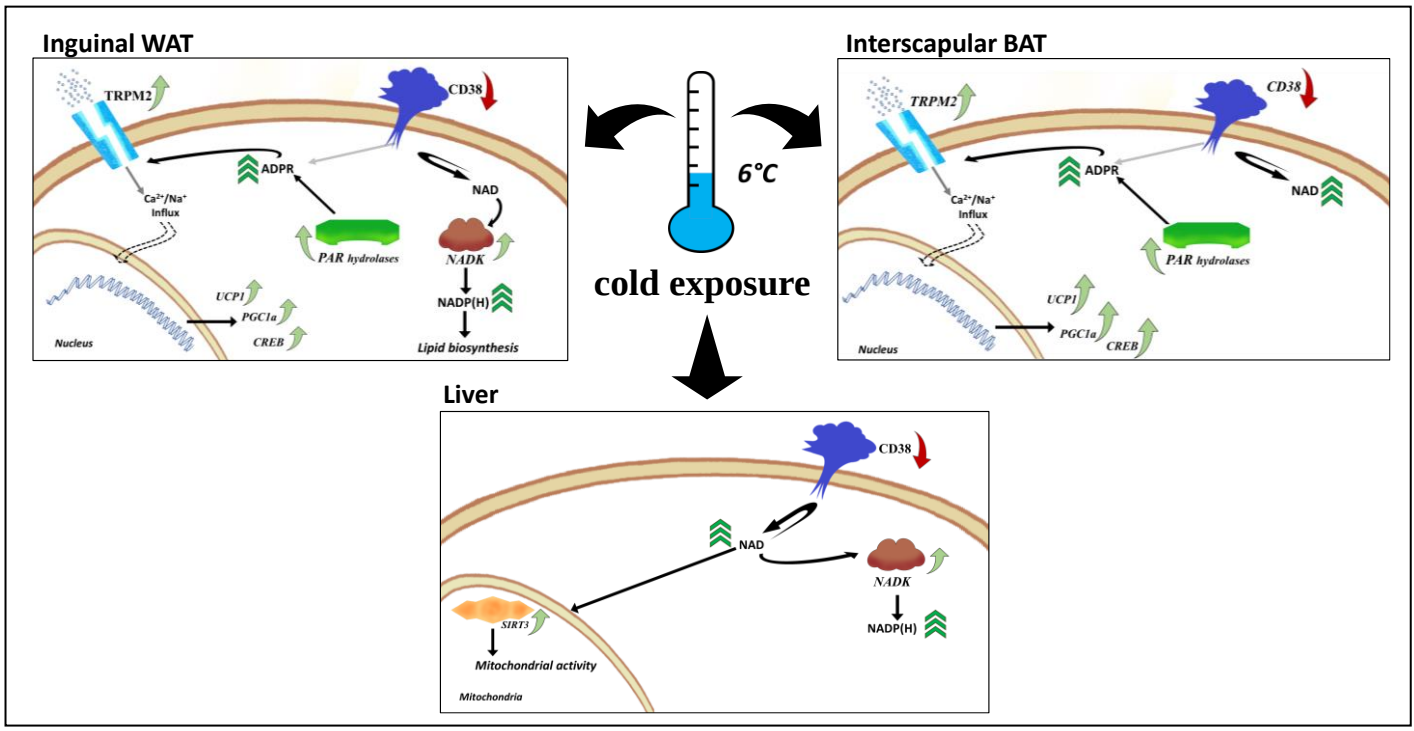

Fig. 17 Graphical rapresentation of NAD-related metabolism in thermogenic tissues during cold exposure.

Summary of the main regulations observed in white and brown adipose tissues (upper side) and liver (lower side) in C57BL/6J mice upon cold exposure: CD38 expression is downregulated, differently affecting NAD(P)(H) pools in the three tissues; conversely, TRPM2 expression and ADPR levels are upregulated in adipose tissues.

4.2 The role of CD38 in liver during thermogenesis

4.2.1 Thermogenesis and liver in WT mice

Besides adipose tissue, CD38 reduction occurred also in liver upon cold exposure (Fig 9H-J). Differently from WAT and BAT, CD38 downregulation in liver of WT mice determined not only an increment in $NAD^{+,}$ but also in NADH levels. This finding suggests that in liver, when energy expenditure is required, NAD^+ saved through CD38 suppression is rapidly reduced. As a consequence, NAD^+/NADH ratio decreased in liver when mice were exposed to cold for 24 h, compared with mice housed at 30°C (Fig 9A, B). In line with our result, Wei and coll. [Wei et al. 2020], performing a similar experiment, observed that cold exposure increases both NAD^+ and NADH levels in liver, and a strong statistical relevance occurred at day 2 of cold acclimation. However, they did not consider CD38 as the reason explaining the increment in NAD(H) levels, rather, they focused on an increased NAD^+ synthesis: NAMPT and NMNAT expression was unchanged after 24 h of cold exposure, as verified at the mRNA and protein levels, but was significantly upregulated after 48 h. In our study, we detected an increase in *Nampt* expression in liver upon 24 hours of cold exposure, that did not translate in a potentiated NAD^+ synthesis rate (Fig 9E, F). It has been observed in different conditions that a reduced ratio NAD^+/NADH is associated to numerous dysfunctions. First of all, high levels of NADH in mitochondria may lead to ROS production. Second, SIRT1 activity is slowed down by low NAD^+/NADH, driving to a reduced PGC-1α activity, that can be associated to a lower number of mitochondria. Nevertheless, in spite of the lower oxidized/reduced ratio, cold exposure led to a higher NAD(H) pool in terms of total amount (40% higher in liver of cold-exposed mice), and not merely to a change in oxidation state of the same pool amount. Possibly, this increment in NAD(H) pool is avoiding negative effect that would be expected with a low NAD^+/NADH ratio. Moreover, our results showed that cold exposure enhanced mitochondrial biogenesis, as determined by the higher levels of mt-DNA in liver of mice exposed to cold (Fig 12B).

A few studies investigated the effect of cold acclimation on the expression of enzymes involved in glucose and lipid metabolism, observing different and sometimes contradictory regulations. Here we reported a marked influence of cold exposure in the regulation of both glucose and lipid metabolism in liver. Our data suggest that glucose oxidation is not the main pathway utilized for energy production in liver of WT mice during thermogenesis. Indeed, in WT mice exposed to cold,

glycolysis appears to be reduced: *Pfk1* and *Gapdh* genes are downregulated (Fig 11A, B); LDH enzymatic activity is reduced (Fig 11C). On the contrary, gluconeogenesis seems to be promoted: *G6Pase* expression and enzymatic activity rise during thermogenesis (Fig 11D, E), likely to release glucose and sustain metabolic pathways in peripheral tissues. In line with this, we observed reduced hepatic G6P levels during thermogenesis in WT mice (Fig 11F), as well as reduced glycogen levels (Fig 11G), which also represents a source of glucose to be released.

Regarding hepatic lipid metabolism, we observed increased TGs upon cold stimulation (Fig 11H), but also a downregulation of *Fasn* gene expression (Fig 11K) occurring in WT mice, confirming previous observations by Wei and coll. and Grefhorst and coll. [Wei et al. 2020, Grefhorst et al. 2018]. Furthermore, we measured the level of acetylation of SOD, being $_{ac}SOD/SOD_{tot}$ regarded as a marker of SIRT3 activity: the activity of SIRT3, a sirtuin with mitochondrial localization, is enhanced upon cold exposure (Fig 12C). This cold-mediated SIRT3 activation has been previously reported to occur in BAT [Shi et al. 2005]. Being SIRT3 a well-known fatty acid oxidation (FAO) promoter, its activation suggests that higher hepatic TG levels observed in cold-exposed WT mice are not due to a slower lipid degradation. The higher hepatic TGs upon col exposure may be due to an accelerated uptake, as reported by Gefhorst and coll. [Gefhorst et al. 2018].

In addition to the NAD(H) pool, we measured $NADP^+$ and NADPH and the main enzymes involved in their metabolism. Differently from our results in WAT, $NADP^+$ pool was unchanged in liver of WT mice exposed to cold (Fig 9C). Despite a rather marked over-expression of *Nadk* mRNA, NADK enzymatic activity was only slightly (not significantly) increased by cold exposure (Fig 10A, B), indicating that post-transcriptional or post-translational regulations may suppress the activity that consuming NAD^+, produces $NADP^+$. Hypothetically, NADK activity may be repressed to avoid NAD^+ "waste" in this specific condition, when NAD^+ is necessary for SIRTs activity.

NADPH, the reduced $NADP^+$ form, allows ROS-removing processes and lipid synthesis. High mitochondrial activity produces a large amount of ROS, that must be metabolized to avoid excessive intracellular stress. In line with this, we observed that during thermogenesis, when ROS production is high [Chouchani et al 2016], NADPH levels were reduced in liver of WT mice, possibly to protect cells from ROS. Indeed, a previous study reported overexpression of glutathione peroxidase [Shore AM 2013]. Moreover, being the expression of enzymes involved in lipid synthesis repressed upon cold stimulation (Fig 11J, K), it is unlikely that our data reflect the NADPH utilization for lipid production. Cold exposure negatively regulated the expression of the two major $NADP^+$-reducing enzymes, *G6pdx* and *Me1* (Fig 10C, D), and the measurement of

G6PD total enzymatic activity confirmed the gene expression data (Fig 10E). The lower expression of G6PD and malic enzyme is in line with the lower NADPH observed (Fig 9D). In light of these results, we hypothesize that G6PD expression is reduced to avoid that G6P is directed towards the PPP pathway, when it must be instead dephosphorylated and used to release glucose, and lipid synthesis is not necessary. Curiously, the use of NADPH to counteract ROS production during cold appears then not to be sustained by a stronger $NADP^+$ reduction to NADPH. However, the present study was performed by exposing mice to cold for a rather short time: the influence of a longer cold exposure needs to be investigated to unveil whether NADPH-producing mechanisms begin to be promoted after 24 hours of cold stimulation.

In WAT undergoing beiging, G6PD expression is regulated differently than in liver: G6PD was increased in WAT, likely to sustain the promoted lipogenesis induced by cold exposure, when the NADPH demand rises. At the best of our knowledge, this is the first study reporting the effect of cold exposure in liver on NADP(H) pool and the main enzymes involved in their synthesis, unveiling a different modulation in different organs during thermogenic stimulation.

4.2.2 Thermogenesis and liver in Cd38$^{-/-}$ mice

Another key aspect in our project was the role of CD38 in adipose tissue and in liver. As already observed in adipose tissues, *Cd38* ablation drove to extremely high levels of NAD^+ and NADH also in liver. As a consequence, an alteration of the hepatic metabolic response of *Cd38*$^{-/-}$ mice may be expected.

The first difference observed in liver between WT and *Cd38*$^{-/-}$ mice, is that the glycolytic pathway was not modified by cold acclimation in *Cd38*$^{-/-}$ mice. As a matter of fact, we did not observe *Pfk1* and *Gapdh* down-modulation in liver of cold-exposed *Cd38*$^{-/-}$ mice (Fig 11A, B), differently from what we observed in WT mice. Indeed, expression of these two glycolytic enzymes was even slightly, but significantly, increased upon cold stimulation. In line with these data, LDH activity was not reduced, as instead occurred in liver of WT mice upon cold exposure (Fig 11C).

Furthermore, *Cd38*$^{-/-}$ mice exhibited only a very modest induction of *G6Pase* mRNA expression (Fig 11D), and the increment in G6Pase enzymatic activity was completely lost (Fig 11E). In addition, we observed higher glycogen levels in liver from *Cd38*$^{-/-}$ mice in comparison with WT mice, at 30°C (Fig 11G). However, cold exposure caused glycogen consumption at 6°C in *cd38*$^{-/-}$

as well. G6P levels breakdown during cold exposure, on the other hand, was not lost in *Cd38*$^{-/-}$ mice (Fig 11F).

Taken together our data suggest a role for CD38 in regulating glycolysis and gluconeogenesis in liver during thermogenesis. Previous studies investigated the effect of CD38 absence on glucagon-stimulated hepatic cells [Rah et al. 2015]: the Authors found a link between the NAD^+-derived, CD38-mediated Ca^{2+} signaling and glucagon-induced metabolic redirection towards gluconeogenesis. In their study, glucagon treatment induced the expression of enzymes that take part in gluconeogenesis, whereas CD38 inhibition or genetically depletion made the hepatic cells less sensible to the stimulation. Indeed, the levels of expression of *Pck1* gene (encoding for the gluconeogenic enzyme Phosphoenolpyruvate carboxykinase 1) were unchanged in glucagon-stimulated *Cd38*$^{-/-}$ hepatocytes. This result is in line with our data on the lack of stimulation of G6Pase upon cold exposure in *Cd38*$^{-/-}$ mice, and it may be also in agreement with the lower levels of glycerol observed in cold-stimulated *Cd38*$^{-/-}$ mice (Fig 11I). Indeed, glycerol can be produced through glyceroneogenesis, using the first steps of gluconeogenesis, and glycerol production seems to be reduced in *Cd38*$^{-/-}$ mice. In addition, Rah and coll. reported that *Cd38*$^{-/-}$ mice-derived hepatocytes displayed higher basal glycogen levels [Rah et al. 2015], in line with our data (Fig 11G). Overall, Rah and coll. ascribed the effects of the lack of CD38 to the impaired Ca^{2+} signalling. We suggest that (some) metabolic alterations observed in *Cd38*$^{-/-}$ mice could be also due to the strong impact of the lack of CD38 on the NAD(P)(H) pool. For instance, it has been reported that the NAD^+/NADH, give information regarding how glycolysis and gluconeogenesis are regulated: low NAD^+/NADH ratio is associated to a promoted gluconeogenesis [Toews et al. 1970, Sistare et al. 1985]. In our condition, NAD^+/NADH ratio decreases in WT mice during cold exposure, in line with a promoted gluconeogenesis. Instead, NAD^+/NADH ratio in *Cd38*$^{-/-}$ mice is not modified during thermogenesis, being higher than in cold-exposed WT mice. Thus, the altered NAD/NADH ratio in WT and *Cd38*$^{-/-}$ mice might be also responsible for the different regulation of glucose metabolism in hepatocytes, together with the different calcium signaling, during cold/glucagon stimulation.

Regarding hepatic lipid metabolism, as for WT, in *Cd38*$^{-/-}$ mice TGs levels rise, as well as *Fasn* and *Acaca* are decreased, after 24 hours of cold acclimation (Fig 11H, J, K).

Furthermore, our findings indicate that *Cd38*$^{-/-}$ mice have higher hepatic SIRT3 activity in basal conditions (Fig 12E), but cold exposure has no effect in modulating SIRT3 activity (Fig 12D): in other words, cold exposure *per se* has no effect on SIRT3 activity in *Cd38*$^{-/-}$ mice, in which NAD

levels are very high. This finding may suggest that availability of the substrate NAD^+ is the main regulator of SIRT3 activity. Chini and coll. already investigated SIRT3 regulation as a consequence of *Cd38* genetic ablation in 2016, although not in a thermogenic-stimulating experimental setting. In that study, they reported that the absence of CD38 leads to an enhanced SIRT3 total enzymatic activity. In addition, they demonstrated that upon boosting NAD^+ levels (obtained with exogenous NAD^+ supplementation), SIRT3 activity reaches the same peak of activity observed in *Cd38*$^{-/-}$ mice, which on the other hand, display an already high SIRT3 activity that cannot be further enhanced [Camacho-Pereira et al. 2016]. Thus, these data are in perfect agreement with our results, demonstrating that: cold exposure increases NAD^+ levels and enhances hepatic SIRT3 enzymatic activity (Fig 9A and Fig 12C); the basal SIRT3 activity in liver in *Cd38*$^{-/-}$ mice is comparable to that observed in WT mice stimulated by cold (Fig 12C, E); cold stimulus has no effect on SIRT3 activity in *Cd38*$^{-/-}$ mice (Fig 12D).

Being SIRT3 activity promoted upon cold exposure, it is conceivable to find a high number of mitochondria, ready to better handle fatty acids breakdown. Indeed, our results on mt-DNA suggest that cold exposure induces mitochondria generation in liver of WT mice (Fig 12B). A similar trend was observed in *Cd38*$^{-/-}$ mice (Fig 12B). Nevertheless, *Cd38*$^{-/-}$ mice display lower mt-DNA levels than WT, both at 30°C and at 6°C (Fig 12B). These data are in agreement with the study from Chini and coll., that reported higher mt-DNA levels in a cell line in which CD38 was overexpressed [Camacho-Pereira et al. 2016]. They discussed this finding as a kind of compensatory mechanism that, due to the low NAD^+ levels (as a consequence of CD38 overexpression), promotes mitochondrial biogenesis. On the contrary, we can speculate that being NAD(H) levels so high in *Cd38*$^{-/-}$ mice, mitochondrial biogenesis is suppressed to avoid a ROS overload in liver. Regarding the NAD phosphorylated pool in liver, $NADP^+$ levels were higher in *Cd38*$^{-/-}$ compared to WT mice at all temperatures, and they were not modified during thermogenesis (Fig 9C). In line with this, *Nadk* expression and enzymatic activity were not modulated in liver of *Cd38*$^{-/-}$ mice exposed to cold (Fig 10A, B). NADPH levels were higher in *Cd38*$^{-/-}$ mice in comparison with WT mice at all temperature (Fig 9D). However, cold exposure determines a NADPH decline also in *Cd38*$^{-/-}$ mice, reflecting the same trend observed in WT mice (Fig 9D). Accordingly, *G6pdx* and *Me1* genes, and G6PD enzymatic activity as well, were downmodulated mimicking the regulation observed in WT mice (Fig 10C, D, E). As previously discussed, being TGs synthesis suppressed during cold exposure, we suppose that NADPH decline

is likely a consequence of the promoted ROS production, and at the same time is surely caused by a drastic reduction in the NADPH synthetizing enzymes.

4.3 The role of TRPM2 in WAT and BAT during thermogenesis

The last goal of the study was to evaluate the impact of *Trpm2* ablation in WAT and BAT during thermogenesis. As already mentioned above, CD38 enzymatic activity generates ADPR, the main TRPM2 agonist. For this reason, CD38 and TRPM2 are linked through a wire that put CD38 in the context of calcium homeostasis. Thus, mice lacking *Trpm2* allowed us to clarify whether the results obtained from *Cd38*$^{-/-}$ mice in adipose tissues are a consequence, not only of an altered NAD^+ metabolism, but also of an altered calcium homeostasis.

The role of TRPs channels in adipose tissue metabolism has been extensively studied in the last two decades. TRPV1, is a calcium channel activated by capsaicin and, when activated by agonists, prevents obesity induces by HFD: the effect was abolished in mice lacking this channel [Lee et al. 2015]. In addition, dietary TRPV1 activators are involved in adrenaline secretion from the nervous system, thus enhancing WAT beiging and in turn, energy expenditure [Ohyama et al. 2016]. On the contrary, TRPV4 seems to play a detrimental role in thermogenesis. Indeed, the expression of browning markers Pgc1a and Ucp1 is promoted upon TRPV4 suppression [Ye et al. 2012]. In addition, mice lacking TRPV4 are resistant to HFD-induced obesity [Kusudo et al. 1985]. Anyhow, the most studied TRP channel in the context of adipose tissue and thermogenesis is TRPM8. As a thermoreceptor, this channel is activated not only by cold-mimicking compounds (such as menthol and icilin), but also by cold temperature [Liu et al. 2020]. Different studies reported that TRPM8 activation through menthol administration *in vitro* enhances UCP1 expression, mitochondrial activation and heat production, and thus promotes WAT beiging and BAT activation [Khare et al. 2018, Ma et al. 2012, Jiang et al. 2017, Sanders et al. 2021, Rossato et al. 2014]. Furthermore, *in vivo* dietary menthol supplementation reduces insulin resistance and ameliorates HFD-induced obesity [Jiang et al. 2017, Ma et al. 2012].

Thus, since a number of calcium channel are involved in WAT beiging and BAT activation, it is reasonable to suppose that also TRPM2 may play a role. However, our data on the role of CD38 during thermogenesis in adipose tissue indicate that mice lacking *Cd38* exhibit enhanced thermogenesis, as measured by the expression of the two main browning markers (Fig 1A-D). Hence, it would be reasonable to hypothesize that ADPR-induced TRPM2 signaling could be

detrimental for the induction of the thermogenic program in adipose tissue. Instead, our data did not confirm this hypothesis. Indeed, mice lacking *Trpm2* exhibit lower respiration rate and reduced energy expenditure when thermogenesis is stimulated both by cold temperature and by β3-adrenergic receptor activation (Fig 13). In addition, gene expression analyses confirmed that the browning process is reduced in WAT (Fig 13D, E, F) and BAT (Fig 13A, B, C) in *Trpm2*$^{-/-}$ mice upon 24 h of cold exposure, confirming that TRPM2 takes part in the thermogenic response as one of the major players. Notably, *Trpm2* overexpression occurs also in mice lacking *Cd38* (Fig 15B), suggesting that the two regulations occur independently. Furthermore, the increased expression of TRPM2 in WAT and BAT upon short-term cold exposure suggests that, when energy expenditure is required, white and brown adipocytes promote the production of this channel because of its pivotal role (Fig 15A, C). Usually, TRPM2 activation is considered as downstream to the CD38-mediated production of ADPR. Instead, in thermogenesis, CD38 and TRPM2 are regulated in opposite directions: TRPM2 is overexpressed, whereas CD38 is downregulated (see above). Being CD38 one of the major ADPR producers, its reduced expression could be associated with reduced ADPR levels and, as a consequence, lower TRPM2 activation. Instead, we observed that ADPR levels rise in WAT and BAT when WT mice are exposed to cold, i.e. when CD38 is down-regulated (Fig 15D, E). Moreover, ADPR levels were increased also in BAT of *Cd38*$^{-/-}$ mice (Fig 15E). These findings unveil for the first time that ADPR is likely pivotal in the activation of the thermogenic program in WAT and BAT, possibly by regulating cytosolic Ca^{2+} levels. Our data demonstrate that CD38 is not the enzyme producing ADPR upon cold exposure and suggest that the hydrolysis of poly-ADPR polymers may represent pathway that provides free ADPR to sustain TRPM2 activation (Fig 16). Hence, our project proposes for the first time a metabolic link between poly-ADPR hydrolyses and TRPM2 activation. Previous studies reported alternative TRPM2 activation pathways that do not involve CD38 activity: 2'-O-Acetyl-ADPR (OAADPR) generated by SIRT2 and SIRT3 is able to mediate TRPM2 gating [Grubisha et al. 2006]; OAADPR and/or ADPR produced by SIRT6 regulates TRPM2 gating, that in turn, promotes the release of pro-inflammatory cytokines and pancreatic cell migration [Bauer et al. 2012].

On the other hand, Park and coll. suggested the role of PARPs in TRPM2 activation during high oxidative stress, investigated this mechanism in the context of Alzheimer Disease. They unveiled that Amyloid-beta-induced oxidative stress determines a neurovascular dysfunction through TRPM2 overactivation: TRPM2 inhibition was proposed as a therapeutic target for future clinical treatment [Park et al. 2014].

Regarding the role of PARPs in adipose tissue, PARP1 and 2 inhibition showed a positive effect on energy metabolism, being, PARP1 suppression associated to higher SIRT1 activity, leading to higher energy expenditure and increased mitochondrial activity [Bai et al. 2011]. In line with this, *Parp2* genetic ablation increased energy expenditure in mice and promoted mitochondrial biogenesis in different tissues, including BAT. This is due to the negative effect exherted by PARP2 on *Sirt1* promoters, that suppress its expression [Bai et al 2011].
To the best of our knowledge, our study is the first one reporting an overexpression of the poly-ADPR, as well as mono-ADPR hydrolases, in association to WAT browning, BAT activation, revealing ADPR increase and TRPM2 overexpression.

In conclusion, our project provided important findings regarding NAD^+ and its metabolism during cold acclimation in mammals. The results presented in my thesis are very interesting considering that numerous groups are currently working on NAD^+ and trying to find out innovative strategies to increase its intracellular levels, for the treatment of several pathological conditions. The fact that cold-induced thermogenesis leads to a lower NAD^+ degradation in adipose tissue and liver may unveil a further benefit of this approach, which is under investigation for the amelioration of different dysmetabolisms. Moreover, since *Cd38*$^{-/-}$ mice are able to sustain an enhanced BAT activation and WAT beiging upon cold stimulation, NAD^+ availability seems to be a factor limiting these processes. Indeed, the phenotype we observed in *Cd38*$^{-/-}$ mice upon cold stimulation, is not to be ascribed to the impaired activation of TRPM2 channel, since the lack of TRPM2 leads to a reduced WAT beiging and BAT activation.
Further studies are required to investigate whether pharmacological modulation of NAD^+ levels, for instance by administration of precursors, or of TRPM2 activation, represents new therapeutic strategies for the treatment of the metabolic diseases, aimed at improving WAT beiging and BAT functions.

Abbreviations

2dADPR: 2’-deoxy-ADPR

ACACA: acetyl-CoA carboxylase 1

ADPR: ADP-ribose

ADPRS: ADP-ribose glycohydrolase

ATGL: adipose triglyceride lipase

ATP: adenosine triphosphate

BAs: bile acids

BAT: brown adipose tissue

BV: brillant violet

cADPR: cyclic ADPR

cAMP: cyclic AMP

cGDPR: cyclic GDP-ribose

CREB: cAMP responsive element-binding protein

DIO2: iodothyronine Deiodinase 2

EE: energy expenditure

eNAMPT: extracellular NAMPT

FASN: fatty acid synthase

FFA: free fatty acids

FGF21: fibroblast grow factor 21

G6P: glucose-6 phosphate

G6pase: glucose-6 phosphate phosphatase

G6PD: glucose-6 phosphate dehydrogenase

GAPDH: glyceraldehyde-3-phosphate dehydrogenase

HFD: high fat diet

HIF-1a: hypoxia-inducible factor 1-alpha

HSL: hormone sensitive lipase

iBAT: interscapular BAT

IL-1: interleukin-1

IL-6: interleukin-6

iNAMPT: intracellular NAMPT

iWAT: inguinal WAT

LDL: low density lipoprotein

LPL: lipoprotein lipase

Me1: malic enzyme

MGL: monoacylglycerol lipase

mt-DNA: mitochondrial-DNA

NA: nicotinic acid

NaAD: nicotinic acid adenine dinucleotide

NAADP: nicotinic acid adenine dinucleotide phosphate

NAD: nicotinamide adenine dinucleotide

NAD^+-ase: NAD^+-glycohydrolases

NADH: nicotinamide adenine dinucleotide (reduced form)

NADK: NAD^+ kinase

NADP: nicotinamide adenine dinucleotide phosphate

NADPH: nicotinamide adenine dinucleotide phosphate (reduced form)

NAFLD: nonalcoholic fatty liver diseases

NAM: nicotinamide

NaMN: nicotinic acid mononucleotide

NAMPT: nicotinamide phosphoribosyltransferase

NAOH: sodium hydroxide

NAPRT: nicotinate phosphoribosyltransferase

NE: norepinephrine

NEFAs: non-esterified fatty acids

NGD: nicotinamide guanine dinucleotide

NMN: nicotinamide mononucleotide

NMNAT: nicotinamide/nicotinic acid mononucleotide adenylyltransferase

NMNH: nicotinamide mononucleotide (reduced form)

NO: nitric oxide

NR: nicotinamide riboside

NRH: nicotinamide riboside (reduced form)

OAADPR: 2'-O-Acetyl-ADPR

OARD: O-acyl-ADP-ribose deacylase 1

PARG: poly (ADP-ribose) glycohydrolase

PARPs: poly ADP-ribose polymerases

PCA: perchloric acid

PCK1: phosphoenolpyruvate carboxykinase 1

PDH: pyruvate dehydrogenase

PerCPCy: Peridinin Chlorophyll Protein Complex-cyanin

PFK1: phosphofructokinase 1

PGC-1a: peroxisome proliferator-activated receptor-gamma coactivator-1alpha

PKA: protein kinase A

PPAR: peroxisome proliferator-activated receptor

PRPP: phosphoribosyl pyrophosphate

RER: respiratory exchange ratio

ROS: reactive oxygen species

RT-PCR: real-time PCR

SERCA2b: sarco-Endoplasmic Reticulum Calcium ATPase 2b

SIRTs: sirtuins

SNS: sympathetic nervous system

SOD2: superoxide dismutase 2

T2D: type 2 Diabetes

T3: 3,3',5-triiodothyronine

T4: 3,3',5,5' tetraiodothyroxyne

TBP: TATA-binding protein

TGs: triglycerides

TNFα: tumor necrosis factor-alpha

TRPM2: the transient receptor potential melastatin 2

UCP1: uncoupling protein 1

VEGF: vascular endothelial grow factor

VLDL very low-density lipoprotein

WAT: white adipose tissue

References

- Abdullah A, Peeters A, de Courten M, Stoelwinder J. (2010) The magnitude of association between overweight and obesity and the risk of diabetes: a meta-analysis of prospective cohort studies. Diabetes Res Clin Pract. 89: 309–19.

- Abumrad NA. (2017) The Liver as a Hub in Thermogenesis. Cell Metab. 26: 454-5.

- Admiraal WM, Holleman F, Bahler L, Soeters MR, Hoekstra JB, Verberne JH. (2013) Combining 123I-metaiodobenzylguanidine SPECT/CT and 18F-FDG PET/CT for the assessment of brown adipose tissue activity in humans during cold exposure. Nucl Med. 54: 208-12.

- Adya R, Tan B K, Punn A, Chen J, Randeva H S. (2007) Visfatin induces human endothelial VEGF and MMP-2/9 production via MAPK and PI3K/Akt signalling pathways: novel insights into visfatin-induced angiogenesis. Cardiovasc Res. 78: 356-65.

- Ahmadian M, Suh JM, Hah N, Liddle C, Atkins AR, Downes M, Evans RM. (2013) PPARγ signaling and metabolism: the good, the bad and the future. Nat Med. 19: 557-66.

- Asano A, Irie Y, Saito M. (2001) Isoform-specific regulation of vascular endothelial growth factor (VEGF) family mRNA expression in cultured mouse brown adipocytes. Molecular Cell Endocrinol. 174: 71-6.

- Audrito V, Messana VG, Deaglio S. (2020) NAMPT and NAPRT: Two Metabolic Enzymes with key roles in inflammation. Front Oncol. 10: 358.

- Bai P, Canto C, Brunyánszki A, Huber A, Szántó M, Cen Y, Yamamoto H, Houten SM, Kiss B, Oudart H, Gergely P, Menissier-de Murcia J, Schreiber V, Sauve AA, Auwerx J. (2011) PARP-2 regulates SIRT1 expression and whole-body energy expenditure. Cell Metab.13: 450-60.

- Bai P, Cantó C, Oudart H, Brunyánszki A, Cen Y, Thomas C, Yamamoto H, Huber A, Kiss B, Houtkooper RH, Schoonjans K, Schreiber V, Sauve AA, Menissier-de Murcia J, Auwerx J. (2011) PARP-1 inhibition increases mitochondrial metabolism through SIRT1 activation. Cell Metab. 13: 461-8.

- Barbosa MT, Soares SM, Novak CM, Sinclair D, Levine JA, Aksoy P, Chini EN. (2007) The enzyme CD38 (a NAD glycohydrolase, EC 3.2.2.5) is necessary for the development of diet-induced obesity. FASEB J. 21: 3629–39.

- Bartelt A, Heeren J. (2014) Adipose tissue browning and metabolic health. Nat Rev Endocrinol. 10: 24–36.

- Basile G, Taglialatela-Scafati O, Damonte G, Armirotti A, Bruzzone S, Guida L, Franco L, Usai C, Fattorusso E, De Flora A, Zocchi E. (2005) ADP-ribosyl cyclases generate two unusual adenine homodinucleotides with cytotoxic activity on mammalian cells. Proc Natl Acad Sci USA. 102: 14509-14.

- Bastard JP, Maachi M, Van Nhieu JT, Jardel C, Bruckert E, Grimaldi A, Robert JJ, Capeau J, Hainque B. (2002) Adipose tissue IL-6 content correlates with resistance to insulin activation of glucose uptake both in vivo and in vitro. J Clin Endocrinol Metab. 87: 2084–9.

- Bauer I, Grozio A, Lasigliè D, Basile G, Sturla L, Magnone M, Sociali G, Soncini D, Caffa I, Poggi A, Zoppoli G, Cea M, Feldmann G, Mostoslavsky R, Ballestrero A, Patrone F, Bruzzone S, Nencioni A. (2012) The NAD+-dependent histone deacetylase SIRT6 promotes cytokine production and migration in pancreatic cancer cells by regulating Ca^{2+} responses. J Biol Chem. 287: 40924– 37.

- Becher T, Palanisamy S, Kramer DJ, Eljalby M, Marx SJ, Wibmer AG, Butler SD, Jiang CS, Vaughan R, Schöder H, Mark A, Cohen P. (2021) Brown adipose tissue is associated with cardiometabolic health. Nat Med. 27: 58–65.

- Beck A, Kolisek M, Bagley LA, Fleig A, Penner R. (2006) Nicotinic acid adenine dinucleotide phosphate and cyclic ADP-ribose regulate TRPM2 channels in T lymphocytes. FASEB J. 20: 962–4.

- Belenky P, Bogan KL, Brenner C. (2007) NAD+ metabolism in health and disease. Trends in Biochemical Sciences. 32: 12-9.

- Bertolotti M, Lonardo A, Mussi C, Baldelli E, Pellegrini E, Ballestri S, Romagnoli D, Loria P. (2014) Nonalcoholic fatty liver disease and aging: epidemiology to management. World J Gastroenterol. 20: 14185-204.

- Bing C. (2015) Is interleukin-1β a culprit in macrophage-adipocyte crosstalk in obesity? Adipocyte. 4: 149-52.

- Bolsoni-Lopes A, Alonso-Vale MI. (2015) Lipolysis and lipases in white adipose tissue – An update. Arch Endocrinol Metab. 59:335-42.

- Braidy N, Guillemin GJ, Mansour H, Chan-Ling T, Poljak A, Grant R. (2011) Age related changes in NAD+ metabolism oxidative stress and Sirt1 activity in wistar rats. PLoS ONE. 6: e19194.

- Brandão BB, Poojari A, Rabiee A. (2021) Thermogenic Fat: Development, Physiological Function, and Therapeutic Potential. Int J Mol Sci. 22: 5906.

- Bruzzone S, De Flora A, Usai C, Graeff R, Lee HC. (2003) Cyclic ADP-ribose is a second messenger in the lipopolysaccharide-stimulated proliferation of human peripheral blood mononuclear cells. Biochem J. 375: 395–403.

- Bruzzone S, Fruscione F, Morando S, Ferrando T, Poggi A, Garuti A, D'Urso A, Selmo M, Benvenuto F, Cea M, Zoppoli G, Moran E, Soncini D, Ballestrero A, Sordat B, Patrone F, Mostoslavsky R, Uccelli A, Nencioni A. (2009) Catastrophic NAD+ depletion in activated T lymphocytes through Nampt inhibition reduces demyelination and disability in EAE. PLoS One. 4: e7897.

- Bruzzone S, Moreschi I, Usai C, Guida L, Damonte G, Salis A, Scarfì S, Millo E, De Flora A, Zocchi E. (2007) Abscisic acid is an endogenous cytokine in human granulocytes with cyclic ADP-ribose as second messenger. Proc Natl Acad Sci USA. 104: 5759-64.

- Burhans MS, Hagman DK, Kuzma JN, Schmidt KA, Kratz M. (2018) Contribution of adipose tissue inflammation to the development of type 2 diabetes mellitus. Compr Physiol. 9: 1–58.

- Byrne CD, Targher G. (2015) NAFLD: a multisystem disease. J Hepatol. 62: S47-64.

- Camacho-Pereira J, Tarragó MG, Chini CCS, Nin V, Escande C, Warner GM, Puranik AS, Schoon RA, Reid JM, Galina A, Chini EN. (2016) CD38 Dictates Age-Related NAD Decline and Mitochondrial Dysfunction through an SIRT3-Dependent Mechanism. Cell Metab. 23: 1127-39.

- Chait A, den Hartigh LJ. (2020) Adipose Tissue Distribution, Inflammation and Its Metabolic Consequences, Including Diabetes and Cardiovascular Disease. Front Cardiovasc Med. 7: 22.

- Chang SH, Song NJ, Choi JH, Yun UJ, Park KW. (2019) Mechanisms underlying Ucp1 dependent and independent adipocyte thermogenesis. Obes Rev. 20: 241-51.

- Chang YH, Chang DM, Lin KC, Shin SJ, Lee YJ. (2011) Visfatin in overweight/obesity, type 2 diabetes mellitus, insulin resistance, metabolic syndrome and cardiovascular diseases: a meta-analysis and systemic review. Diabetes Metab Res Rev. 27: 515-27.

- Chini CCS, Peclat TR, Warner GM, Kashyap S, Espindola-Netto JM, de Oliveira GC, Gomez LS, Hogan KA, Tarragó MG, Puranik AS, Agorrody G, Thompson KL, Dang K, Clarke S, Childs BG, Kanamori KS, Witte MA, Vidal P, Kirkland AL, De Cecco M, Chellappa K, McReynolds MR, Jankowski C, Tchkonia T, Kirkland JL, Sedivy JM, van Deursen JM, Baker DJ, van Schooten W, Rabinowitz JD, Baur JA, Chini EN. (2020) CD38 ecto-enzyme in immune cells is induced during aging and regulates NAD(+) and NMN levels. Nat Metab. 2: 1284–304.

- Chini EN, Chini CCS, Espindola Netto JM, de Oliveira GC, van Schooten W. (2018) The Pharmacology of CD38/NADase: An Emerging Target in Cancer and Diseases of Aging. Trends Pharmacol Sci. 39: 424–36.

- Chouchani ET, Kazak L, Jedrychowski MP, Lu GZ, Erickson BK, Szpyt J, Pierce KA, Laznik-Bogoslavski D, Vetrivelan R, Clish CB, Robinson AJ, Gygi SP, Spiegelman BM. (2016) Mitochondrial ROS regulate thermogenic energy expenditure and sulfenylation of UCP1. Nature. 532: 112-6.

- Cinti S. (2018) Pink Adipocytes. Trends Endocrinol Metab. 29: 651-66.

- Corrêa LH, Heyn GS, Magalhaes KG. (2019) The Impact of the Adipose Organ Plasticity on Inflammation and Cancer Progression. Cells. 8: 662.

- Covarrubias AJ, Kale A, Perrone R, Lopez-Dominguez JA, Pisco AO, Kasler HG, Schmidt MS, Heckenbach I, Kwok R, Wiley CD, Wong HS, Gibbs E, Iyer SS, Basisty N, Wu Q, Kim IJ, Silva E,

Vitangcol K, Shin KO, Lee YM, Riley R, Ben-Sahra I, Ott M, Schilling B, Scheibye-Knudsen M, Ishihara K, Quake SR, Newman J, Brenner C, Campisi J, Verdin E.* (2020) Senescent cells promote tissue NAD+ decline during ageing via the activation of CD38+ macrophages. Nat Metab. 2: 1265-83.

- Covarrubias AJ, Perrone R, Grozio A, Verdin E. (2021) NAD+ metabolism and its roles in cellular processes during ageing. Nat Rev Mol Cell Biol. 22: 119–41.

- Cypess AM, Lehman S, Williams G, Tal I, Rodman D, Goldfine AB, Kuo FC, Palmer EL, Tseng YH, Doria A, Kolodny GM, Kahn CR. (2009) Identification and importance of brown adipose tissue in adult humans. N Engl J Med. 360: 1509–1517.

- De Flora A, Guida L, Franco L, Zocchi E, Bruzzone S, Benatti U, Damonte G, Lee HC. (1997) CD38 and ADP-ribosyl cyclase catalyze the synthesis of a dimeric ADP-ribose that potentiates the calcium-mobilizing activity of cyclic ADP-ribose. J Biol Chem. 272: 12945-51.

- Deaglio S, Robson SC. (2011) Ectonucleotidases as regulators of purinergic signaling in thrombosis, inflammation, and immunity. Adv Pharmacol. 61: 301–32.

- Deshpande DA, Guedes AGP, Lund FE, Subramanian S, Walseth TF, Kannan MS. (2017) CD38 in the pathogenesis of allergic airway disease: Potential therapeutic targets. Pharmacol Ther. 172: 116–26.

- Dileepan M, Jude JA, Rao SP, Walseth TF, Panettieri RA, Subramanian S, Kannan MS. (2014) MicroRNA-708 regulates CD38 expression through signaling pathways JNK MAP kinase and PTEN/AKT in human airway smooth muscle cells. Respir Res. 31: 107.

- Dileepan M, Jude JA, Rao SP, Walseth TF, Panettieri RA, Subramanian S, Kannan MS. (2017) CD38 in the pathogenesis of allergic airway disease: potential therapeutic targets. Pharmacol Ther. 172: 116–26.

- Eichmann TO, Kumari M, Haas JT, Farese Jr. RV, Zimmermann R, Lass A, and Zechner R. (2012) Studies on the Substrate and Stereo/Regioselectivity of Adipose Triglyceride Lipase, Hormone-sensitive Lipase, and Diacylglycerol-O-acyltransferases, J Biol Chem. 287: 41446–57.

- Escande C, Nin V, Price NL, Capellini V, Gomes AP, Barbosa MT, O'Neil L, White TA, Sinclair DA, Chini EN. (2013) Flavonoid apigenin is an inhibitor of the NAD+ ase CD38: Implications for cellular NAD+ metabolism, protein acetylation, and treatment of metabolic syndrome. Diabetes. 62: 1084–93.

- Fenzl A, Kiefer FW. (2014) Brown adipose tissue and thermogenesis. Horm Mol Biol Clin Investig. 19: 25-37.

- Fisher FM, Kleiner S, Douris N, Fox EC, Mepani RJ, Verdeguer F, Wu J, Kharitonenkov A, Flier JS, Maratos-Flier E, Spiegelman BM. (2021) FGF21 regulates PGC-1α and browning of white adipose tissues in adaptive thermogenesis. Genes & Dev. 26: 271-81.

- Flegal KM, Kruszon-Moran D, Carroll MD, Fryar CD, Ogden CL. (2016) Trends in Obesity Among Adults in the United States, 2005 to 2014. JAMA. 315: 2284-91.

- Fliegert R, Bauche A, Wolf Pérez AM, Watt JM, Rozewitz MD, Winzer R, Janus M, Gu F, Rosche A, Harneit A, Flato M, Moreau C, Kirchberger T, Wolters V, Potter BVL, Guse AH. (2017) 2'-Deoxyadenosine 5'-diphosphoribose is an endogenous TRPM2 superagonist. Nat Chem Biol. 13: 1036-44.

- Fonfria E, Murdock PR, Cusdin FS, Benham CD, Kelsell RE, McNulty S. (2006) Tissue distribution profiles of the human TRPM cation channel family. J Recept Signal Transduct Res.;26: 159-78.

- Franco L, Bruzzone S, Song P, Guida L, Zocchi E, Walseth TF, Crimi E, Usai C, De Flora A & Brusasco V. (2001) Extracellular cyclic ADP-ribose potentiates ACh-induced contraction in bovine tracheal smooth muscle. Am J Physiol. 280: L98-L106.

- Fried SK, Bunkin DA, Greenberg AS. (1998) Omental and subcutaneous adipose tissues of obese subjects release interleukin-6: depot difference and regulation by glucocorticoid. J Clin Endocrinol Metab. 83: 847–50.

- Fu X, Deja S, Kucejova B, Duarte JAG, McDonald JG, Burgess SC. (2019) Targeted Determination of Tissue Energy Status by LC-MS/MS. Anal Chem. 91: 5881–7.

- Gao M, Du Y, Xie JW, Xue J, Wang YT, Qin L, Ma MM, Tang YB, Li XY. (2018) Redox signal-mediated TRPM2 promotes Ang II-induced adipocyte insulin resistance via Ca^{2+}-dependent CaMKII/JNK cascade. Metabolism. 85: 313-24.

- Giordano A, Smorlesi A, Frontini A, Barbatelli G, Cinti S. (2014) White, brown and pink adipocytes: the extraordinary plasticity of the adipose organ. Eur J Endocrinol. 170: R159-71.

- Giralt M, Villarroya F. (2013) White, Brown, Beige/Brite: Different Adipose Cells for Different Functions? Endocrinology. 154: 2992–3000.

- Goody D, Pfeifer A. (2019) MicroRNAs in brown and beige fat. Biochim Biophys Acta Mol Cell Biol Lipids. 1864: 29–36.

- Graeff RM, Walseth TF, Fryxell K, Branton WD, Lee HC. (1994) Enzymatic synthesis and characterizations of cyclic GDP-ribose. A procedure for distinguishing enzymes with ADP-ribosyl cyclase activity. J Biol Chem. 269: 30260–7.

- Grefhorst A, van den Beukel JC, Dijk W, Steenbergen J, Voortman GJ, Leeuwenburgh S, Visser TJ, Kersten S, Friesema ECH, Themmen APN, Visser JA. (2018)9 Multiple effects of cold exposure on livers of male mice. J Endocrinol. 238: 91-106.

- Grozio A, Sociali G, Sturla L, Caffa I, Soncini D, Salis A, Raffaelli N, De Flora A, Nencioni A, Bruzzone S. (2013) CD73 protein as a source of extracellular precursors for sustained NAD+ biosynthesis in FK866-treated tumor cells. J Biol Chem. 288: 25938–49.

- Grubisha O, Rafty LA, Takanishi CL, Xu X, Tong L, Perraud AL, Scharenberg AM, Denu JM. (2006) Metabolite of SIR2 reaction modulates TRPM2 ion channel. J Biol Chem. 281: 14057-65.

- Guse AH. (2005) Second messenger function and the structure-activity relationship of cyclic adenosine diphosphoribose (cADPR). FEBS J. 272: 4590–7.

- Guse AH, Diercks BP. (2018) Integration of nicotinic acid adenine dinucleotide phosphate (NAADP)-dependent calcium signalling. J Physiol. 596: 2735–43.

- Hankir MK, Klingenspor M. (2018) Brown adipocyte glucose metabolism: a heated subject. EMBO Rep. 19: e46404

- Hao Q, Yadav R, Basse AL, Petersen S, Sonne SB, Rasmussen S, Zhu Q, Lu Z, Wang J, Audouze K, Gupta R, Madsen L, Kristiansen K, Hansen JB. (2015) Transcriptome profiling of brown adipose tissue during cold exposure reveals extensive regulation of glucose metabolism. Am J Physiol Endocrinol Metab. 308: E380-E392.

- Hirschey MD, Shimazu T, Goetzman E, Jing E, Schwer B, Lombard DB, Grueter CA, Harris C, Biddinger S, Ilkayeva OR, Stevens RD, Li Y, Saha AK, Ruderman NB, Bain JR, Newgard CB, Farese RV Jr, Alt FW, Kahn CR, Verdin E. (2010) Nature. 464: 121-5.

- Hogan KA, Chini CCS, Chini EN. (2019) The Multi-faceted Ecto-enzyme CD38: Roles in Immunomodulation, Cancer, Aging, and Metabolic Diseases. Front Immunol. 10: 1187.

- Hondares E, Iglesias R, Giralt A, Gonzalez F J, Giralt M, --Mampel T, Villarroya F. (2011) Thermogenic activation induces FGF21 expression and release in brown adipose tissue. J Biol Chem. 286: 12983-90.

- Hotamisligil GS, Arner P, Caro JF, Atkinson RL, Spiegelman BM. (1995) Increased adipose tissue expression of tumor necrosis factor-alpha in human obesity and insulin resistance. J Clin Invest. 95: 2409–15.

- Howard M, Grimaldi JC, Bazan JF, Lund FE, Santos-Argumedo L, Parkhouse RM, Walseth TF, Lee HC. (1993) Formation and hydrolysis of cyclic ADP-ribose catalyzed by lymphocyte antigen CD38. Science. 262: 1056–9.

- Ikeda K, Maretich P, Kajimura S. (2018) The Common and Distinct Features of Brown and Beige Adipocytes. Trends in Endocrinology & Metabolism. 29: 191-200.

- Ishii M, Shimizu S, Hara Y, Hagiwara T, Miyazaki A, Mori Y, Kiuchi Y. (2006) Intracellular-produced hydroxyl radical mediates H_2O_2-induced Ca^{2+} influx and cell death in rat beta-cell line RIN-5F. Cell Calcium. 39: 487-94.

- Jiang C, Zhai M, Yan D, Li D, Li C, Zhang Y, Xiao L, Xiong D, Deng Q, Sun W. (2017) Dietary menthol-induced TRPM8 activation enhances WAT "browning" and ameliorates diet-induced obesity. Oncotarget. 8: 75114-26.

- Jude JA, Dileepan M, Subramanian S, Solway J, Panettieri RA Jr, Walseth TF, Kannan MS. (2012) miR-140-3p regulation of TNFα-induced CD38 expression in human airway smooth muscle cells. Am J Physiol Lung Cell Mol Physiol. 303: L460–L468.

- Jung SM, Sanchez-Gurmaches J, Guertin DA. (2019) Brown Adipose Tissue Development and Metabolism. Handb Exp Pharmacol. 251: 3-36.

- Kahn SE, Hull RL, Utzschneider KM. (2006) Mechanisms linking obesity to insulin resistance and type 2 diabetes. Nature. 444: 840-6.

- Kendrick AA, Choudhury M, Rahman SM, McCurdy CE, Friederich M, Van Hove JL, Watson PA, Birdsey N, Bao J, Gius D, Sack MN, Jing E, Kahn CR, Friedman JE, Jonscher KR. (2011) Fatty liver is associated with reduced SIRT3 activity and mitochondrial protein hyperacetylation. Biochem J. 433: 505–14.

- Khare P, Mangal P, Baboota RK, Jagtap S, Kumar V, Singh DP, Boparai RK, Sharma SS, Khardori R, Bhadada SK, Kondepudi KK, Chopra K, Bishnoi M. (2018) Involvement of Glucagon in Preventive Effect of Menthol Against High Fat Diet Induced Obesity in Mice. Front Pharmacol. 9: 1244.

- Kim HJ, Cho H, Alexander R, Patterson HC, Gu M, Lo KA, Xu D, Goh VJ, Nguyen LN, Chai X, Huang CX, Kovalik JP, Ghosh S, Trajkovski M, Silver DL, Lodish H, Sun L. (2014) MicroRNAs are required for the feature maintenance and differentiation of brown adipocytes. Diabetes. 63: 4045-56.

- Kim SY, Cho BH, Kim UH. (2010) CD38-mediated Ca^{2+} signaling contributes to angiotensin II-induced activation of hepatic stellate cells: attenuation of hepatic fibrosis by CD38 ablation. J Biol Chem. 285: 576-82.

- Konen JM, Fradette JJ, Gibbons DL. (2019) The Good, the Bad and the Unknown of CD38 in the Metabolic Microenvironment and Immune Cell Functionality of Solid Tumors. Cells. 9: 52.

- Kotzbeck P, Giordano A, Mondini E, Murano I, Severi I, Venema W, Cecchini MP, Kershaw EE, Barbatelli G, Haemmerle G, Zechner R, Cinti S. (2018) Brown adipose tissue whitening leads to brown adipocyte death and adipose tissue inflammation. J Lipid Res. 59: 784-94.

- Kühn FJP, Lückhoff A. (2004) Sites of the NUDT9-H domain critical for ADP-ribose activation of the cation channel TRPM2. J Biol Chem. 279: 46431-7.

- Kunitoshi U, Makoto T. (2014) The role of TRPM2 in pancreatic β-cells and the development of diabetes, Cell Calcium, 56: 332-9.

- Kusminski CM, Bickel PE, Scherer PE. (2016) Targeting adipose tissue in the treatment of obesity-associated diabetes. Nat Rev Drug Discov. 15: 639-60.

- Kusudo T, Wang Z, Mizuno A, Suzuki M, Yamashita H. (1985) TRPV4 deficiency increases skeletal muscle metabolic capacity and resistance against diet-induced obesity. J Appl Physiol. 112: 1223-32.

- Kwok KHM, Lam KSL, Xu A. (2016) Heterogeneity of white adipose tissue: molecular basis and clinical implications. Experimental & Molecular Medicine. 48: e215.

- Leckie CP, McAinsh MR, AllenGJ, Sanders D & Hetherington AM. (1998) Abscisic acid-induced stomatal closure mediated by cyclic ADP-ribose. Proc Natl Acad Sci USA. 95: 15837-42.

- Lee E, Jung DY, Kim JH, Patel PR, Hu X, Lee Y, Azuma Y, Wang HF, Tsitsilianos N, Shafiq U, Kwon JY, Lee HJ, Lee KW, Kim JK. (2015) Transient receptor potential vanilloid type-1 channel regulates diet-induced obesity, insulin resistance, and leptin resistance. FASEB J. 29: 3182-92.

- Lee JH, Park A, Oh KJ, Lee SC, Kim WK, Bae KH. (2019) The Role of Adipose Tissue Mitochondria: Regulation of Mitochondrial Function for the Treatment of Metabolic Diseases. Int J Mol Sci. 20: 4924.

- Lee P, Smith S, Linderman J, Courville AB, Brychta RJ, Dieckmann W, Werner CD, Chen KY, Celi FS. (2014) Temperature-acclimated brown adipose tissue modulates insulin sensitivity in humans. Diabetes. 63: 3686–98.

- Leinninger GM, Myers Jr MG. (2008) LRb signals act within a distributed network of leptin-responsive neurones to mediate leptin action. Acta Physiol (Oxf). 192 :49-59.

- Lindquist JA, Mertens PR. (2018) Cold shock proteins: from cellular mechanisms to pathophysiology and disease. Cell Commun. Signal. 16: 63.

- Liu Y, Mikrani R, He Y, Faran Ashraf Baig MM, Abbas M, Naveed M, Tang M, Zhang Q, Li C, Zhou X. (2020) TRPM8 channels: A review of distribution and clinical role. Eur J Pharmacol. 882: 173312.

- Livak KJ, Schmittgen TD. (2001) Analysis of relative gene expression data using realtime quantitative PCR and the 2−ΔΔCt method. Methods. 25: 402–8.

- Ma S., Yu H., Zhao Z., Luo Z., Chen J., Ni Y., et al. (2012). Activation of the cold-sensing TRPM8 channel triggers UCP1-dependent thermogenesis and prevents obesity. J Mol Cell Biol. 4: 88–96.

- Maciejewska U. (1990) Effects of cold on NAD+ kinase activity in winter rape plants. Physiol Plant. 80: 133-5.

- Malavasi F, Deaglio S, Funaro A, Ferrero E, Horenstein AL, Ortolan E, Vaisitti T, Aydin S. (2008) Evolution and function of the ADP ribosyl cyclase/CD38 gene family in physiology and pathology. Physiol Rev. 88: 841–86.

- Martínez-Sánchez N. (2020) There and Back Again: Leptin Actions in White Adipose Tissue. Int J Mol Sci. 21: 6039.

- Matoušková P, Bártíková H, Boušová I, Hanušová V, Szotáková B, Skálová L. (2014) Reference genes for real-time PCR quantification of messenger RNAs and microRNAs in mouse model of obesity. PLoS One. 9: e86033.

- Morandi F, Airoldi I, Marimpietri D, Bracci C, Faini AC, Gramignoli R. (2019) CD38, a Receptor with Multifunctional Activities: From Modulatory Functions on Regulatory Cell Subsets and Extracellular Vesicles to a Target for Therapeutic Strategies. Cells. 8: 1527.

- Moreschi I, Bruzzone S, Melone L, De Flora A & Zocchi E. (2006) NAADP+ synthesis from cADPRP and nicotinic acid by ADP-ribosyl cyclases. Biochem Biophys Res Commun. 345: 573–80.

- Morita K, Kitayama S, Dohi T. (1997) Stimulation of cyclic ADP-ribose synthesis by acetylcholine and its role in catecholamine release in bovine adrenal chromaffin cells. J Biol Chem. 272: 21002-9.

- Morroni M, Giordano A, Zingaretti MC, Boiani R, De Matteis R, Kahn BB, Nisoli E, Tonello C, Pisoschi C, Luchetti MM, Marelli M, Cinti S. (2004) Reversible transdifferentiation of secretory epithelial cells into adipocytes in the mammary gland. Proc Natl Acad Sci USA. 101: 16801-6.

- Mottillo EP, Balasubramanian P, Lee YH, Weng C, Kershaw EE, Granneman JG. (2014) Coupling of lipolysis and de novo lipogenesis in brown, beige, and white adipose tissues during chronic β3-adrenergic receptor activation. J Lipid Res. 55: 2276-86.

- Mu J, Feng B, Ye Z., Yuan F, Zeng W, Luo Z, Qi W. (2011) Visfatin is related to lipid dysregulation, endothelial dysfunction and atherosclerosis in patients with chronic kidney disease. J Nephrol. 24: 177-84.

- Munshi CB, Graeff R, Lee HC. (2002) Evidence for a causal role of CD38 expression in granulocytic differentiation of human HL-60 cells. J Biol Chem. 277: 49453-49458.

- Nisoli E, Clementi E, Tonello C, Sciorati C, Briscini L, Carruba MO. (1988) Effects of nitric oxide on proliferation and differentiation of rat brown adipocytes in primary cultures. Br J Pharmacol. 125: 888–94.

- Ohyama K, Nogusa Y, Shinoda K, Suzuki K, Bannai M, Kajimura S. (2016) A Synergistic Antiobesity Effect by a Combination of Capsinoids and Cold Temperature Through Promoting Beige Adipocyte Biogenesis. Diabetes. 65: 1410-23.

- Park L, Wang G, Moore J, Girouard H, Zhou P, Anrather J, Iadecola C. (2014) The key role of transient receptor potential melastatin-2 channels in amyloid-beta-induced neurovascular dysfunction. Nat Commun. 5: 5318.

- Pham TX, Bae M, Kim MB, Lee Y, Hu S, Kang H, Park YK, Lee JY. Nicotinamide riboside, an NAD+ precursor, attenuates the development of liver fibrosis in a diet-induced mouse model of liver fibrosis. Biochim Biophys Acta Mol Basis Dis. 1865: 2451-2463.

- Podestà, M, Pitto A, Figari O, Bacigalupo A, Bruzzone S, Guida L, Franco L, De Flora A & Zocchi E. (2003) Cyclic ADP-ribose generation by CD38 improves human hemopoietic stem cell engraftment into NOD/SCID mice. FASEB J. 17: 310-2.

- Rabiee A. (2020) Beige Fat Maintenance; Toward a Sustained Metabolic Health. Front Endocrinol. 11: 634.

- Radenkovic D, Verdin E. (2020) Clinical Evidence for Targeting NAD Therapeutically. Pharmaceuticals. 13: 247.

- Rah SY, Kim UH. (2015) CD38-mediated Ca^{2+} signaling contributes to glucagon-induced hepatic gluconeogenesis. Sci Rep. 5: 10741

- Rajman L, Chwalek K, Sinclair DA. (2018) Therapeutic Potential of NAD-Boosting Molecules: The In Vivo Evidence. Cell Metab. 27: 529–47.

- Ramnanan CJ, Edgerton DS, Kraft G, Cherrington AD. (2011) Physiologic action of glucagon on liver glucose metabolism. Diabetes Obes Metab. 13: 118-25.

- Revollo JR, Körner A, Mills KF, Satoh A, Wang T, Garten A, Dasgupta B, Sasaki Y, Wolberger C, Townsend RR, Milbrandt J, Kiess W, Imai S. (2007) Nampt/PBEF/Visfatin regulates insulin secretion in beta cells as a systemic NAD biosynthetic enzyme. Cell Metab. 6: 363-75.

- Reynés B, van Schothorst EM, García-Ruiz E, Keijer J, Palou A, Oliver P. (2017) Cold exposure down-regulates immune response pathways in ferret aortic perivascular adipose tissue. Thromb Haemost. 117: 981-91.

- Ricquier D. (2011) Uncoupling protein 1 of brown adipocytes, the only uncoupler: a historical perspective. Front Endocrinol (Lausanne). 2: 85.

- Rossato M, Granzotto M, Macchi V, Porzionato A, Petrelli L, Calcagno A, Vencato J, De Stefani D, Silvestrin V, Rizzuto R, Bassetto F, De Caro R, Vettor R. (2014) Human white adipocytes express the cold receptor TRPM8 which activation induces UCP1 expression, mitochondrial activation and heat production. Mol Cell Endocrinol. 383:137-46.

- Rui L. (2014) Energy metabolism in the liver. Compr Physiol. 4: 177-97.

- Saely CH, Geiger K, Drexel H. (2012) Brown versus white adipose tissue: a mini-review. Gerontology. 58: 15-23.

- Sanders OD, Rajagopal JA, Rajagopal L. (2021) Menthol to Induce Non-shivering Thermogenesis via TRPM8/PKA Signaling for Treatment of Obesity. J Obes Metab Syndr. 30: 4-11.

- Scheja L, Heeren J. (2016) Metabolic interplay between white, beige, brown adipocytes and the liver. J Hepatol. 64: 1176-1186.

- Shi T, Wang F, Stieren E, Tong Q. (2005) SIRT3, a mitochondrial sirtuin deacetylase, regulates mitochondrial function and thermogenesis in brown adipocytes. J Biol Chem. 280: 13560-7.

- Shore AM, Karamitri A, Kemp P, Speakman JR, Graham NS, Lomax MA. (2013) Cold-induced changes in gene expression in brown adipose tissue, white adipose tissue and liver. PLoS One. 8: e68933.

- Siegrist-Kaiser CA, Pauli V, Juge-Aubry CE, Boss O, Pernin A, Chin WW, Cusin I, Rohner-Jeanrenaud F, Burger AG, Zapf J, Meier CA. (1997) Direct effects of leptin on brown and white adipose tissue. J Clin Invest. 100 :2858-64.

- Sistare FD, Haynes RC Jr. (1985) The interaction between the cytosolic pyridine nucleotide redox potential and gluconeogenesis from lactate/pyruvate in isolated rat hepatocytes. Implications for investigations of hormone action. J Biol Chem. 260: 12748-53.

- Sociali G, Grozio A, Caffa I, Schuster S, Becherini P, Damonte P, Sturla L, Fresia C, Passalacqua M, Mazzola F, Raffaelli N, Garten A, Kiess W, Cea M, Nencioni A, Bruzzone S. (2019) SIRT6 deacetylase activity regulates NAMPT activity and NAD(P)(H) pools in cancer cells. FASEB J. 33: 3704-3717.

- Stromsdorfer KL, Yamaguchi S, Yoon MJ, Moseley AC, Franczyk MP, Kelly SC, Qi N, Imai SI, Yoshino J. (2016) NAMPT-Mediated NAD(+) Biosynthesis in Adipocytes Regulates Adipose Tissue Function and Multi-organ Insulin Sensitivity in Mice. Cell Rep. 16: 1851-60.

- Sturla L, Fresia C, Guida L, Bruzzone S, Scarfi S, Usai C, Fruscione F, Magnone M, Millo E, Basile G, Grozio A, Jacchetti E, Allegretti M, De Flora A, Zocchi E. (2009) LANCL2 is necessary for abscisic acid binding and signaling in human granulocytes and in rat insulinoma cells. J Biol Chem. 284: 28045–57.

- Sturla L, Mannino E, Scarfi S, Bruzzone S, Magnone M, Sociali G, Booz V, Guida L, Vigliarolo T, Fresia C, Emionite L, Buschiazzo A, Marini C, Sambuceti G, De Flora A, Zocchi E. (2017) Abscisic acid enhances glucose disposal and induces brown fat activity in adipocytes in vitro and in vivo. Biochim Biophys Acta Mol Cell Biol Lipids. 1862: 131–44.

- Suchacki KJ, Stimson RH. (2021) Nutritional Regulation of Human Brown Adipose Tissue. Nutrients. 13: 1748.

- Sun K, Kusminski CM, Luby-Phelps K, Spurgin SB, An YA, Wang QA, Holland WL, Scherer PE. (2014) Brown adipose tissue derived VEGF-A modulates cold tolerance and energy expenditure. Mol Metab. 3: 474–83.

- Sun W, Li C, Zhang Y, Jiang C, Zhai M, Zhou Q, Xiao L, Deng Q. (2017) Gene expression changes of thermo-sensitive transient receptor potential channels in obese mice. Cell Biol Int. 41: 908-13.

- Tarragó MG, Chini CCS, Kanamori KS, Warner GM, Caride A, de Oliveira GC, Rud M, Samani A, Hein KZ, Huang R, Jurk D, Cho DS, Boslett JJ, Miller JD, Zweier JL, Passos JF, Doles JD, Becherer DJ, Chini EN. (2018) A Potent and Specific CD38 Inhibitor Ameliorates Age-Related Metabolic Dysfunction by Reversing Tissue NAD+ Decline. Cell Metab. 27: 1081–95.

- Toews CJ, Lowy C, Ruderman NB. (1970) The regulation of gluconeogenesis. The effect of pent-4-enoic acid on gluconeogenesis and on the gluconeogenic metabolite concentrations of isolated perfused rat liver.J Biol Chem. 245: 818-24

- Torres N, Vargas-Castillo AE, Tovar AR. (2016) Adipose Tissue: White Adipose Tissue Structure and Function. Encyclopedia of Food and Health. p35-42.

- Travelli C, Aprile S, Mattoteia D, Colombo G, Clemente N, Scanziani E, Terrazzino S, Alisi MA, Polenzani L, Grosa G, Genazzani AA, Tron GC, Galli U. (2019) Identification of potent triazolylpyridine nicotinamide phosphoribosyltransferase (NAMPT) inhibitors bearing a 1,2,3-triazole tail group. Eur J Med Chem. 181: 111576.

- Vaisitti T, Audrito V, Serra S, Buonincontri R, Sociali G, Mannino E, Pagnani A, Zucchetto A, Tissino E, Vitale C, Coscia M, Usai C, Pepper C, Gattei V, Bruzzone S, Deaglio S. (2015) The enzymatic activities of CD38 enhance CLL growth and trafficking: Implications for therapeutic targeting. Leukemia. 29: 356–68.

- van de Donk NWCJ, Richardson PG, Malavasi F. (2018) CD38 antibodies in multiple myeloma: Back to the future. Blood. 131: 13–29.

- van Marken Lichtenbelt WD, Vanhommerig JW, Smulders NM, Drossaerts JM, Kemerink GJ, Bouvy ND, Schrauwen P, Teule GJ. (2009) Cold-activated brown adipose tissue in healthy men. N Engl J Med. 360: 1500–8.

- Virtanen KA, Lidell ME, Orava J, Heglind M, Westergren R, Niemi T, Taittonen M, Laine J, Savisto NJ, Enerbäck S, Nuutila P. (2009) Functional brown adipose tissue in healthy adults. N Engl J Med. 360: 1518-1525.

- Wang Ling-Fang, Lian-Jie Miao, Xiao-Nv Wang, Cong-Cong Huang, Yi-Song Qian, Xuan Huang, Xiao-Lei Wang, Wan-Zhu Jin, Guang-Ju Ji, Mingui Fu, Ke-Yu Deng, Hong-Bo Xin. (2018) CD38 deficiency suppresses adipogenesis and lipogenesis in adipose tissues through activating Sirt1/PPARγ signaling pathway. J Cell Mol Med. 22101–10.

- Wang Z, Yu X, Chen Y. (2021) Recruitment of Thermogenic Fat: Trigger of Fat Burning. Front Endocrinol (Lausanne). 12: 696505.

- Wehage E, Eisfeld J, Heiner I, Jüngling E, Zitt C, Lückhoff A. (2002) Activation of the cation channel long transient receptor potential channel 2 (LTRPC2) by hydrogen peroxide. A splice variant reveals a mode of activation independent of ADP-ribose. J Biol Chem. 277: 23150-6.

- Wei X, Jia R, Yang Z, Jiang J, Huang J, Yan J, Luo X. (2020) NAD+ /sirtuin metabolism is enhanced in response to cold-induced changes in lipid metabolism in mouse liver. FEBS Lett. 594: 1711-1725.

- Weiner J, Hankir M, Heiker JT, Fenske W, Krause K. (2017) Thyroid hormones and browning of adipose tissue. Molecular and Cellular Endocrinology. 458: 156-159.

- Weir JB. (1949) New methods for calculating metabolic rate with special reference to protein metabolism. J Physiol. 109: 1-9.

- Weisberg SP, McCann D, Desai M, Rosenbaum M, Leibel RL and Ferrante AW Jr. (2003) Obesity is associated with macrophage accumulation in adipose tissue. J Clin Invest. 112: 1796–808.

- Worthmann A, John C, Rühlemann MC, Baguhl M, Heinsen FA, Schaltenberg N, Heine M, Schlein C, Evangelakos I, Mineo C, Fischer M, Dandri M, Kremoser C, Scheja L, Franke A, Shaul PW, Heeren J. (2017) Cold-induced conversion of cholesterol to bile acids in mice shapes the gut microbiome and promotes adaptive thermogenesis. Nat Med. 23: 839-49.

- Xiao W, Wang RS, Handy DE, Loscalzo J. (2018) NAD(H) and NADP(H) Redox Couples and Cellular Energy Metabolism. Antioxid Redox Signal. 28: 251-72.

- Xie L, Wen K, Li Q, Huang CC, Zhao JL, Zhao QH, Xiao YF, Guan XH, Qian YS, Gan L, Wang LF, Deng KY, Xin HB. (2021) CD38 Deficiency Protects Mice from High Fat Diet-Induced Nonalcoholic Fatty Liver Disease through Activating NAD(+)/Sirtuins Signaling Pathways-Mediated Inhibition of Lipid Accumulation and Oxidative Stress in Hepatocytes. Int J Biol Sci. 17: 4305-15.

- Xu F, Zheng X, Lin B, Liang H, Cai M, Cao H, Ye J, Weng J. (2016) Diet-induced obesity and insulin resistance are associated with brown fat degeneration in SIRT1-deficient mice. Obesity (Silver Spring). 24: 634-42.

- Xue B, Greenberg AG, Kraemer FB, Zemel MB. (2001) Mechanism of intracellular calcium ($[Ca^{2+}]_i$) inhibition of lipolysis in human adipocytes. FASEB J. 15: 2527-9.

- Xue Y, Petrovic N, Cao R, Larsson O, Lim S, Chen S, Feldmann HM, Liang Z, Zhu Z, Nedergaard J, Cannon B, Cao Y. (2009) Hypoxia-independent angiogenesis in adipose tissues during cold acclimation. Cell Metab. 9: 99-109.

- Yamaguchi S, Franczyk MP, Chondronikola M, Qi N, Gunawardana SC, Stromsdorfer KL, Porter LC, Wozniak DF, Sasaki Y, Rensing N, Wong M, Piston DW, Klein S, Yoshino J. (2019) Adipose tissue NAD+ biosynthesis is required for regulating adaptive thermogenesis and whole-body energy homeostasis in mice. Proc Natl Acad Sci U S A. 116: 23822-28.

- Yang Y, Zhang N, Zhang G, Sauve AA. (2020) NRH salvage and conversion to NAD(+) requires NRH kinase activity by adenosine kinase. Nat Metab. 2: 364–79.

- Yau WW, Yen PM. (2020) Thermogenesis in Adipose Tissue Activated by Thyroid Hormone. Int J Mol Sci. 21: 3020.

- Ye L, Kleiner S, Wu J, Sah R, Gupta RK, Banks AS, Cohen P, Khandekar MJ, Boström P, Mepani RJ, Laznik D, Kamenecka TM, Song X, Liedtke W, Mootha VK, Puigserver P, Griffin PR, Clapham DE, Spiegelman BM. (2012) TRPV4 is a regulator of adipose oxidative metabolism, inflammation, and energy homeostasis. Cell. 151: 96-110.

- Yoon MJ, Yoshida M, Johnson S, Takikawa A, Usui I, Tobe K, Nakagawa T, Yoshino J, Imai S. (2015) SIRT1-Mediated eNAMPT Secretion from Adipose Tissue Regulates Hypothalamic NAD+ and Function in Mice. Cell Metab. 21: 706-17.

- Yoshida M, Satoh A, Lin JB, Mills KF, Sasaki Y, Rensing N, Wong M, Apte RS, Imai SI. (2019) Extracellular Vesicle-Contained eNAMPT Delays Aging and Extends Lifespan in Mice. Cell Metab. 30: 329-342.

- Yoshino J, Mills KF, Yoon MJ, Imai S. (2011) Nicotinamide mononucleotide, a key NAD(+) intermediate, treats the pathophysiology of diet- and age-induced diabetes in mice. Cell Metab. 14: 528–36.

- Yoshino M, Yoshino J, Kayser BD, Patti GJ, Franczyk MP, Mills KF, Sindelar M, Pietka T, Patterson BW, Imai SI, Klein S. (2021) Nicotinamide mononucleotide increases muscle insulin sensitivity in prediabetic women. Science. 372: 1224–9.

- Young GS, Choleris E, Lund FE, Kirkland JB. (2006) Decreased cADPR and increased NAD+ in the $Cd38^{-/-}$ mouse. Biochem Biophys Res Commun. 346: 188–92.

- Zapata-Pérez R, Tammaro A, Schomakers BV, Scantlebery AML, Denis S, Elfrink HL, Giroud-Gerbetant J, Cantó C, López-Leonardo C, McIntyre RL, van Weeghel M, Sánchez-Ferrer Á, Houtkooper RH. Reduced nicotinamide mononucleotide is a new and potent NAD+ precursor in mammalian cells and mice. FASEB J. 35: e21456.

- Zhang Y, Proenca R, Maffei M, Barone M, Leopold L, Friedman JM. (1994) Positional cloning of the mouse obese gene and its human homologue. Nature. 372: 425–32.

- Zhang Z, Zhang W, Jung DY, Ko HJ, Lee Y, Friedline RH, Lee E, Jun J, Ma Z, Kim F, Tsitsilianos N, Chapman K, Morrison A, Cooper MP, Miller BA & Kim JK. (2012) TRPM2 Ca^{2+} channel regulates energy balance and glucose metabolism. American Journal of Physiology - Endocrinology and Metabolism. 302: E807-E816.

- Zhang R. (2013) MNADK, a novel liver-enriched mitochondrion-localized NAD kinase. Biol. Open 2: 432–8.

- Zocchi E, Daga A, Usai C, Franco L, Guida L, Bruzzone S, Costa A, Marchetti C, De Flora A. (1998) Expression of CD38 increases intracellular calcium concentration and reduces doubling time in HeLa and 3T3 cells. J Biol Chem. 273: 8017–24.

- Zoppoli G, Cea M, Soncini D, Fruscione F, Rudner J, Moran E, Caffa I, Bedognetti D, Motta G, Ghio R, Ferrando F, Ballestrero A, Parodi S, Belka C, Patrone F, Bruzzone S, Nencioni A. (2010) Potent synergistic interaction between the Nampt inhibitor APO866 and the apoptosis activator TRAIL in human leukemia cells. Exp Hematol. 38: 979–88.
- Zuo W, Liu N, Zeng Y, Liu Y, Li B, Wu K, Xiao Y, Liu Q. (2020) CD38: A Potential Therapeutic Target in Cardiovascular Disease. Cardiovasc Drugs Ther. 35: 815–28.